

This version of the ESI published 09/08/2023 replaces the previous version published 24/05/2023 to include Sections 5-8.

Substituent Effects on Aromatic Interactions in Water

Gloria Tobajas-Curiel,¹ Qingqing Sun,^{2,3} Jeremy K. M. Sanders,¹ Pablo Ballester,^{2,4,*} Christopher A. Hunter^{1,*}

¹*Yusuf Hamied Department of Chemistry, University of Cambridge, Cambridge CB2 1EW, U.K.
Email: herchelsmith.orgchem@ch.cam.ac.uk*

²*Institute of Chemical Research of Catalonia (ICIQ), Barcelona Institute of Science and Technology (BIST), Av. Països Catalans, 16, 43007, Tarragona, Spain. Email: pballester@iciq.es*

³*Yangzhou University, School of Chemistry and Chemical Engineering, Yangzhou, 225002 Jiangsu (China). Email: sunqingqing@snnu.edu.cn.*

⁴*ICREA, Passeig Lluís Companys 23, 08010, Barcelona, Spain.*

Supporting Information

1. General methods.....	3
2. Chemistry procedures	4
2.1. General experimental procedure for the synthesis of 4-arylpyridine <i>N</i> -oxides 5-14	4
2.2. General experimental procedure for the synthesis of 4-arylpyridine <i>N</i> -oxides 15-17	4
2.3. Physical data of the 4-arylpyridine <i>N</i> -oxides 5-17	5
3. Isothermal titration calorimetry (ITC) experiments	31
3.1. Octapyridinium-super-aryl-extended calix[4]pyrrole 1	31
3.1.1. Complex C of the DMC	31
3.1.2. Complex A of the DMC	32
3.2. Tetrapyridinium-aryl-extended calix[4]pyrrole 3	39
3.2.1. Complex D of the DMC	39
3.2.2. Complex B of the DMC	40
3.3. Octachloro-super-aryl-extended calix[4]pyrrole 2	47
3.3.1. Complex C of the DMC	47
3.3.2. Complex A of the DMC	48
3.4. Tetrachloro-aryl-extended calix[4]pyrrole 4.....	55

3.4.1.	Complex D of the DMC	55
3.4.2.	Complex B of the DMC	56
4.	Pairwise ¹ H NMR competitive titrations	63
4.1.	Octapyridinium-super-aryl-extended calix[4]pyrrole 1	63
4.2.	Octachloro-super-aryl-extended calix[4]pyrrole 2	70
4.3.	Tetrachloro-aryl-extended calix[4]pyrrole 4.....	77
5.	Results of titration experiments	78
6.	¹ H NMR analysis of the structures of complex A of the DMC	82
7.	Analysis of the DMC results	84
8.	References	88

1. General methods

All the reagents and materials used in the synthesis of the compounds described below were obtained from commercial sources and used without prior purification. Compounds **1-4** were prepared as reported in literature.¹⁻³ Thin layer chromatography was carried out using Silica gel 60F on glass plates. Flash chromatography was carried out on an automated system (Combiflash Companion, Combiflash Rf+ or Combiflash Rf Lumen) using prepacked cartridges of silica (25 μm or 50 μm PuriFlash® Columns). ^1H and ^{13}C NMR spectra were recorded on Bruker 400 MHz DPX400, 400 MHz AVIII400, 500 MHz DCH cryoprobe or 500 MHz TCI Cryoprobe spectrometer at 298.0 ± 0.1 K unless specifically stated otherwise. Residual solvent was used as an internal standard for referencing. In chloroform-*d*, ^1H spectra were referenced to δ 7.26 ppm and ^{13}C spectra to δ 77.06 ppm for the solvent signal. In dimethyl sulfoxide-*d*₆, ^1H spectra were referenced to δ 2.50 ppm and ^{13}C spectra to δ 39.52 ppm. In deuterium oxide, ^1H spectra were referenced to δ 4.79 ppm. All chemical shifts are quoted in ppm on the δ scale and the coupling constants expressed in Hz. Signal splitting patterns are described as follows: s (singlet), br s (broad singlet), d (doublet), t (triplet), q (quartet), m (multiplet). FT-IR spectra were recorded on a PerkinElmer Spectrum One FT-IR spectrometer equipped with an ATR cell. The LCMS analysis of samples was performed using a Waters Acquity H-Class UPLC coupled with a single quadrupole Waters SQD2 or a Waters Xevo G2-S bench top QTOF machine. Melting points were measured on a Mettler Toledo MP90 melting point apparatus. ITC titrations were carried out on a Malvern MicroCal VP-ITC MicroCalorimeter.

2. Chemistry procedures

2.1. General experimental procedure for the synthesis of 4-arylpyridine *N*-oxides 5-14

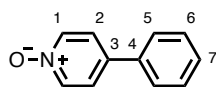
To a solution of 4-chloro pyridine *N*-oxide (0.50 mmol, 1 equiv.) in dioxane (4 mL) under nitrogen, the corresponding aryl boronic acid (1.00 mmol, 2 equiv.), palladium tetrakis triphenylphospine (0.03 mmol, 0.05 equiv.) and sodium carbonate (2 M solution in water, 1 mL) were added. The mixture was stirred at 80 °C for 16 h. Ethyl acetate (10 mL) and water (5 mL) were then added. The black precipitate was filtered off through Celite® and the filtrate was extracted with ethyl acetate (3 x 10 mL). The combined organic layers were washed with brine, dried over anhydrous MgSO₄ and the solvents evaporated under reduced pressure. The crude product was purified by flash column chromatography on silica gel (methanol in dichloromethane 0 to 5 % in 20 minutes) to yield the corresponding 4-arylpyridine *N*-oxides **5-14**.

2.2. General experimental procedure for the synthesis of 4-arylpyridine *N*-oxides 15-17

To a solution of 4-chloro pyridine *N*-oxide (1.25 mmol, 5 equiv.) in dioxane (4 mL) under nitrogen, the corresponding aryl boronic acid (0.25 mmol, 1 equiv.), palladium tetrakis triphenylphospine (0.01 mmol, 0.05 equiv.) and sodium carbonate (2 M solution in water, 0.5 mL) were added. The mixture was stirred at 80 °C for 16 h. Ethyl acetate (10 mL) and water (5 mL) were then added. The black precipitate was filtered off through Celite® and the filtrate was extracted with ethyl acetate (3 x 10 mL). The combined organic layers were washed with brine, dried over anhydrous MgSO₄ and the solvents evaporated under reduced pressure. The crude product was purified by reverse phase flash column chromatography on C-18 (acetonitrile in water 10 to 50 % in 20 minutes) to yield the corresponding 4-halophenyl pyridine *N*-oxides **15-17**.

2.3. Physical data of the 4-arylpyridine *N*-oxides 5-17

4-Phenylpyridine 1-oxide (5)



Off white solid (59 mg, 0.34 mmol, 69 % yield)

M.p.: 151 – 153 °C.

¹H NMR (400 MHz, DMSO-*d*₆): δ_{H} = 8.26 (d, J = 7.1 Hz, 2H, H-1), 7.79 – 7.76 (m, 4H, H-2, H-5), 7.50 (t, J = 7.5 Hz, 2H, H-6), 7.45 – 7.41 (m, 1H, H-7).

¹³C NMR (101 MHz, DMSO-*d*₆): δ_{C} = 138.9 (C-1), 136.0 (C-3), 135.6 (C-4), 129.2 (C-6), 128.8 (C-7), 126.2 (C-5), 123.6 (C-2).

HRMS (ES⁺): calculated for C₁₁H₁₀NO 172.0757 [M+H⁺], found 172.0755 [M+H⁺].

FT-IR (ATR): ν_{max} 3335, 3109, 1687, 1472, 1431, 1230, 1183, 843, 779, 576 cm⁻¹.

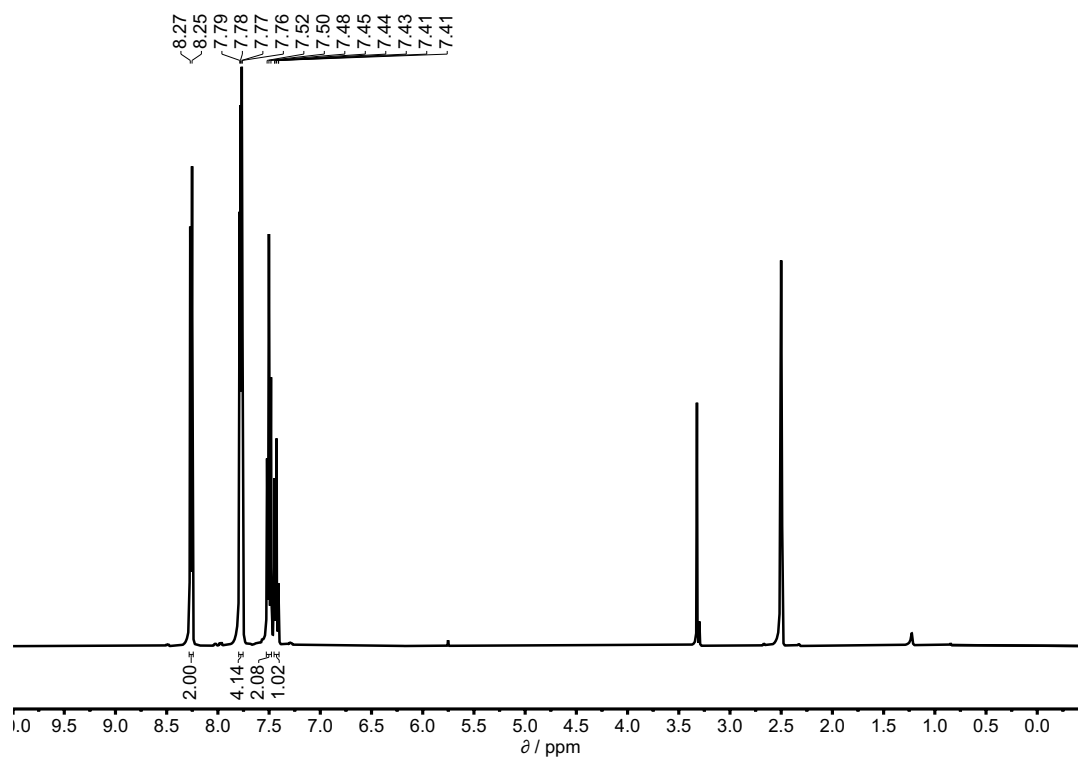


Figure S1. ^1H NMR spectrum (400 MHz, DMSO-d_6) of compound **5**.

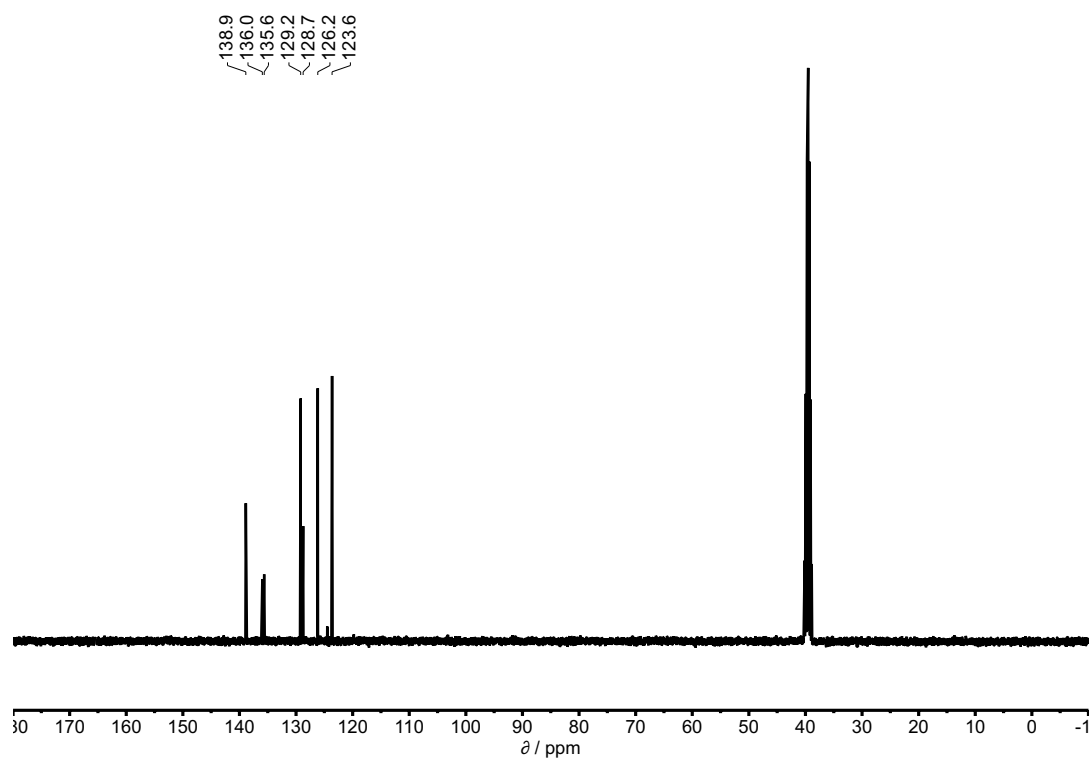
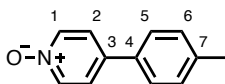


Figure S2. ^{13}C NMR spectrum (101 MHz, DMSO-d_6) of compound **5**.

4-(*p*-Tolyl)pyridine 1-oxide (6)



Pink solid (73 mg, 0.39 mmol, 79 % yield)

M.p.: 136 – 138 °C.

¹H NMR (400 MHz, DMSO-*d*₆): δ_{H} = 8.23 (d, J = 7.1 Hz, 2H, H-1), 7.74 (d, J = 7.1 Hz, 2H, H-2), 7.67 (d, J = 8.0 Hz, 2H, H-5), 7.30 (d, J = 8.0 Hz, 2H, H-6), 2.34 (s, 3H, CH₃).

¹³C NMR (101 MHz, DMSO-*d*₆): δ_{C} = 138.8 (C-1), 138.4 (C-7), 136.0 (C-3), 132.7 (C-4), 129.8 (C-6), 126.0 (C-5), 123.3 (C-2), 20.7 (CH₃).

HRMS (ES⁺): calculated for C₁₂H₁₂NO 186.0913 [M+H⁺], found 186.0909 [M+H⁺].

FT-IR (ATR): ν_{max} 3506, 3034, 1480, 1243, 1181, 1027, 815, 679, 532 cm⁻¹.

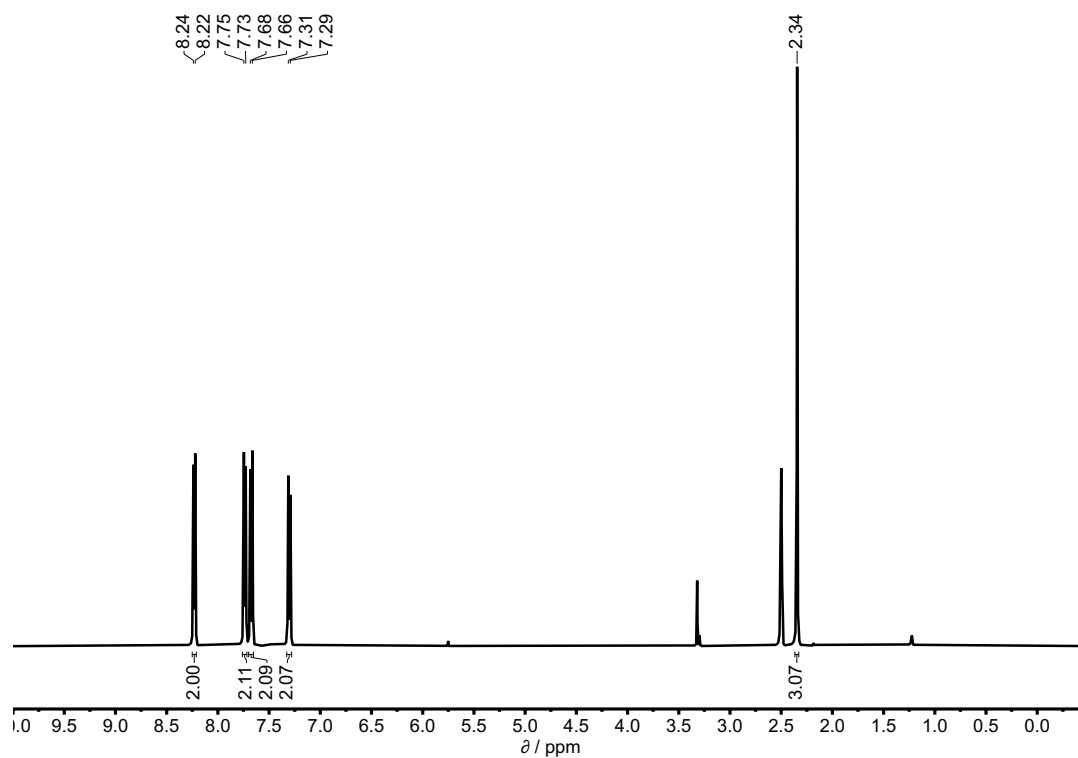


Figure S3. ^1H NMR spectrum (400 MHz, DMSO-d_6) of compound **6**.

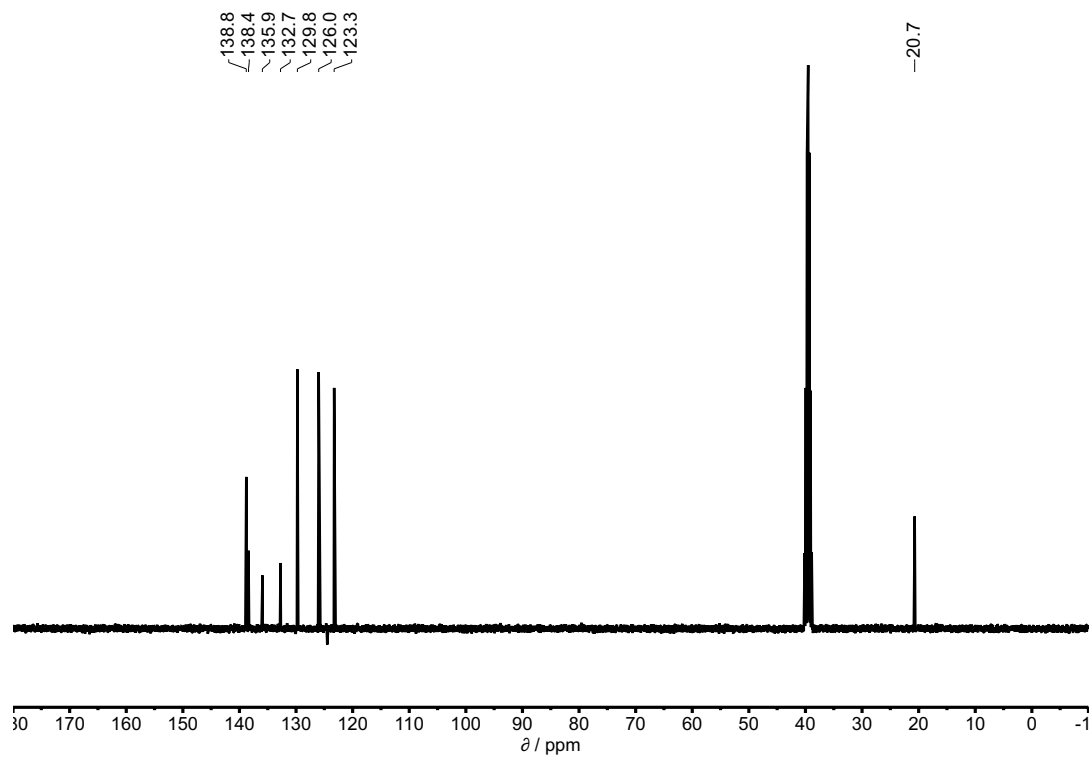
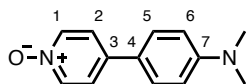


Figure S4. ^{13}C NMR spectrum (101 MHz, DMSO-d_6) of compound **6**.

4-(4-(Dimethylamino)phenyl)pyridine 1-oxide (7)



Brown solid (78 mg, 0.36 mmol, 73 % yield)

M.p.: 242 – 244 °C.

¹H NMR (400 MHz, DMSO-*d*₆): δ_H = 8.14 (d, *J* = 7.1 Hz, 2H, H-1), 7.67 – 7.62 (m, 4H, H-2, H-5), 6.79 (d, *J* = 8.9 Hz, 2H, H-6), 2.96 (s, 6H, N(CH₃)₂).

¹³C NMR (101 MHz, DMSO-*d*₆): δ_C = 150.6 (C-7), 138.6 (C-1), 136.6 (C-3), 126.8 (C-5), 122.4 (C-4), 121.8 (C-2), 112.4 (C-6), 39.8 (N(CH₃)₂).

HRMS (ES⁺): calculated for C₁₃H₁₅N₂O 215.1179 [M+H⁺], found 215.1173 [M+H⁺].

FT-IR (ATR): ν_{max} 2899, 1604, 1471, 1365, 1252, 1183, 1028, 813, 660 cm⁻¹.

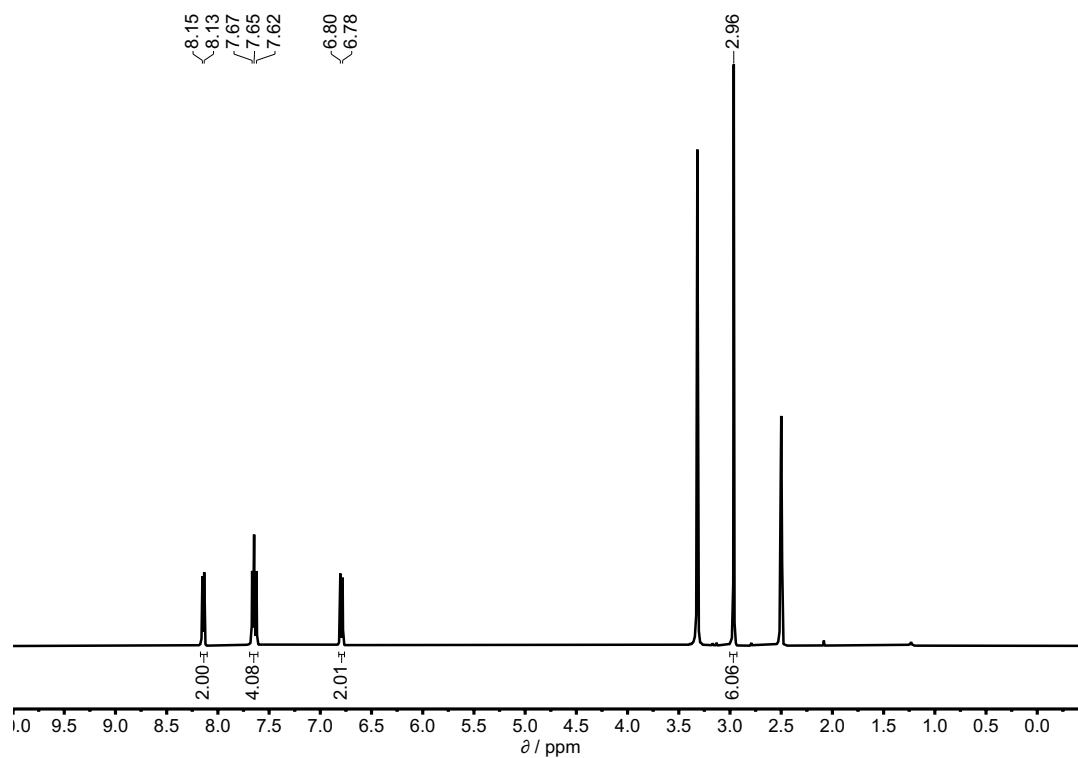


Figure S5. ^1H NMR spectrum (400 MHz, DMSO-d_6) of compound 7.

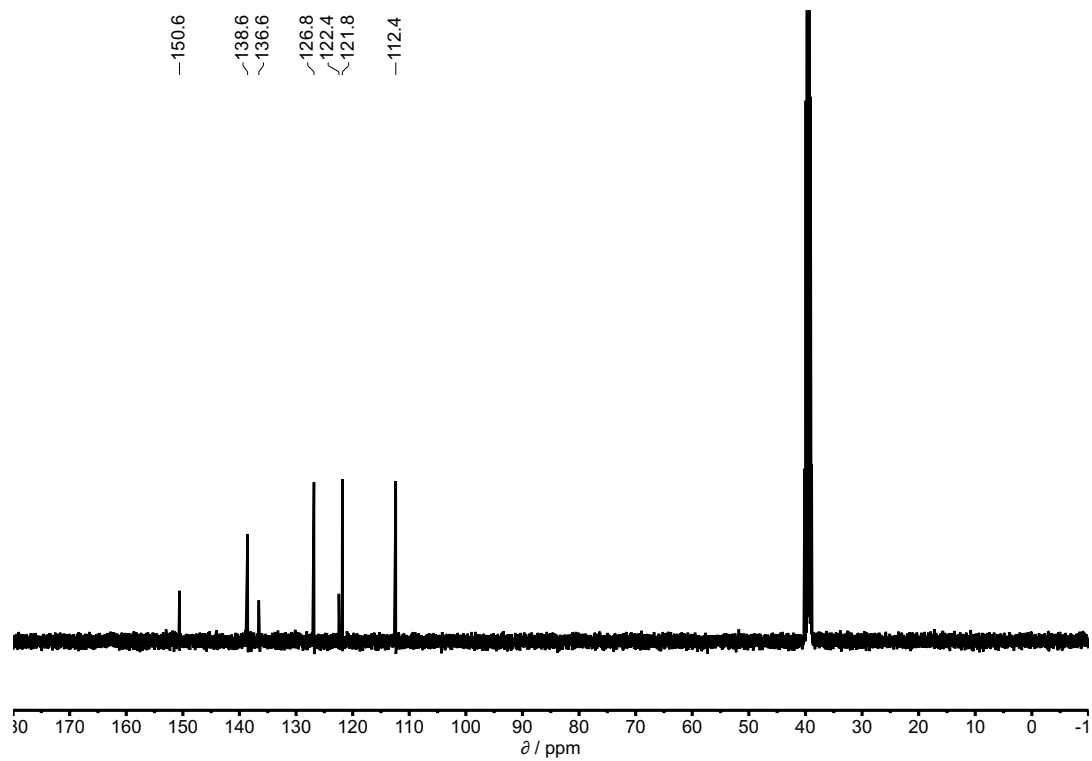
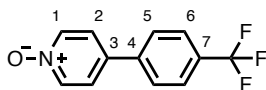


Figure S6. ^{13}C NMR spectrum (101 MHz, DMSO-d_6) of compound 7.

4-(4-(Trifluoromethyl)phenyl)pyridine 1-oxide (8)



Off-white solid (84 mg, 0.35 mmol, 70 % yield)

M.p.: 177 – 179 °C.

¹H NMR (400 MHz, DMSO-*d*₆): δ_{H} = 8.32 (d, J = 7.1 Hz, 2H, H-1), 8.01 (d, J = 8.2 Hz, 2H, H-5), 7.87 – 7.84 (m, 4H, H-2, H-6).

¹³C NMR (101 MHz, DMSO-*d*₆): δ_{C} = 139.7 (CF₃), 139.1 (C-1), 134.2 (C-3), 127.1 (C-5), 126.0 (C-6), 124.5 (C-4), 124.2 (C-2).

HRMS (ES+): calculated for C₁₂H₉F₃NO 240.0631 [M+H⁺], found 240.0625 [M+H⁺].

FT-IR (ATR): ν_{max} 3436, 3115, 1615, 1483, 1328, 1115, 1074, 850, 717 cm⁻¹.

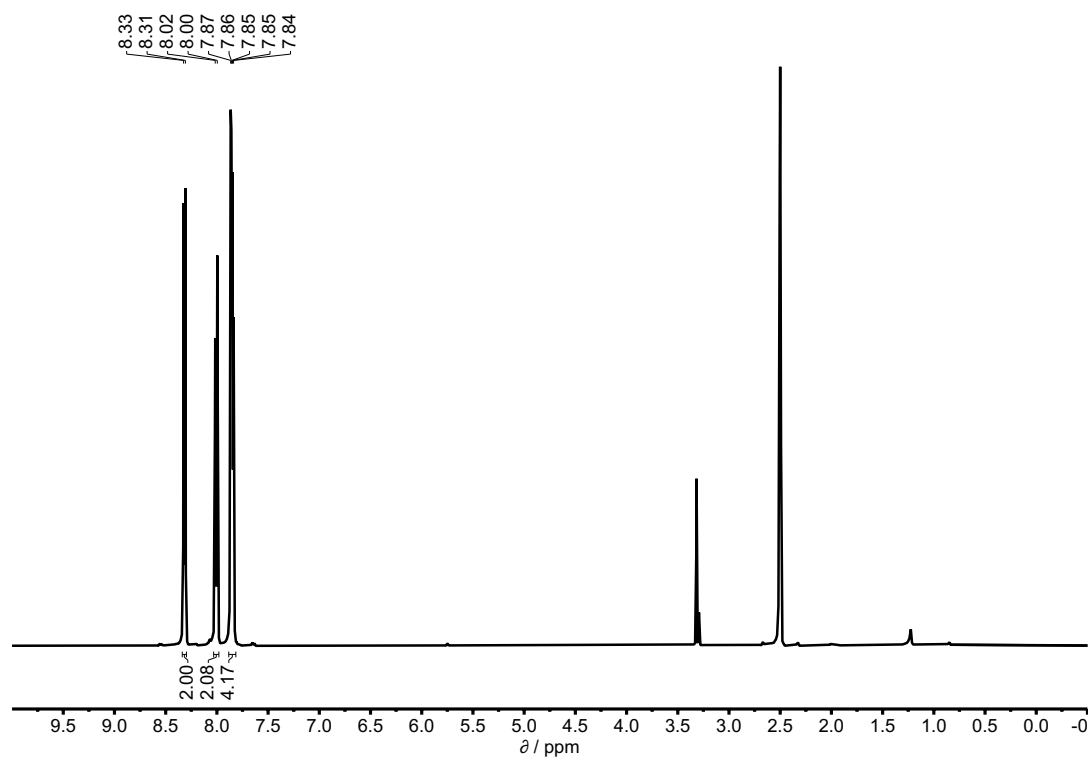


Figure S7. ^1H NMR spectrum (400 MHz, DMSO-d_6) of compound **8**.

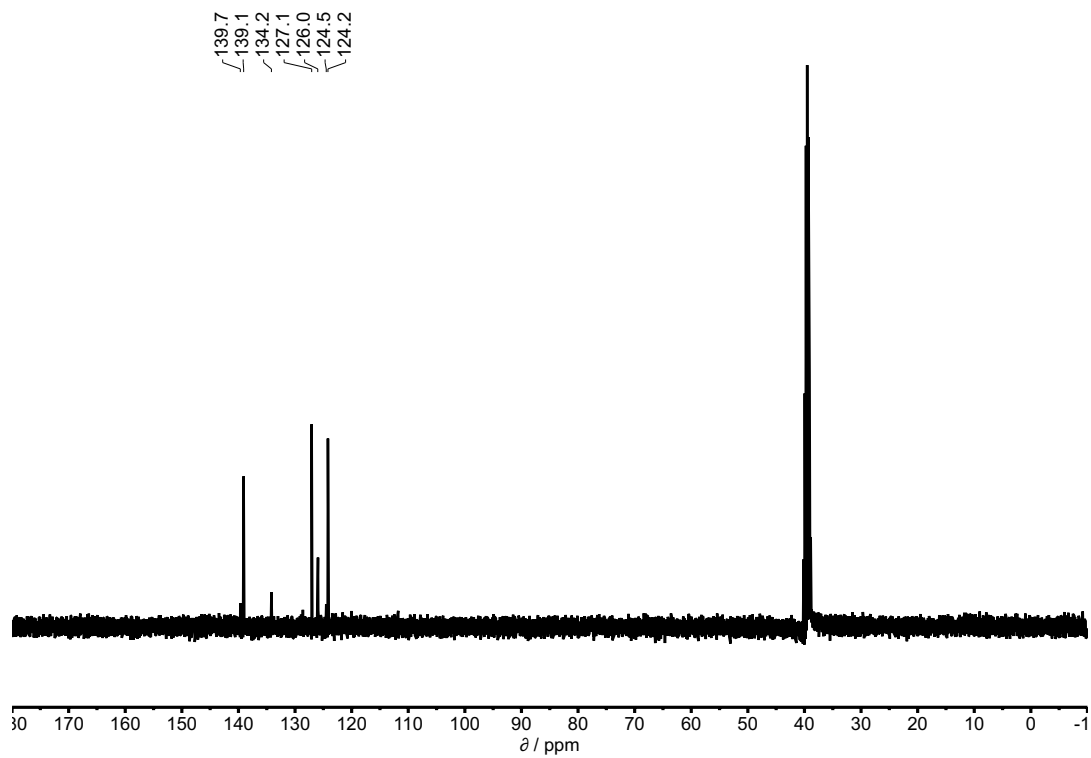
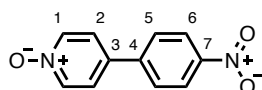


Figure S8. ^{13}C NMR spectrum (101 MHz, DMSO-d_6) of compound **8**.

4-(4-Nitrophenyl)pyridine 1-oxide (9)



Yellow solid (82 mg, 0.38 mmol, 75 % yield)

M.p.: 218 – 200 °C.

¹H NMR (400 MHz, DMSO-*d*₆): δ_{H} = 8.34 – 8.30 (m, 4H, H-1, H-6), 8.07 (d, J = 8.9 Hz, 2H, H-5), 7.90 (d, J = 7.1 Hz, 2H, H-2).

¹³C NMR (101 MHz, DMSO-*d*₆): δ_{C} = 147.2 (C-7), 141.9 (C-3), 139.2 (C-1), 133.4 (C-4), 127.5 (C-5), 124.4 (C-2), 124.2 (C-6).

HRMS (ES+): calculated for C₁₁H₉N₂O₃ 217.0608 [M+H⁺], found 217.0603 [M+H⁺].

FT-IR (ATR): ν_{max} 1600, 1511, 1475, 1345, 1254, 1201, 835, 755 cm⁻¹.

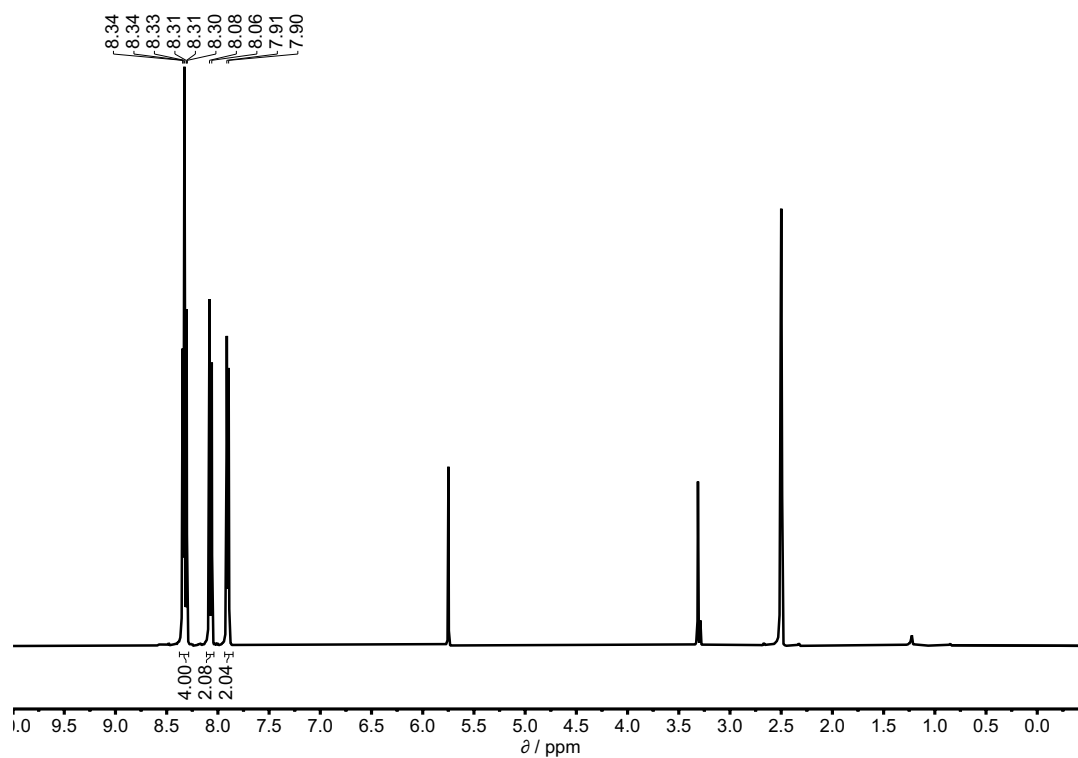


Figure S9. ^1H NMR spectrum (400 MHz, DMSO-d_6) of compound **9**.

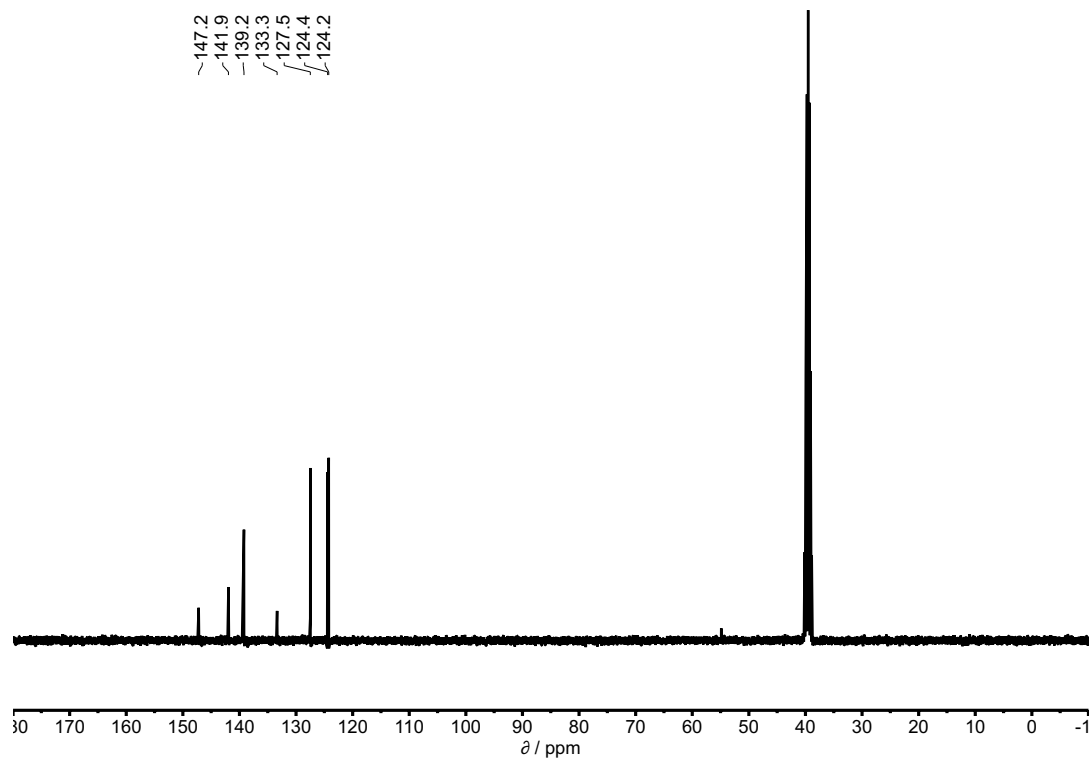
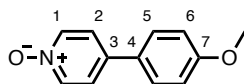


Figure S10. ^{13}C NMR spectrum (101 MHz, DMSO-d_6) of compound **9**.

4-(4-Methoxyphenyl)pyridine 1-oxide (10)



Off-white solid (67 mg, 0.33 mmol, 66 % yield)

M.p.: 113 – 116 °C.

¹H NMR (400 MHz, DMSO-*d*₆): δ_{H} = 8.21 (d, J = 7.2 Hz, 2H, H-1), 7.75 – 7.70 (m, 4H, H-2, H-5), 7.05 (d, J = 8.8 Hz, 2H, H-6), 3.81 (s, 3H, OCH₃).

¹³C NMR (101 MHz, DMSO-*d*₆): δ_{C} = 159.9 (C-7), 138.8 (C-1), 135.8 (C-3), 127.9 (C-4), 127.5 (C-5), 122.9 (C-2), 114.6 (C-6), 55.3 (OCH₃).

HRMS (ES+): calculated for C₁₂H₁₂NO₂ 202.0868 [M+H⁺], found 202.0874 [M+H⁺].

FT-IR (ATR): ν_{max} 3380, 1607, 1478, 1289, 1231, 1177, 1036, 826, 800, 552 cm⁻¹.

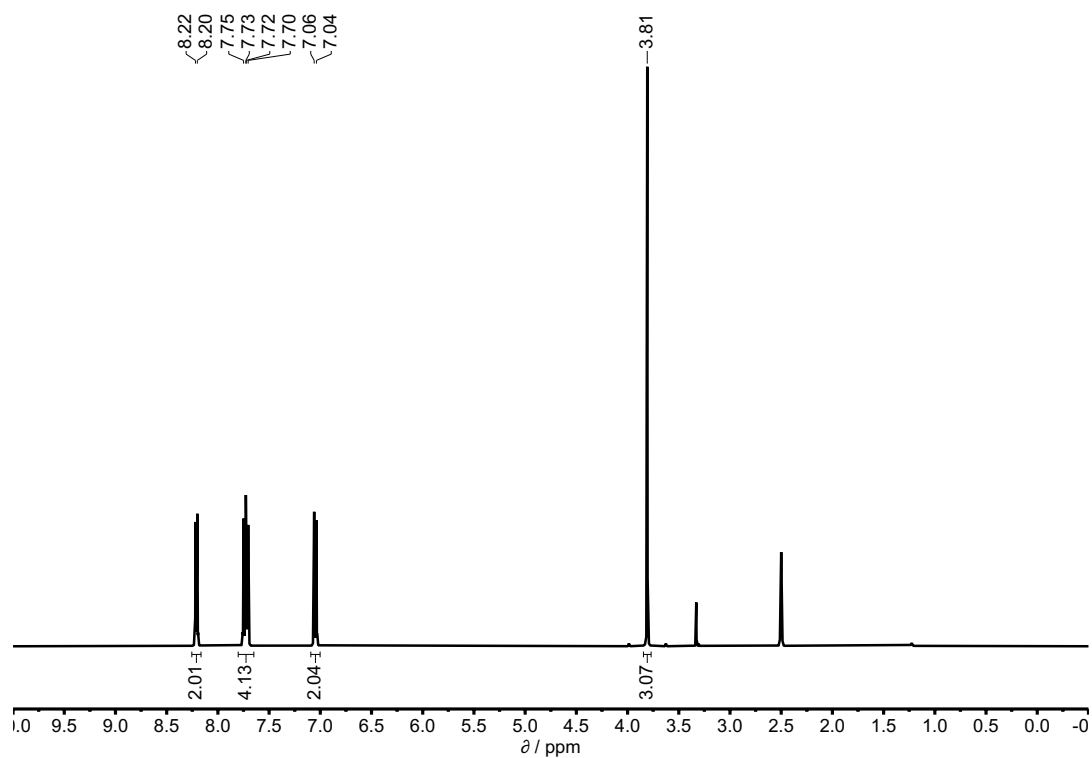


Figure S11. ^1H NMR spectrum (400 MHz, DMSO-d_6) of compound **10**.

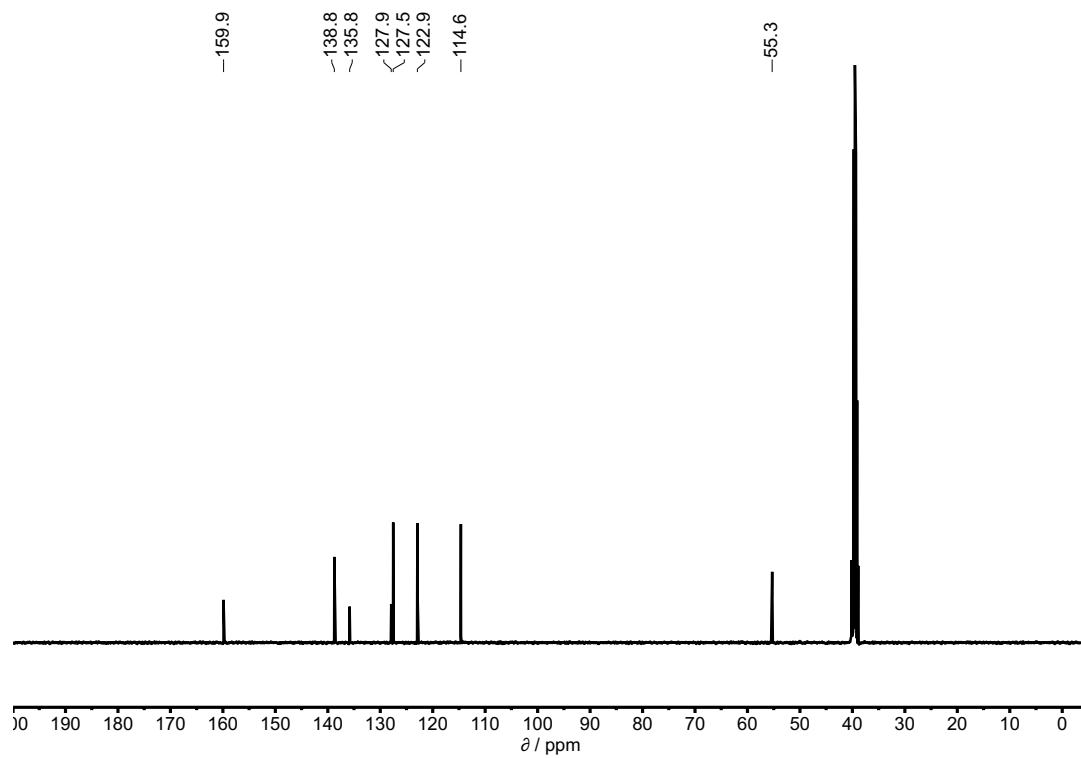
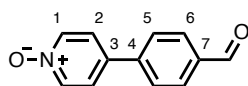


Figure S12. ^{13}C NMR spectrum (101 MHz, DMSO-d_6) of compound **10**.

4-(4-Formylphenyl)pyridine 1-oxide (11)



White solid (65 mg, 0.33 mmol, 65 % yield)

M.p.: 185 – 187 °C.

¹H NMR (400 MHz, DMSO-*d*₆): δ_{H} = 10.06 (s, 1H, CHO), 8.32 (d, J = 5.8 Hz, 2H, H-1), 8.02 (s, 4H, H-6, H-5), 7.88 (d, J = 5.8 Hz, 2H, H-2).

¹³C NMR (101 MHz, DMSO-*d*₆): δ_{C} = 192.7 (C=O), 141.1 (C-4), 139.1 (C-1), 135.8 (C-7), 134.4 (C-3), 130.2 (C-6), 126.9 (C-5), 124.2 (C-2).

HRMS (ES⁺): calculated for C₁₂H₁₀NO₂ 200.0712 [M+H⁺], found 200.0717 [M+H⁺].

FT-IR (ATR): ν_{max} 3326, 1697, 1605, 1479, 1252, 1184, 856, 831, 818, 714 cm⁻¹.

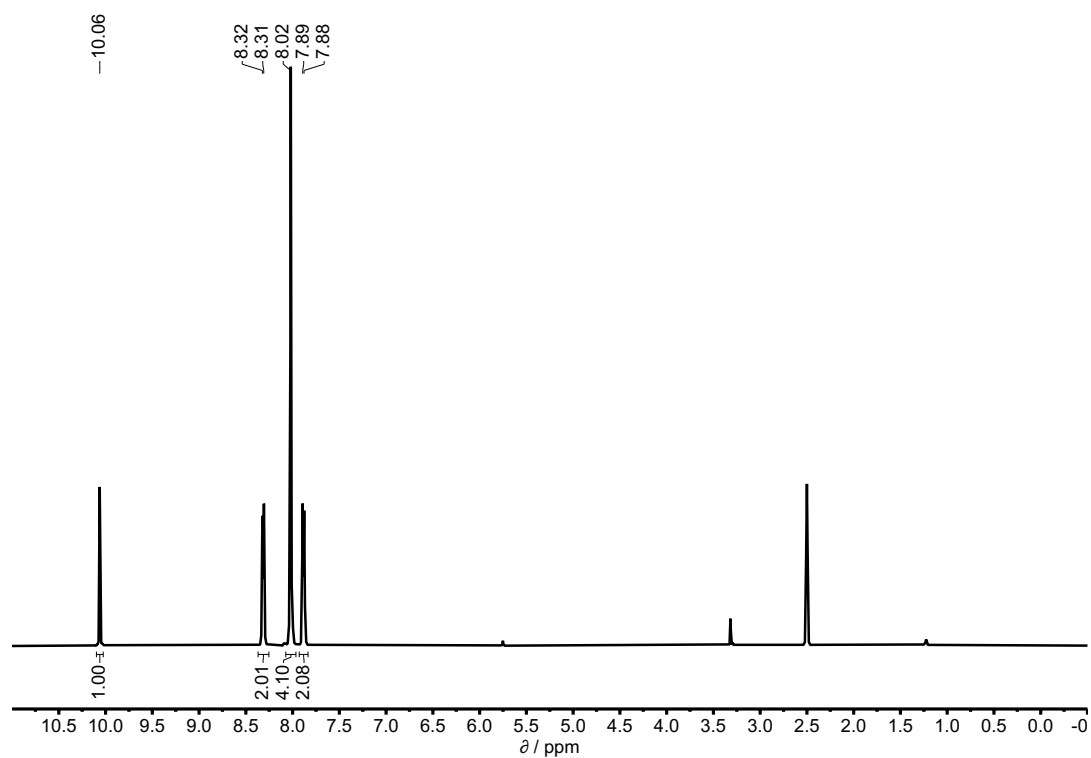


Figure S13. ^1H NMR spectrum (400 MHz, DMSO-d_6) of compound 11.

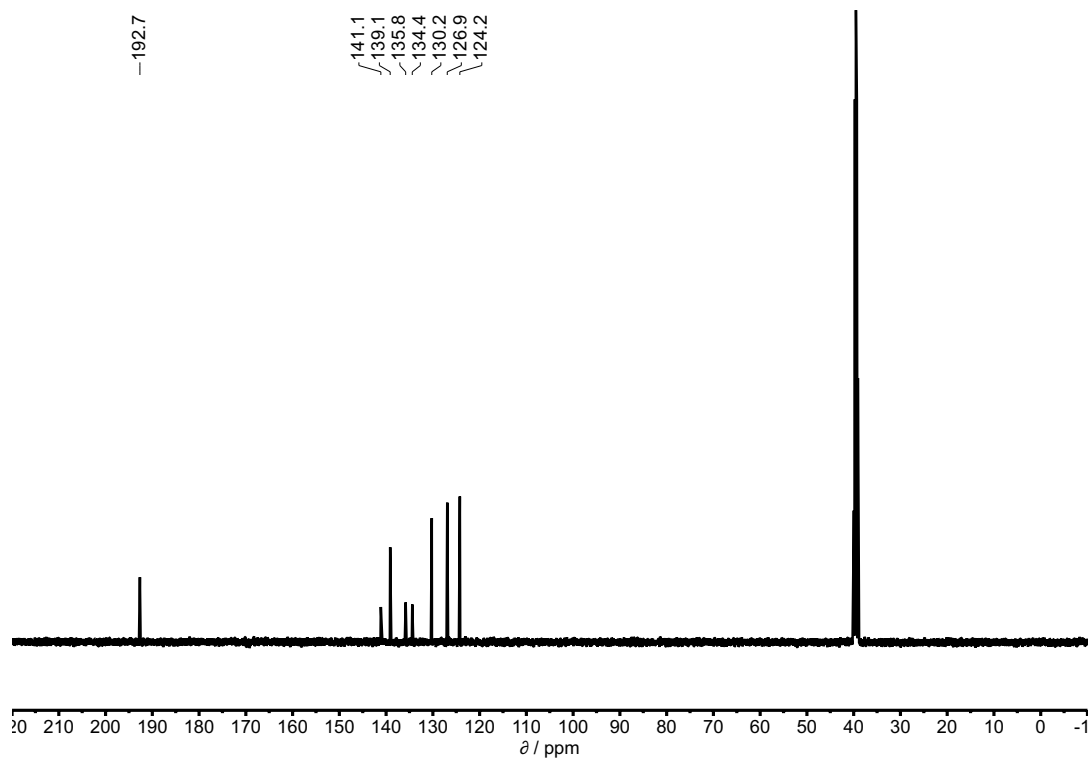
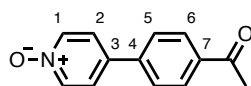


Figure S14. ^{13}C NMR spectrum (101 MHz, DMSO-d_6) of compound 11.

4-(4-Acetylphenyl)pyridine 1-oxide (12)



Off-white solid (85 mg, 0.40 mmol, 79 % yield)

M.p.: 161 – 163 °C.

¹H NMR (400 MHz, DMSO-*d*₆): δ_{H} = 8.30 (d, J = 7.4 Hz, 2H, H-1), 8.05 (d, J = 8.7 Hz, 2H, H-6), 7.94 (d, J = 8.7 Hz, 2H, H-5), 7.87 (d, J = 7.4 Hz, 2H, H-2), 2.62 (s, 3H, COCH₃).

¹³C NMR (101 MHz, DMSO-*d*₆): δ_{C} = 197.4 (C=O), 139.8 (C-4), 139.1 (C-1), 136.5 (C-7), 134.5 (C-3), 129.0 (C-6), 126.4 (C-5), 124.1 (C-2), 26.8 (COCH₃).

HRMS (ES⁺): calculated for C₁₃H₁₂NO₂ 214.0868 [M+H⁺], found 214.0872 [M+H⁺].

FT-IR (ATR): ν_{max} 3335, 1688, 1605, 1480, 1268, 1245, 1196, 850, 820, 657 cm⁻¹.

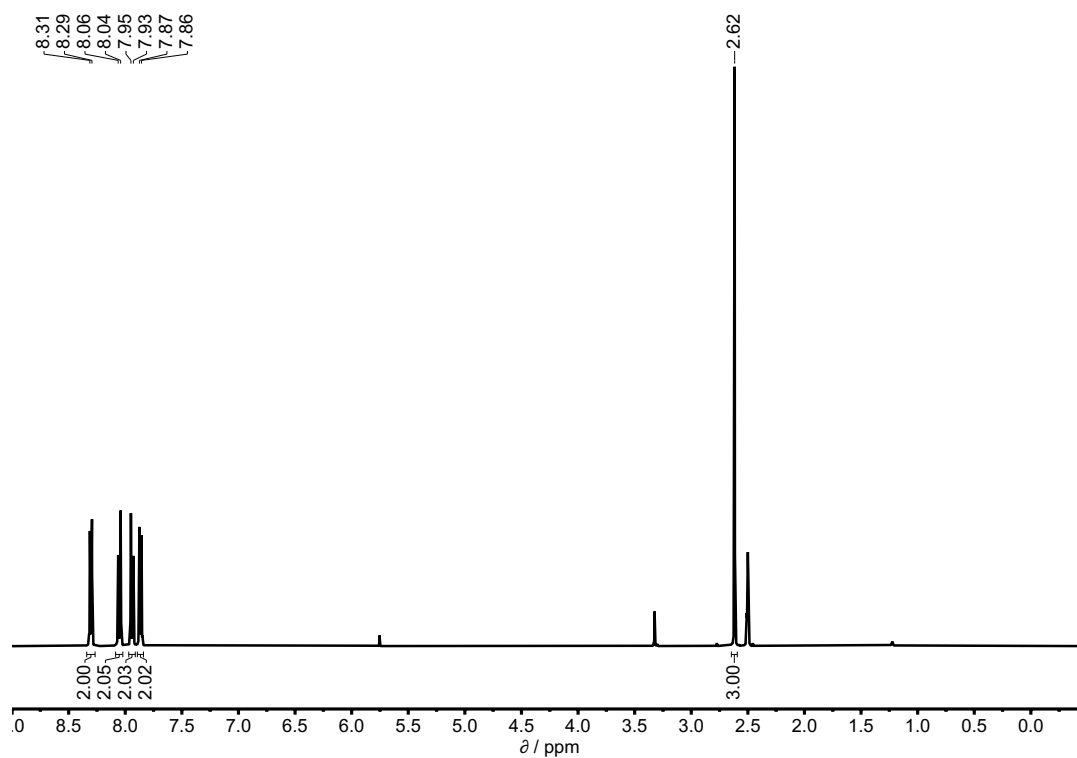


Figure S15. ^1H NMR spectrum (400 MHz, DMSO-d_6) of compound 12.

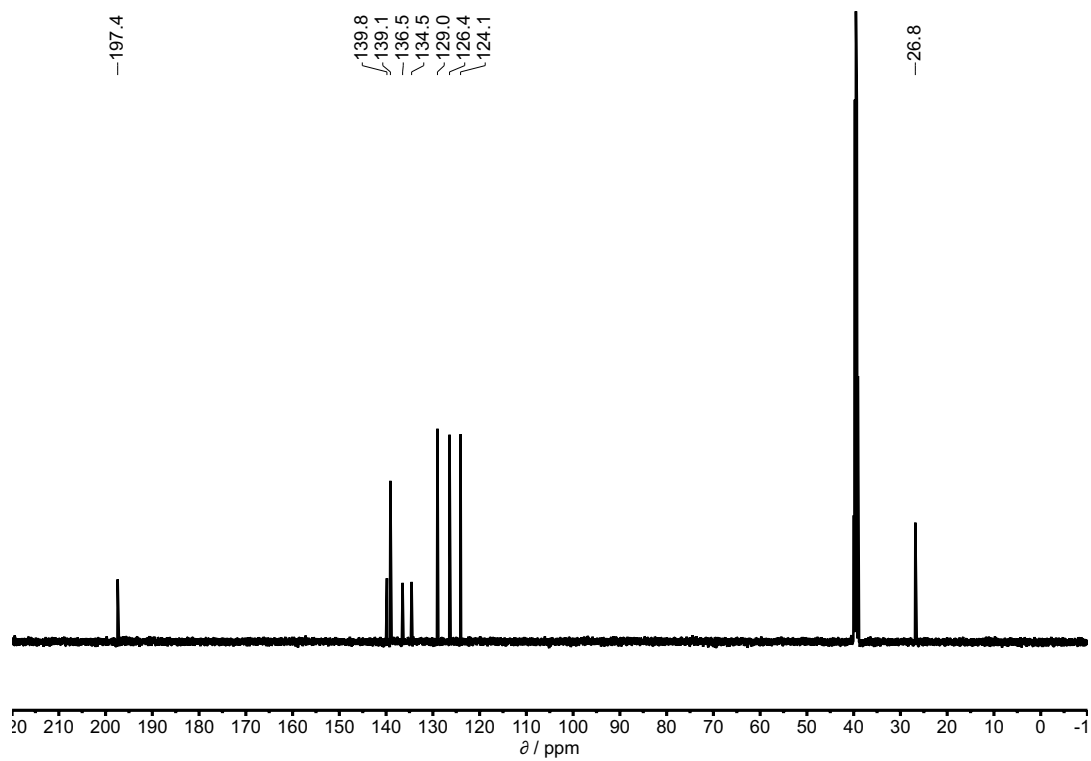
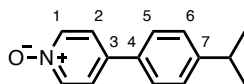


Figure S16. ^{13}C NMR spectrum (101 MHz, DMSO-d_6) of compound 12.

4-(4-Isopropylphenyl)pyridine 1-oxide (13)



Pink solid (74 mg, 0.35 mmol, 69 % yield)

M.p.: 143 – 145 °C.

¹H NMR (400 MHz, DMSO-*d*₆): δ_{H} = 8.24 (d, J = 7.3 Hz, 2H, H-1), 7.74 (d, J = 7.3 Hz, 2H, H-2), 7.69 (d, J = 8.5 Hz, 2H, H-5), 7.36 (d, J = 8.2 Hz, 2H, H-6), 2.93 (p, J = 6.9 Hz, 1H, CH), 1.22 (d, J = 6.9 Hz, 6H, CH₃).

¹³C NMR (101 MHz, DMSO-*d*₆): δ_{C} = 149.2 (C-7), 138.8 (C-1), 136.1 (C-3), 133.2 (C-4), 127.2 (C-6), 126.2 (C-5), 123.4 (C-2), 33.1 (CH), 23.7 (CH₃).

HRMS (ES⁺): calculated for C₁₄H₁₆NO 214.1232 [M+H⁺], found 214.1240 [M+H⁺].

FT-IR (ATR): ν_{max} 3360, 2959, 1476, 1409, 1237, 1179, 1025, 847, 823, 770, 713, 665 cm⁻¹.

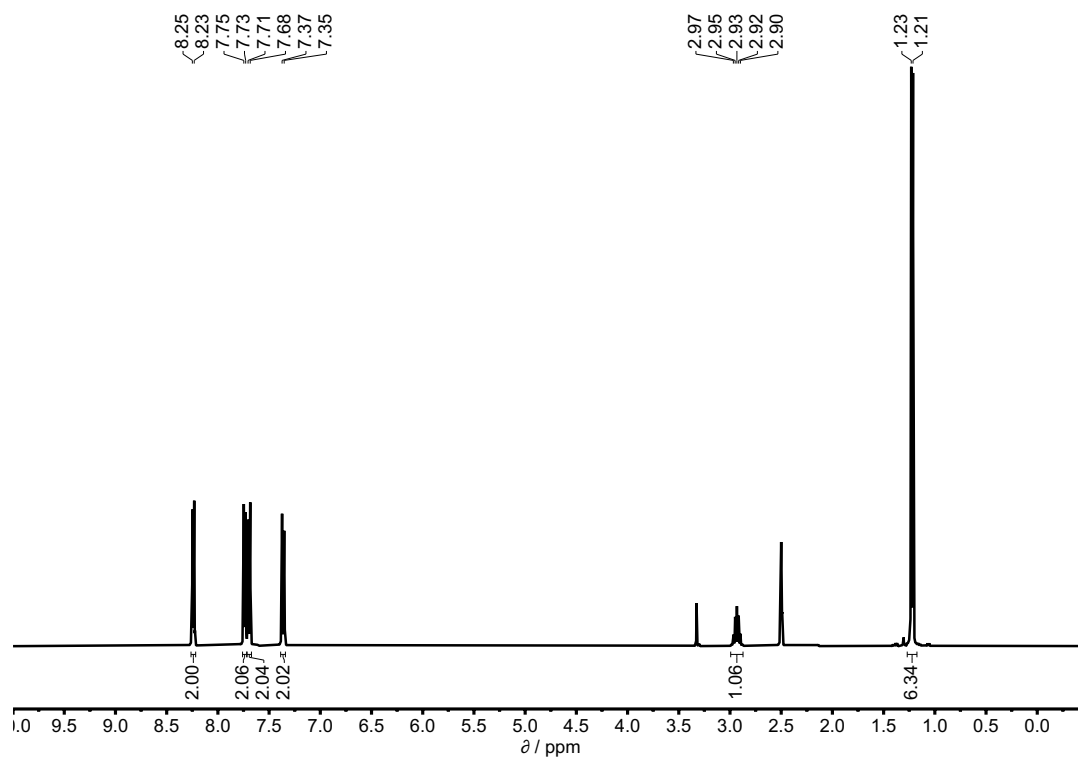


Figure S17. ^1H NMR spectrum (400 MHz, DMSO-d_6) of compound **13**.

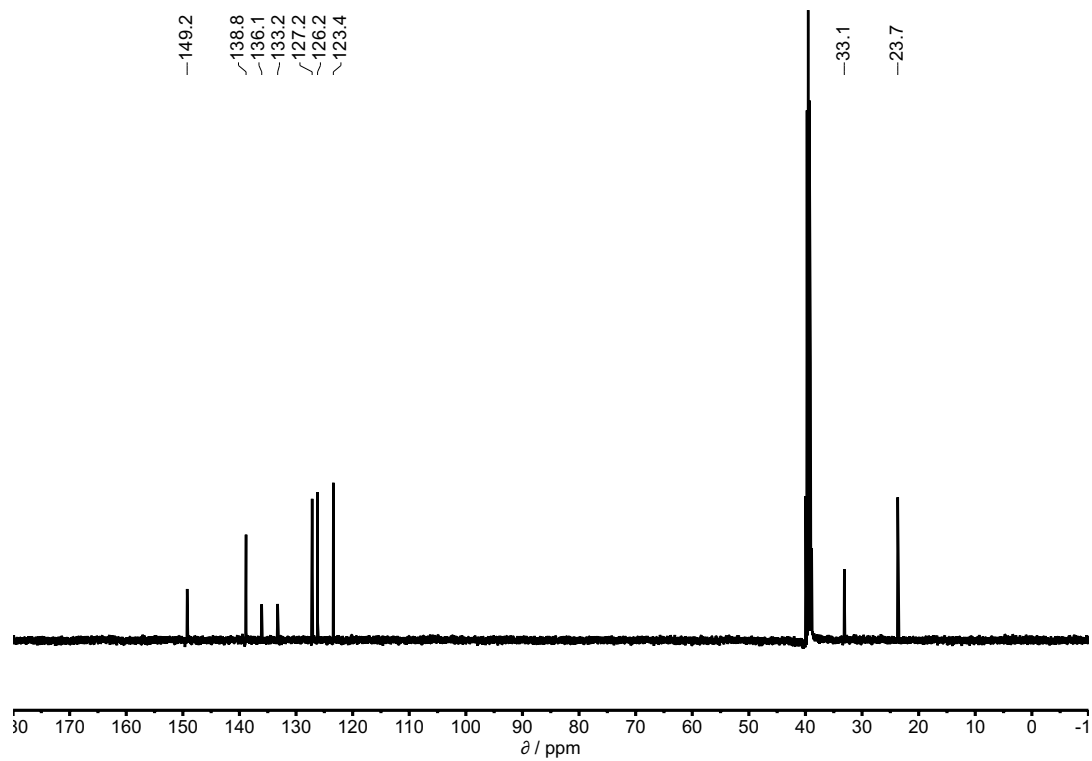
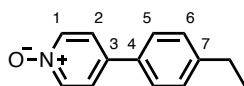


Figure S18. ^{13}C NMR spectrum (101 MHz, DMSO-d_6) of compound **13**.

4-(4-Ethylphenyl)pyridine 1-oxide (14)



Brown solid (73 mg, 0.37 mmol, 73 % yield)

M.p.: 116 – 118 °C.

¹H NMR (400 MHz, DMSO-*d*₆): δ_{H} = 8.24 (d, J = 5.6 Hz, 2H, H-1), 7.74 (d, J = 5.6 Hz, 2H, H-2), 7.69 (d, J = 6.7 Hz, 2H, H-5), 7.33 (d, J = 7.0 Hz, 2H, H-6), 2.65 (q, J = 7.6 Hz, 2H, CH₂), 1.20 (t, J = 7.6 Hz, 3H, CH₃).

¹³C NMR (101 MHz, DMSO-*d*₆): δ_{C} = 144.7 (C-7), 138.8 (C-1), 136.0 (C-3), 133.1 (C-4), 128.6 (C-6), 126.1 (C-5), 123.4 (C-2), 27.8 (CH₂), 15.4 (CH₃).

HRMS (ES⁺): calculated for C₁₃H₁₄NO 200.1075 [M+H⁺], found 200.1081 [M+H⁺].

FT-IR (ATR): ν_{max} 3379, 2964, 1474, 1450, 1408, 1234, 1176, 1029, 848, 822, 784, 711, 672, 637 cm⁻¹.

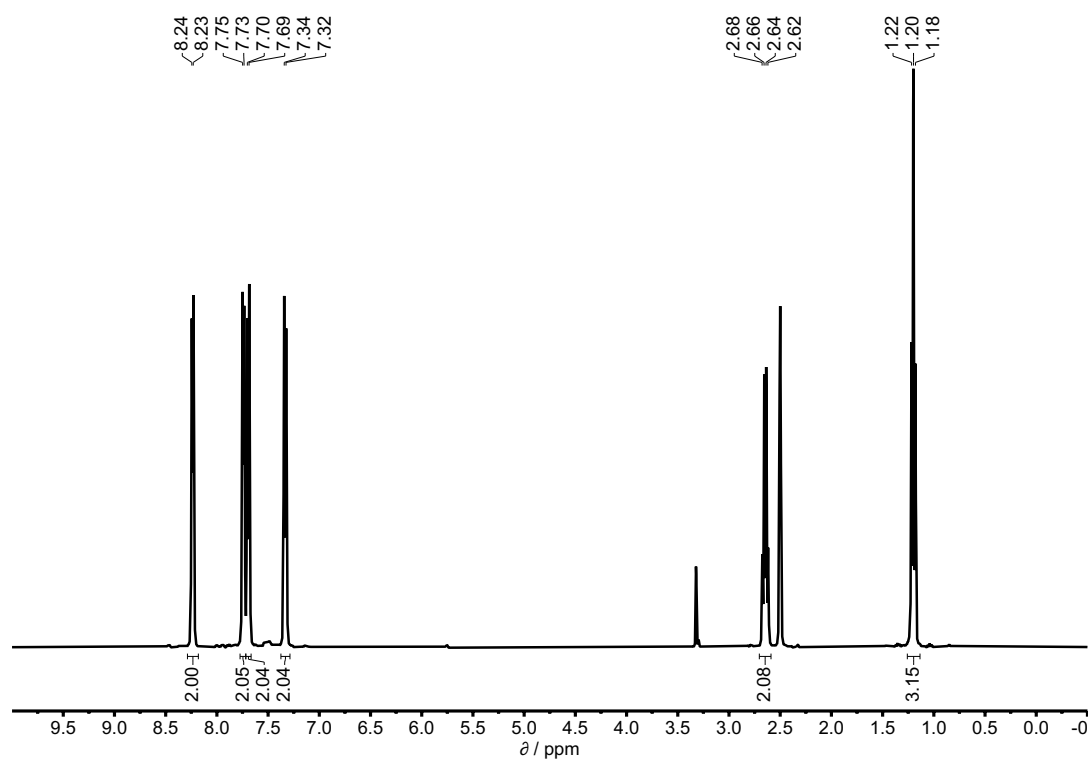


Figure S19. ^1H NMR spectrum (400 MHz, DMSO-d_6) of compound 14.

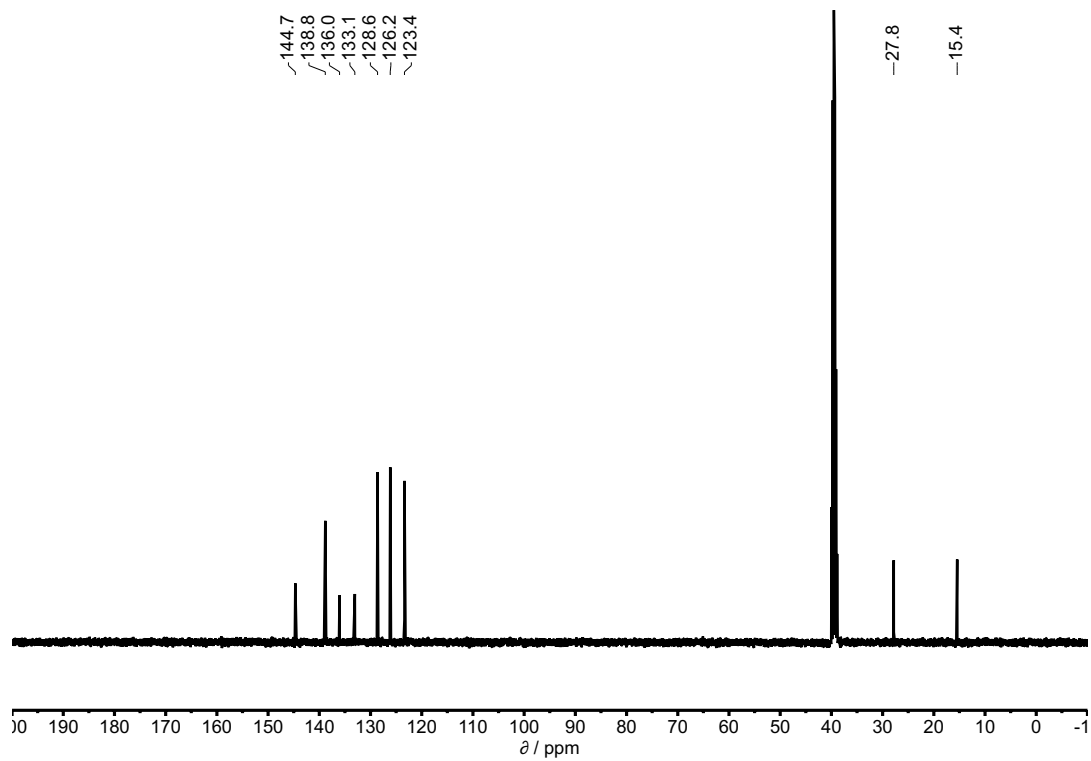
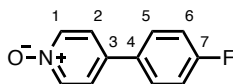


Figure S20. ^{13}C NMR spectrum (101 MHz, DMSO-d_6) of compound 14.

4-(4-Fluorophenyl)pyridine 1-oxide (15)



White solid (13 mg, 0.07 mmol, 14 % yield)

M.p.: 157 – 159 °C.

¹H NMR (400 MHz, DMSO-*d*₆): δ_H = 8.26 (d, *J* = 5.3 Hz, 2H, H-1), 7.84 (t, *J* = 6.3 Hz, 2H, H-5), 7.76 (d, *J* = 5.5 Hz, 2H, H-2), 7.33 (t, *J* = 8.8 Hz, 2H, H-6).

¹³C NMR (101 MHz, DMSO-*d*₆): δ_C = 163.7 (C-7), 138.8 (C-1), 134.9 (C-3), 132.1 (C-4), 128.4 (C-5), 123.6 (C-2), 116.1 (C-6).

HRMS (ES⁺): calculated for C₁₁H₉FNO 190.0668 [M+H⁺], found 190.0673 [M+H⁺].

FT-IR (ATR): ν_{max} 3112, 3039, 1600, 1518, 1475, 1450, 1405, 1247, 1224, 1179, 1162, 1024, 814 cm⁻¹.

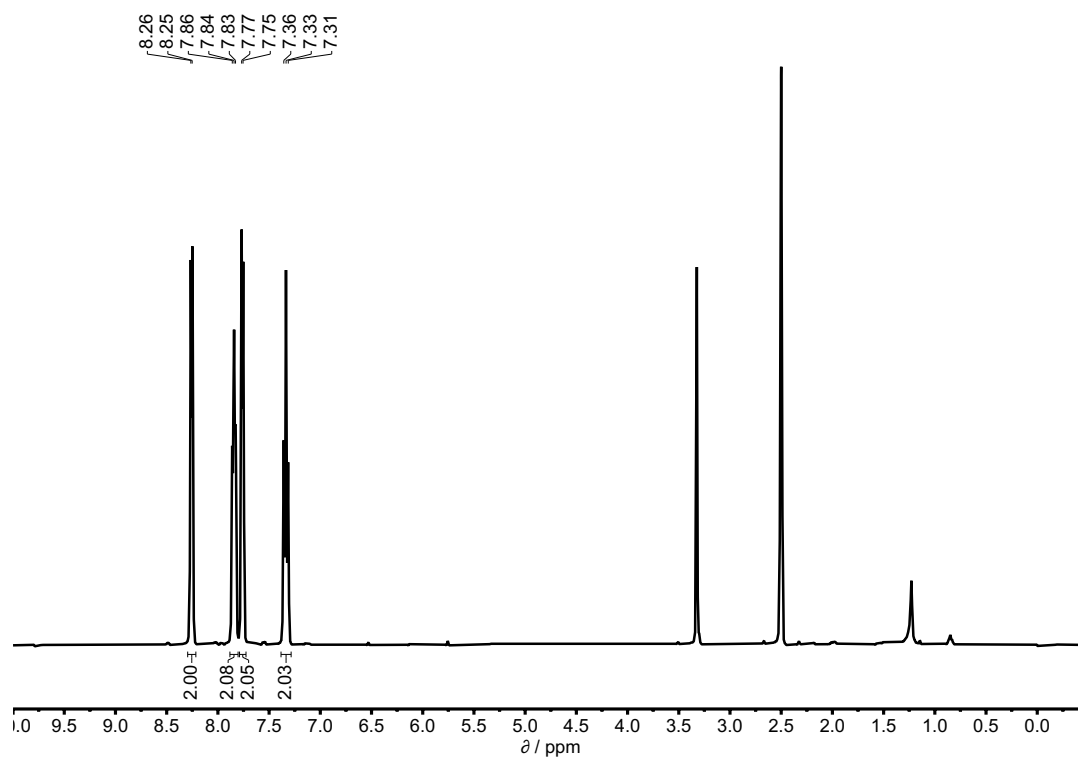


Figure S21. ^1H NMR spectrum (400 MHz, DMSO-d_6) of compound 15.

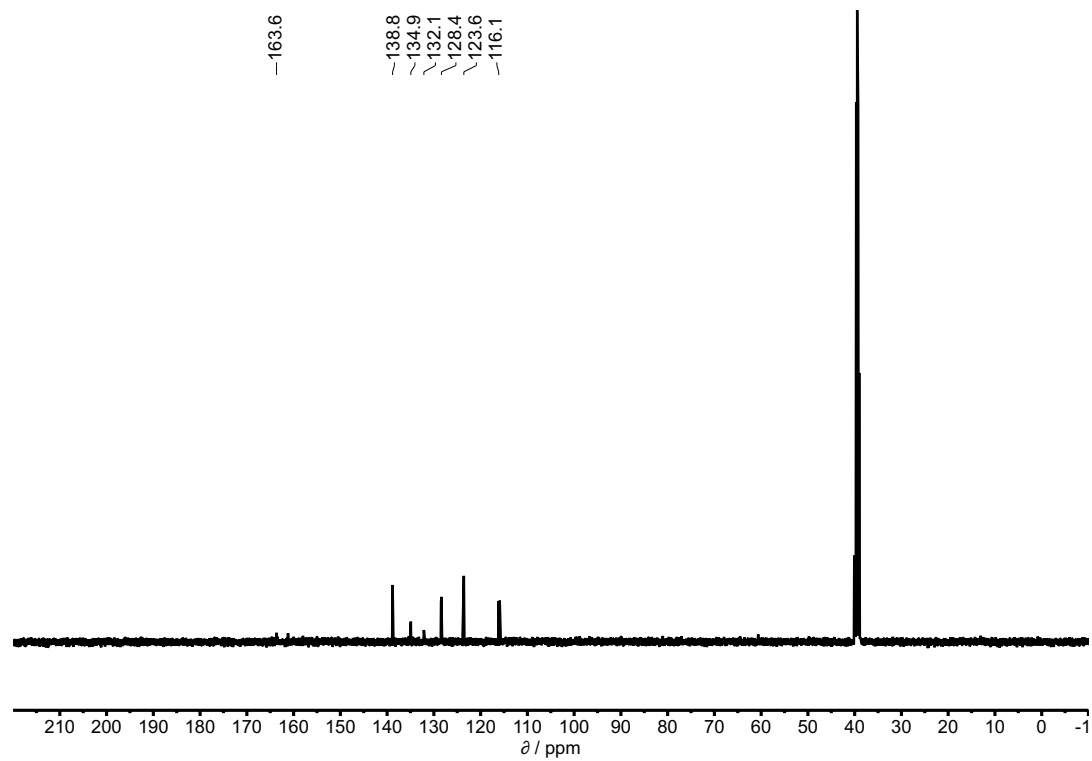
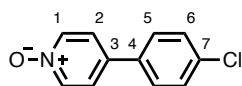


Figure S22. ^{13}C NMR spectrum (101 MHz, DMSO-d_6) of compound 15.

4-(4-Chlorophenyl)pyridine 1-oxide (16)



White solid (42 mg, 0.20 mmol, 41 % yield)

M.p.: 166 – 168 °C

¹H NMR (400 MHz, DMSO-*d*₆): δ_H = 8.27 (d, J = 7.3 Hz, 2H, H-1), 7.83 – 7.77 (m, 4H, H-2, H-5), 7.55 (d, J = 8.7 Hz, 2H, H-6).

¹³C NMR (101 MHz, DMSO-*d*₆): δ_C = 139.0 (C-1), 134.6 (C-4), 134.5 (C-3), 133.6 (C-7), 129.2 (C-6), 128.0 (C-5), 123.7 (C-2).

HRMS (ES⁺): calculated for C₁₁H₉ClNO 206.0373 [M+H⁺], found 206.0382 [M+H⁺].

FT-IR (ATR): ν_{max} 3387, 3110, 1472, 1397, 1244, 1180, 1101, 1024, 816, 753 cm⁻¹.

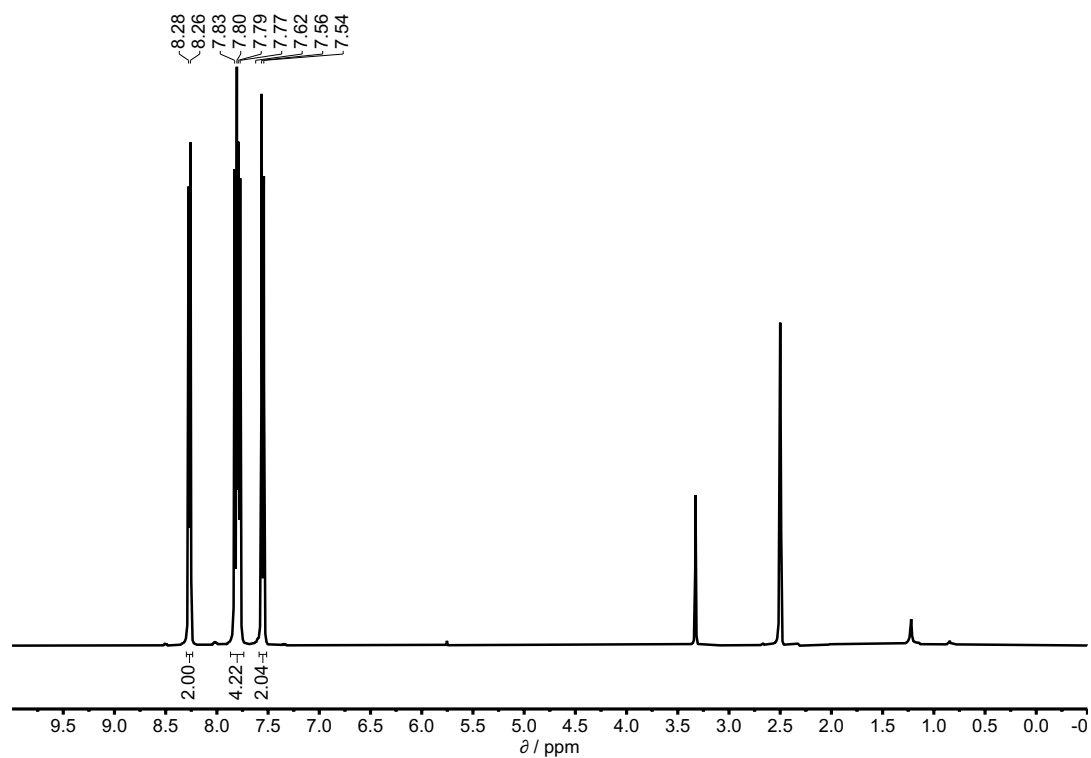


Figure S23. ^1H NMR spectrum (400 MHz, DMSO-d_6) of compound 16.

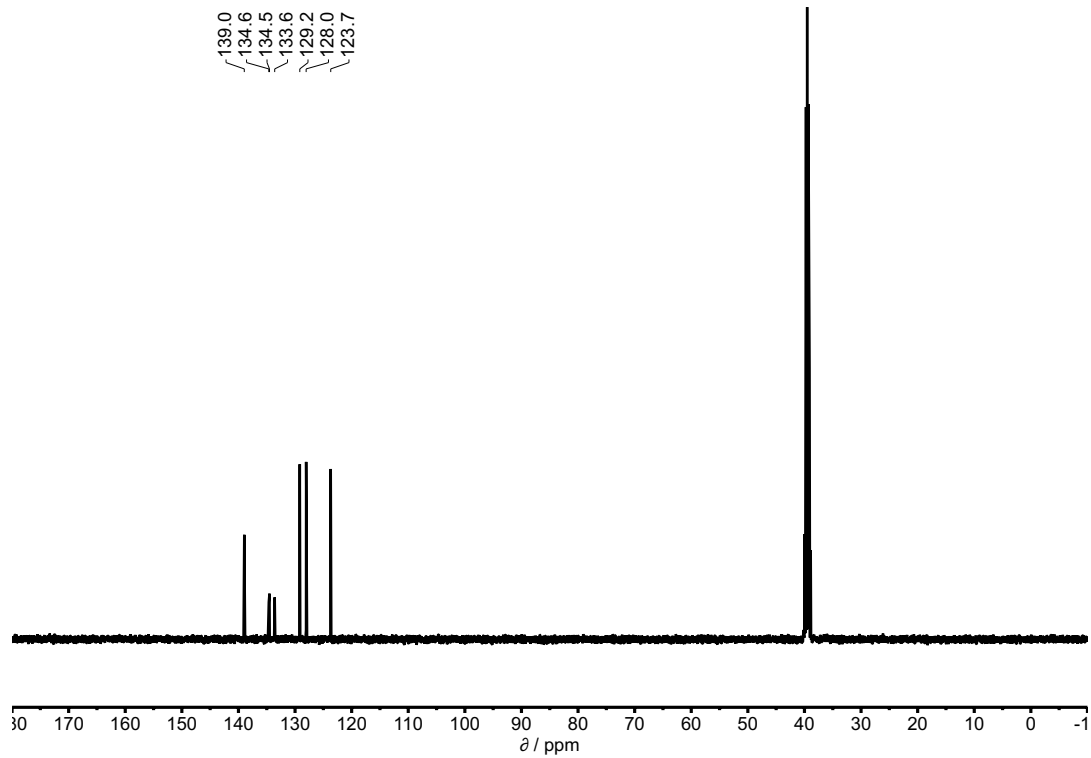
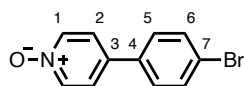


Figure S24. ^{13}C NMR spectrum (101 MHz, DMSO-d_6) of compound 16.

4-(4-Vromophenyl)pyridine 1-oxide (17)



Off-white solid (35 mg, 0.14 mmol, 28 % yield)

M.p.: 162 – 164 °C.

¹H NMR (400 MHz, DMSO-*d*₆): $\delta_{\text{H}} = 8.27$ (d, $J = 7.3$ Hz, 2H, H-1), 7.80 – 7.75 (m, 4H, H-2, H-5), 7.70 (d, $J = 8.7$ Hz, 2H, H-6).

¹³C NMR (101 MHz, DMSO-*d*₆): $\delta_{\text{C}} = 139.0$ (C-1), 134.9 (C-4), 134.7 (C-3), 132.1 (C-6), 128.3 (C-5), 123.7 (C-2), 122.3 (C-7).

HRMS (ES⁺): calculated for C₁₁H₉BrNO 249.9868 [M+H⁺], found 249.9871 [M+H⁺].

FT-IR (ATR): ν_{max} 3387, 3111, 1472, 1448, 1393, 1245, 1195, 1178, 1076, 1022, 1006, 849, 816, 741, 613 cm⁻¹.

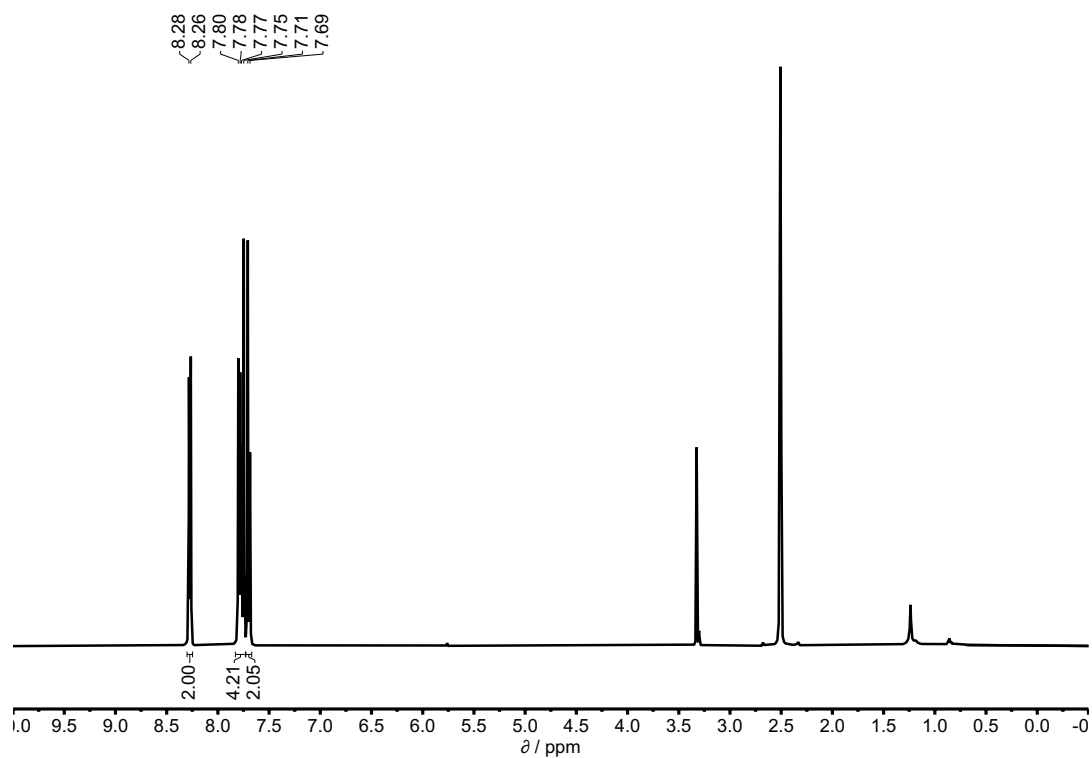


Figure S25. ^1H NMR spectrum (400 MHz, DMSO-d_6) of compound 17.

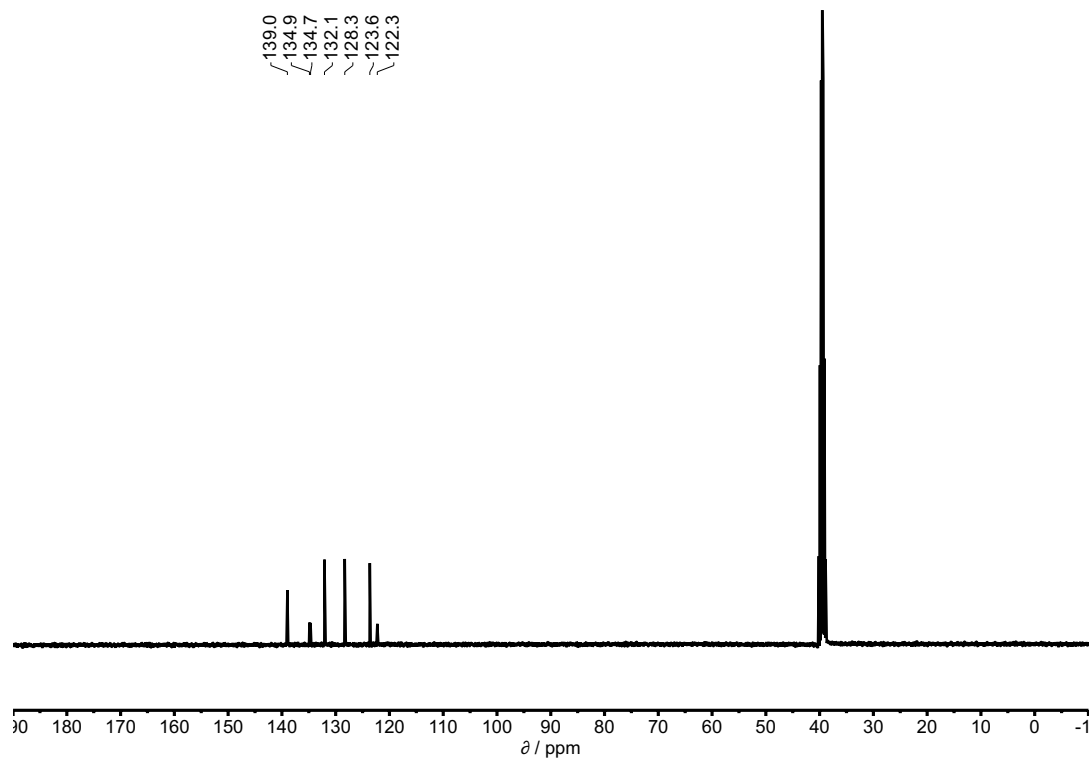


Figure S26. ^{13}C NMR spectrum (101 MHz, DMSO-d_6) of compound 17.

3. Isothermal titration calorimetry (ITC) experiments

In a typical ITC experiment, the host (**1-4**) was dissolved in HPLC grade water or chloroform with a concentration 30-40 times the expected dissociation constant, and the solution was loaded into the sample cell of the microcalorimeter. A 7-10 times more concentrated solution of guest (**5-17** and **PNO**) was loaded into the injection syringe. The number of injections was 35, and the volume of the injections was 8 μL . The thermogram peaks were integrated and thermodynamic parameters were calculated using the MicroCal PEAQ-ITC Analysis Software which uses the least-squares minimisation to obtain globally minimised parameters. In all cases the data fitted well to a simple 1:1 binding model.

3.1. Octapyridinium-super-aryl-extended calix[4]pyrrole **1**

3.1.1. Complex C of the DMC

The C-value for this experiment is 141, so the data could be used to determine both K and ΔH° .

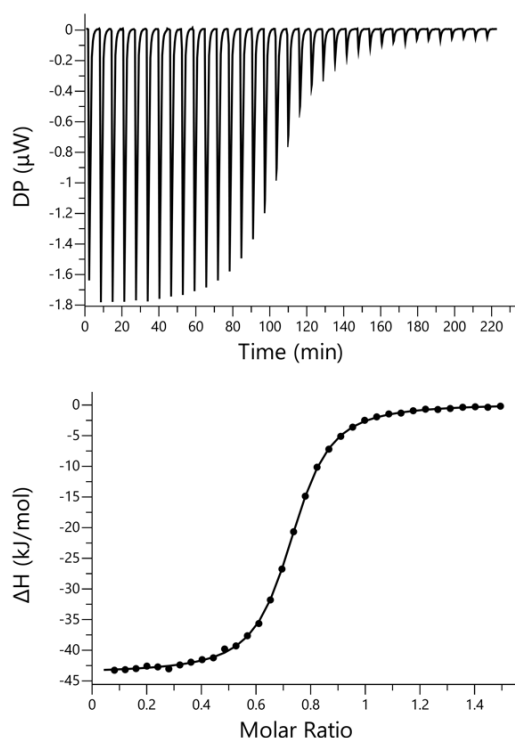


Figure S27. ITC data for titration of **PNO** (0.28 mM) into **1** (0.04 mM) in water at 298 K. The raw data for each injection is shown (differential power, DP), along with the least-squares-fit of the enthalpy change per mole of guest (ΔH) to a 1:1 binding isotherm.

3.1.2. Complex A of the DMC

The C-values for these experiments are in the range $10^5 - 10^8$, so the data could only be used to determine ΔH° . The values of K were determined separately by NMR competition experiments.

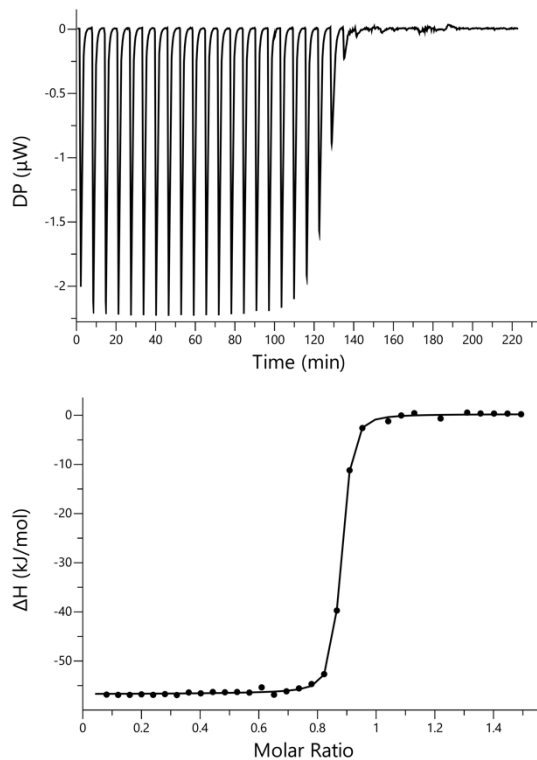


Figure S28. ITC data for titration of **5** (0.28 mM) into **1** (0.04 mM) in water at 298 K. The raw data for each injection is shown (differential power, DP), along with the least-squares-fit of the enthalpy change per mole of guest (ΔH) to a 1:1 binding isotherm.

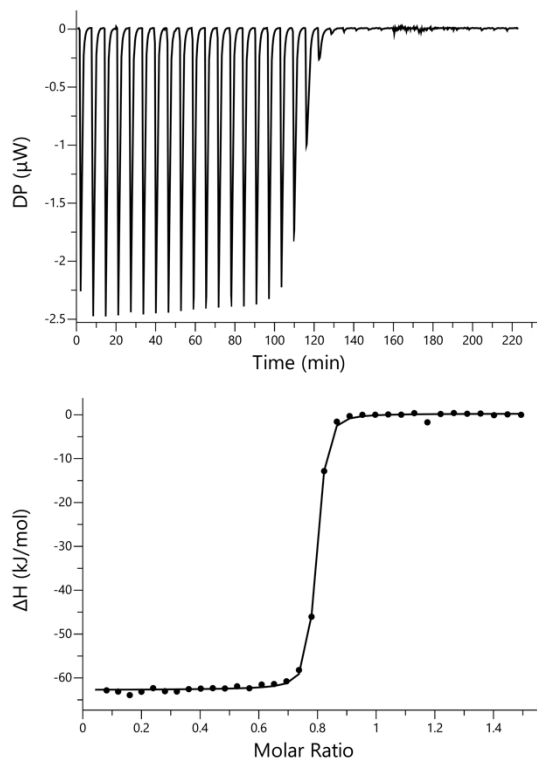


Figure S29. ITC data for titration of **6** (0.28 mM) into **1** (0.04 mM) in water at 298 K. The raw data for each injection is shown (differential power, DP), along with the least-squares-fit of the enthalpy change per mole of guest (ΔH) to a 1:1 binding isotherm.

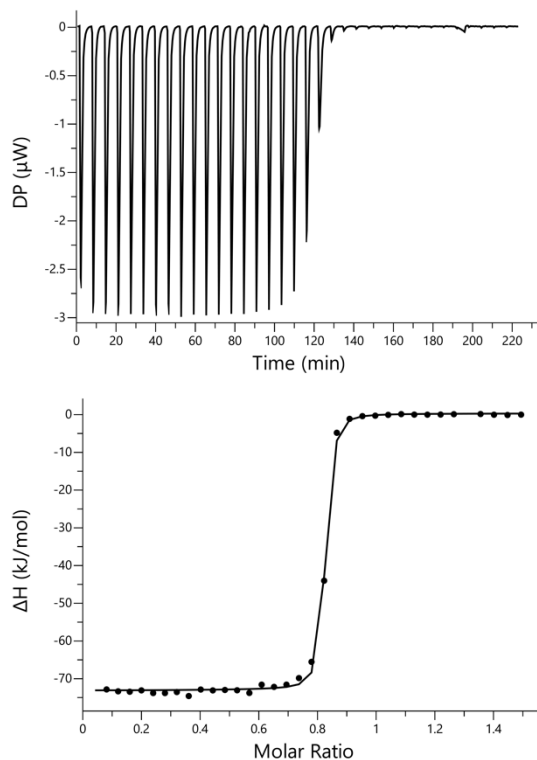


Figure S30. ITC data for titration of **7** (0.28 mM) into **1** (0.04 mM) in water at 298 K. The raw data for each injection is shown (differential power, DP), along with the least-squares-fit of the enthalpy change per mole of guest (ΔH) to a 1:1 binding isotherm.

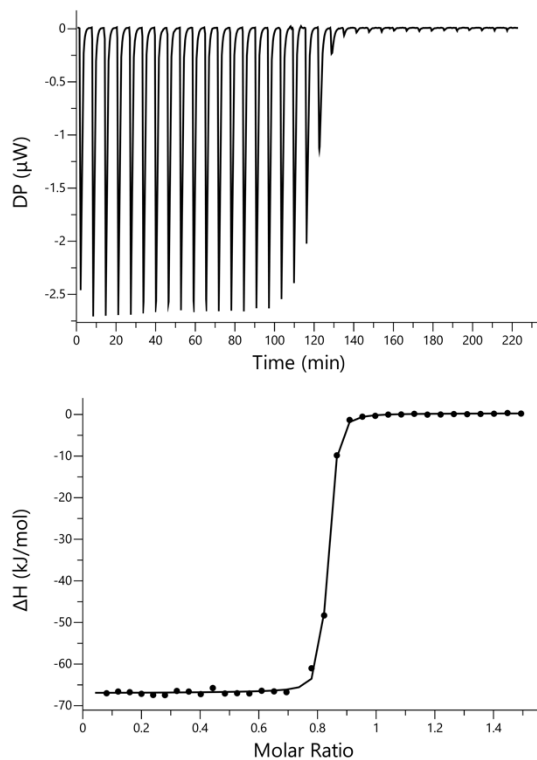


Figure S31. ITC data for titration of **8** (0.28 mM) into **1** (0.04 mM) in water at 298 K. The raw data for each injection is shown (differential power, DP), along with the least-squares-fit of the enthalpy change per mole of guest (ΔH) to a 1:1 binding isotherm.

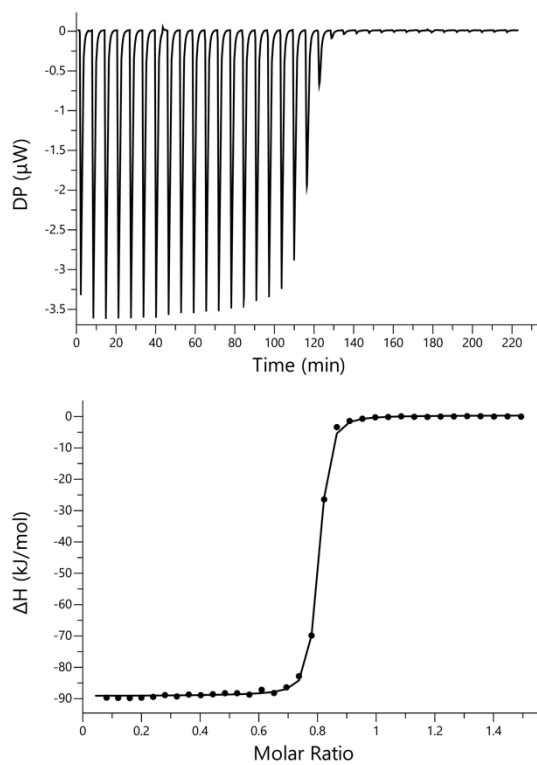


Figure S32. ITC data for titration of **9** (0.28 mM) into **1** (0.04 mM) in water at 298 K. The raw data for each injection is shown (differential power, DP), along with the least-squares-fit of the enthalpy change per mole of guest (ΔH) to a 1:1 binding isotherm.

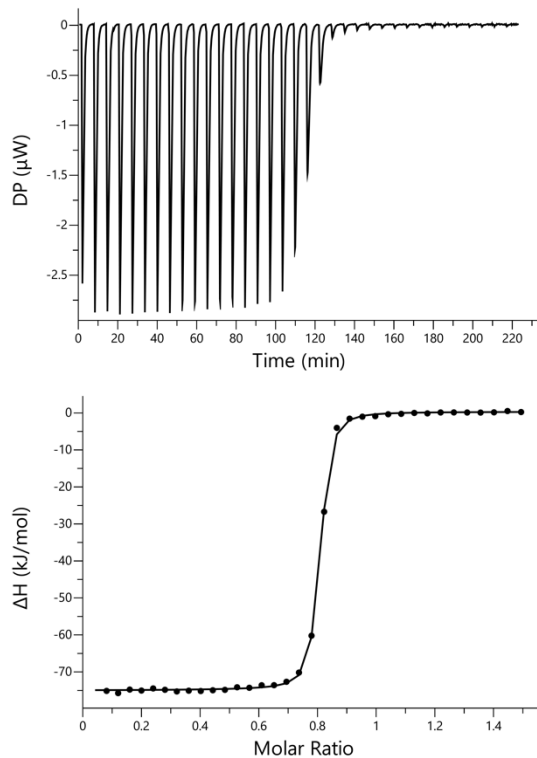


Figure S33. ITC data for titration of **10** (0.28 mM) into **1** (0.04 mM) in water at 298 K. The raw data for each injection is shown (differential power, DP), along with the least-squares-fit of the enthalpy change per mole of guest (ΔH) to a 1:1 binding isotherm.

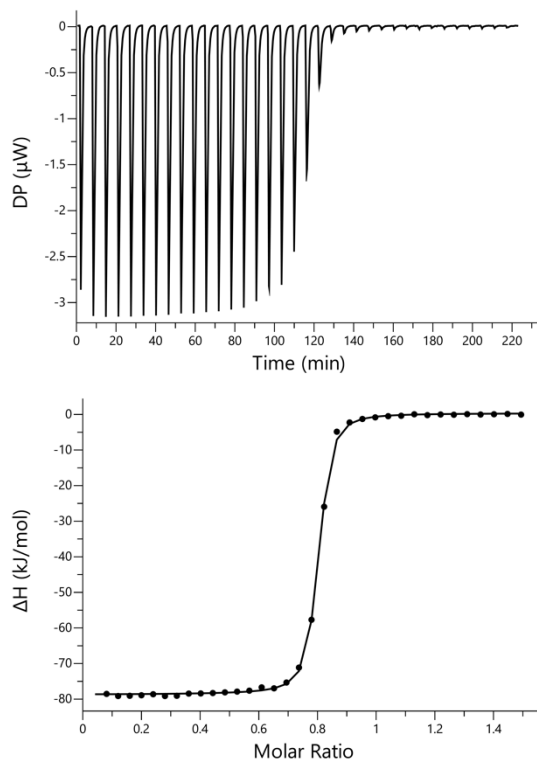


Figure S34. ITC data for titration of **11** (0.28 mM) into **1** (0.04 mM) in water at 298 K. The raw data for each injection is shown (differential power, DP), along with the least-squares-fit of the enthalpy change per mole of guest (ΔH) to a 1:1 binding isotherm.

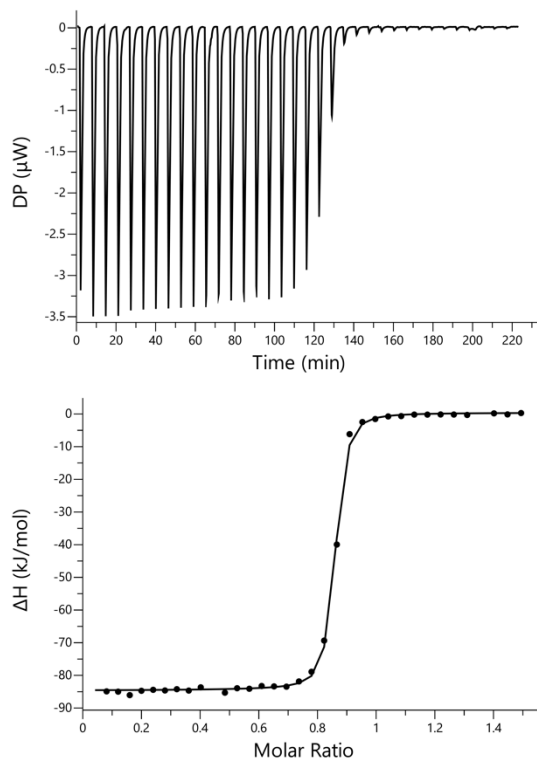


Figure S35. ITC data for titration of **12** (0.28 mM) into **1** (0.04 mM) in water at 298 K. The raw data for each injection is shown (differential power, DP), along with the least-squares-fit of the enthalpy change per mole of guest (ΔH) to a 1:1 binding isotherm.

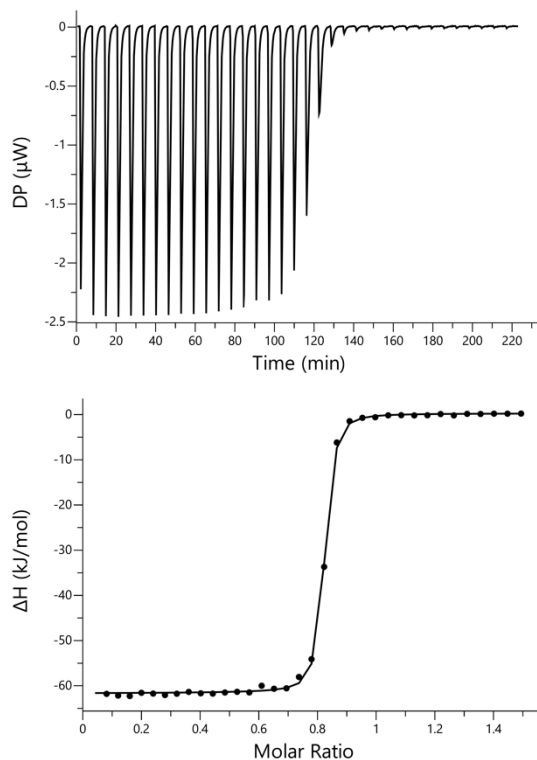


Figure S36. ITC data for titration of **13** (0.28 mM) into **1** (0.04 mM) in water at 298 K. The raw data for each injection is shown (differential power, DP), along with the least-squares-fit of the enthalpy change per mole of guest (ΔH) to a 1:1 binding isotherm.

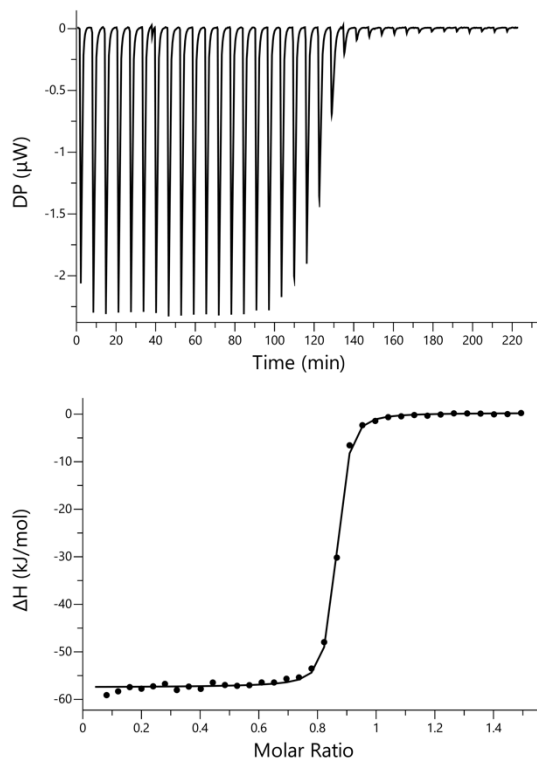


Figure S37. ITC data for titration of **14** (0.28 mM) into **1** (0.04 mM) in water at 298 K. The raw data for each injection is shown (differential power, DP), along with the least-squares-fit of the enthalpy change per mole of guest (ΔH) to a 1:1 binding isotherm.

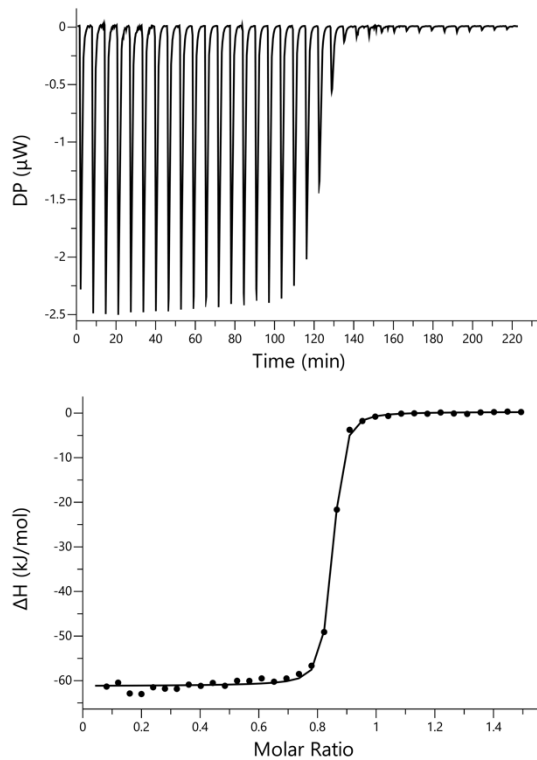


Figure S38. ITC data for titration of **15** (0.28 mM) into **1** (0.04 mM) in water at 298 K. The raw data for each injection is shown (differential power, DP), along with the least-squares-fit of the enthalpy change per mole of guest (ΔH) to a 1:1 binding isotherm.

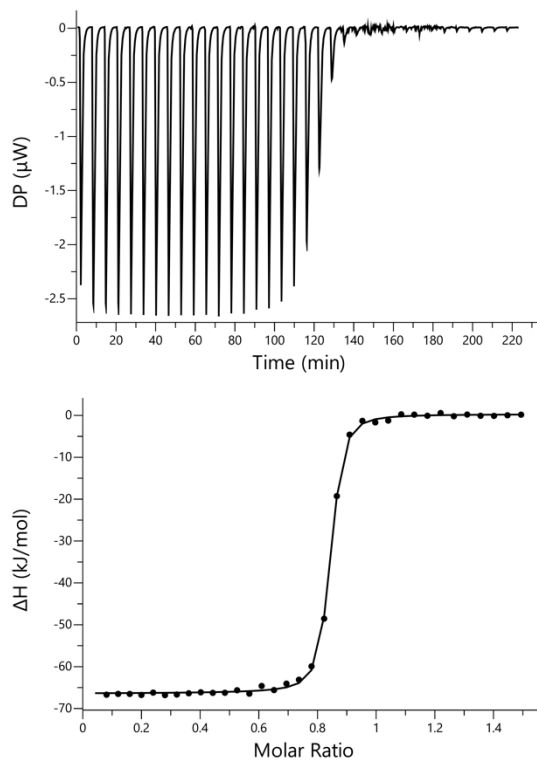


Figure S39. ITC data for titration of **16** (0.28 mM) into **1** (0.04 mM) in water at 298 K. The raw data for each injection is shown (differential power, DP), along with the least-squares-fit of the enthalpy change per mole of guest (ΔH) to a 1:1 binding isotherm.

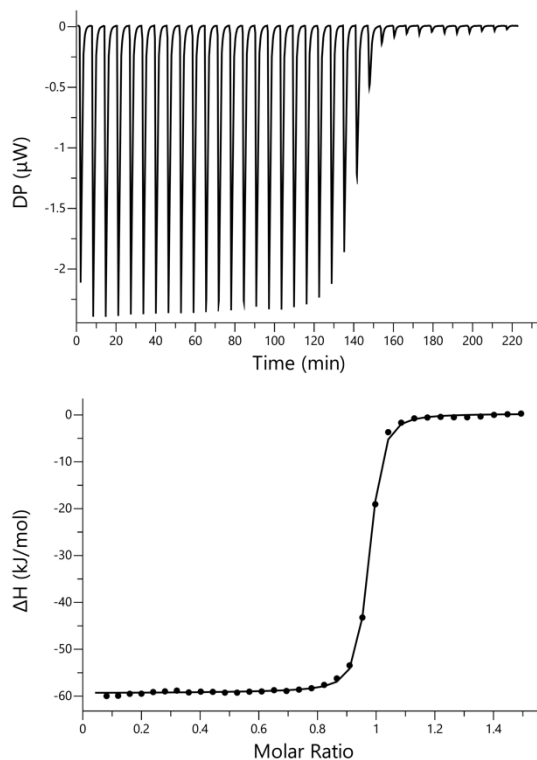


Figure S40. ITC data for titration of **17** (0.28 mM) into **1** (0.04 mM) in water at 298 K. The raw data for each injection is shown (differential power, DP), along with the least-squares-fit of the enthalpy change per mole of guest (ΔH) to a 1:1 binding isotherm.

3.2. Tetrapyridinium-aryl-extended calix[4]pyrrole **3**

3.2.1. Complex D of the DMC

The C-value for this experiment is 13, so the data could be used to determine both K and ΔH° .

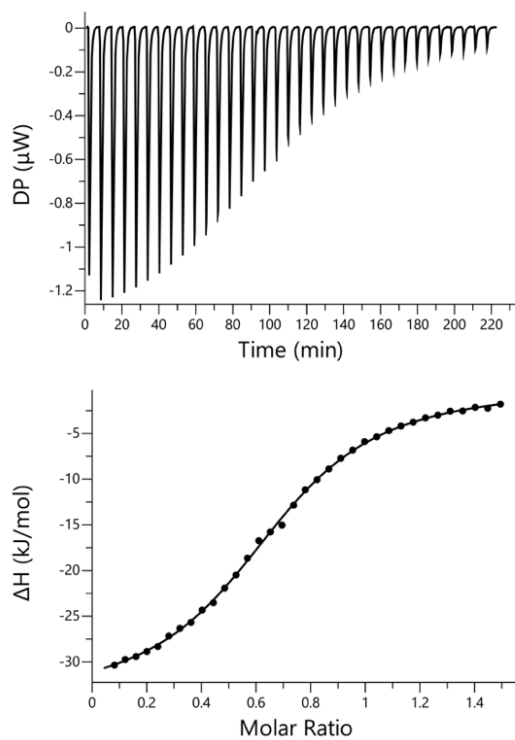


Figure S41. ITC data for titration of **PNO** (0.28 mM) into **3** (0.04 mM) in water at 298 K. The raw data for each injection is shown (differential power, DP), along with the least-squares-fit of the enthalpy change per mole of guest (ΔH) to a 1:1 binding isotherm.

3.2.2. Complex B of the DMC

The C-values for these experiments are in the range 37 – 54, so the data could be used to determine both K and ΔH° .

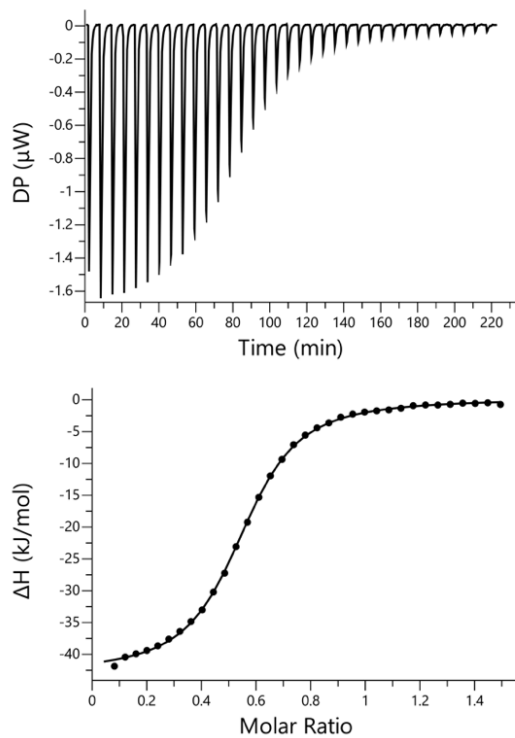


Figure S42. ITC data for titration of **5** (0.28 mM) into **3** (0.04 mM) in water at 298 K. The raw data for each injection is shown (differential power, DP), along with the least-squares-fit of the enthalpy change per mole of guest (ΔH) to a 1:1 binding isotherm.

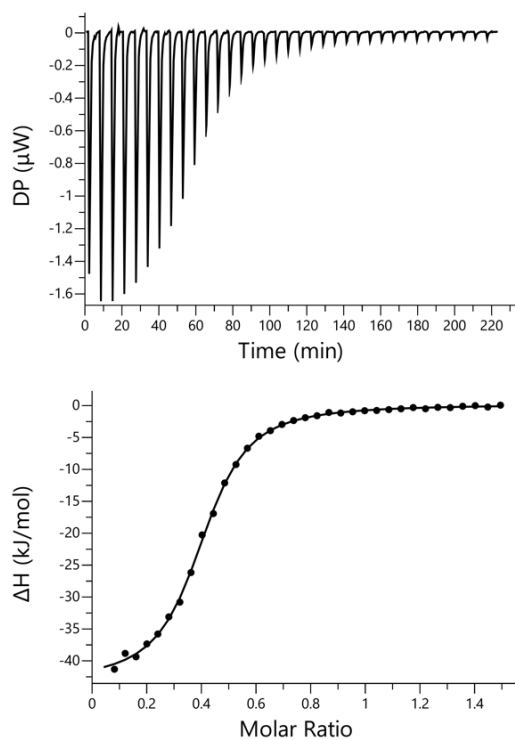


Figure S43. ITC data for titration of **6** (0.28 mM) into **3** (0.04 mM) in water at 298 K. The raw data for each injection is shown (differential power, DP), along with the least-squares-fit of the enthalpy change per mole of guest (ΔH) to a 1:1 binding isotherm.

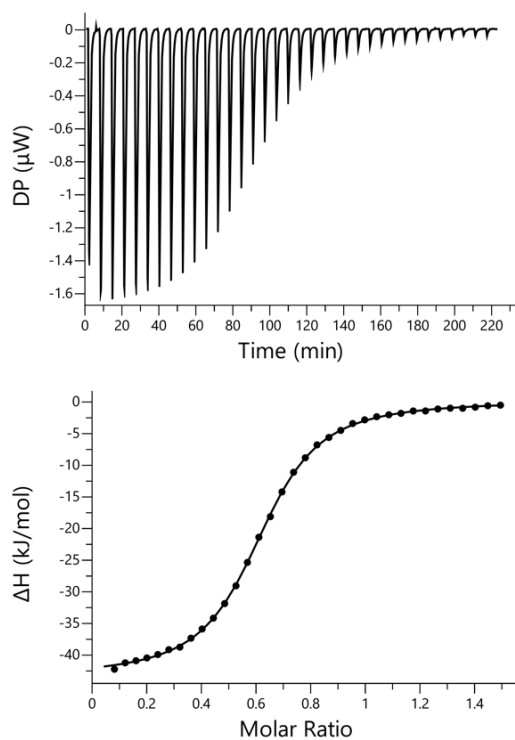


Figure S44. ITC data for titration of **7** (0.28 mM) into **3** (0.04 mM) in water at 298 K. The raw data for each injection is shown (differential power, DP), along with the least-squares-fit of the enthalpy change per mole of guest (ΔH) to a 1:1 binding isotherm.

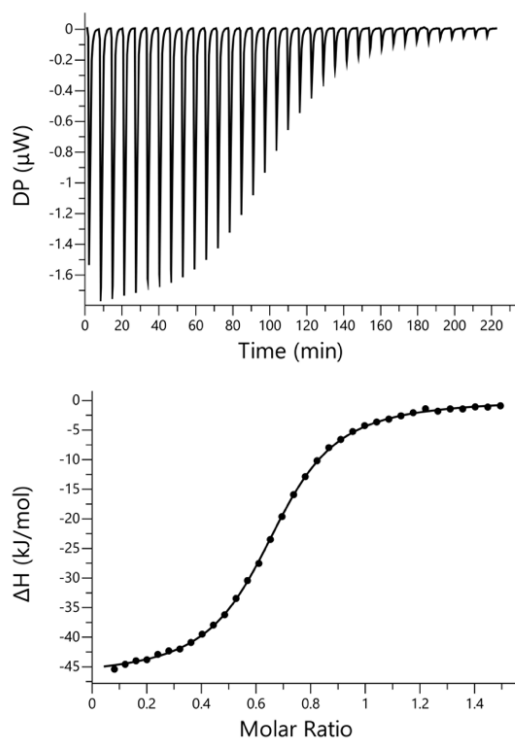


Figure S45. ITC data for titration of **8** (0.28 mM) into **3** (0.04 mM) in water at 298 K. The raw data for each injection is shown (differential power, DP), along with the least-squares-fit of the enthalpy change per mole of guest (ΔH) to a 1:1 binding isotherm.

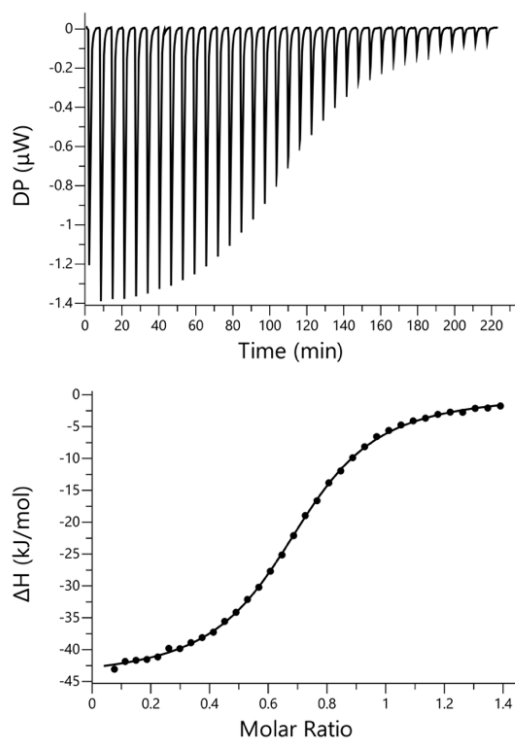


Figure S46. ITC data for titration of **9** (0.28 mM) into **3** (0.04 mM) in water at 298 K. The raw data for each injection is shown (differential power, DP), along with the least-squares-fit of the enthalpy change per mole of guest (ΔH) to a 1:1 binding isotherm.

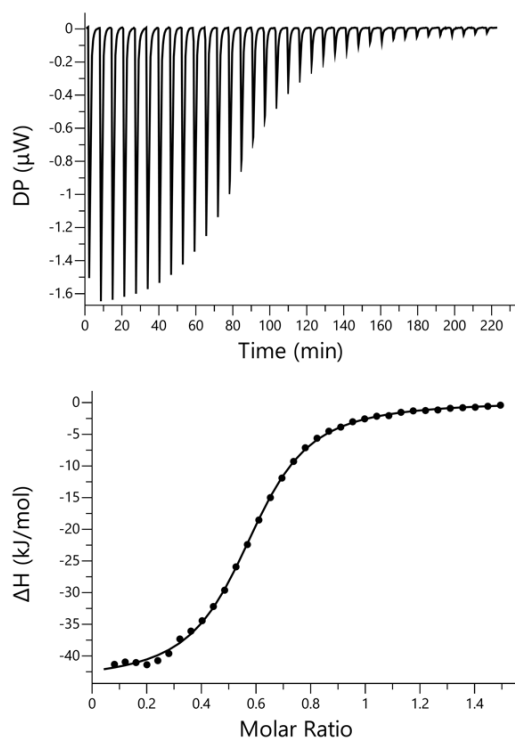


Figure S47. ITC data for titration of **10** (0.28 mM) into **3** (0.04 mM) in water at 298 K. The raw data for each injection is shown (differential power, DP), along with the least-squares-fit of the enthalpy change per mole of guest (ΔH) to a 1:1 binding isotherm.

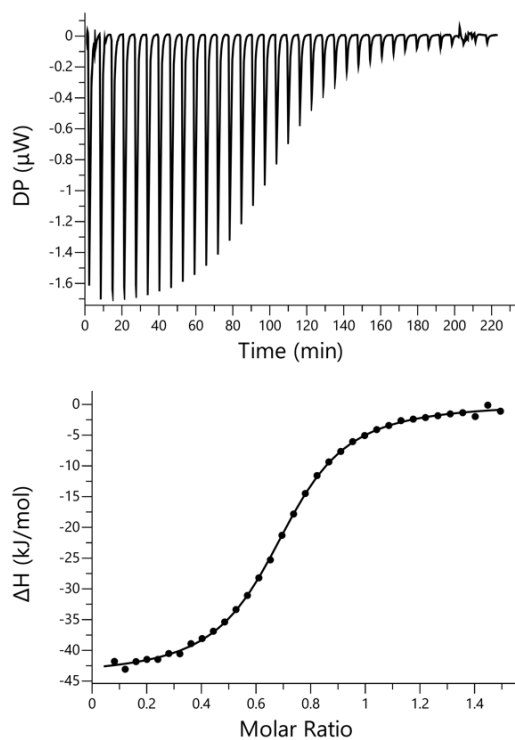


Figure S48. ITC data for titration of **11** (0.28 mM) into **3** (0.04 mM) in water at 298 K. The raw data for each injection is shown (differential power, DP), along with the least-squares-fit of the enthalpy change per mole of guest (ΔH) to a 1:1 binding isotherm.

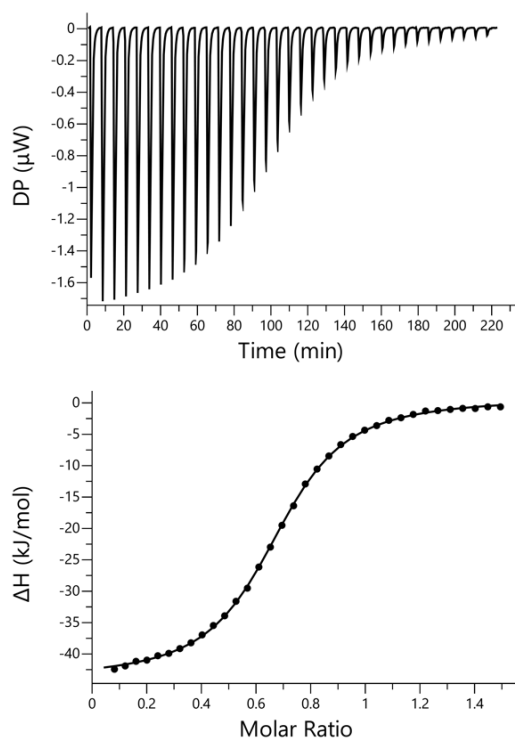


Figure S49. ITC data for titration of **12** (0.28 mM) into **3** (0.04 mM) in water at 298 K. The raw data for each injection is shown (differential power, DP), along with the least-squares-fit of the enthalpy change per mole of guest (ΔH) to a 1:1 binding isotherm.

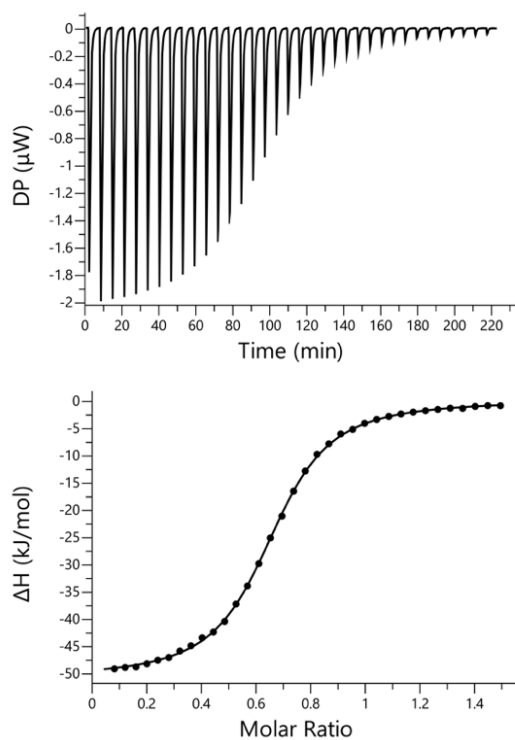


Figure S50. ITC data for titration of **13** (0.28 mM) into **3** (0.04 mM) in water at 298 K. The raw data for each injection is shown (differential power, DP), along with the least-squares-fit of the enthalpy change per mole of guest (ΔH) to a 1:1 binding isotherm.

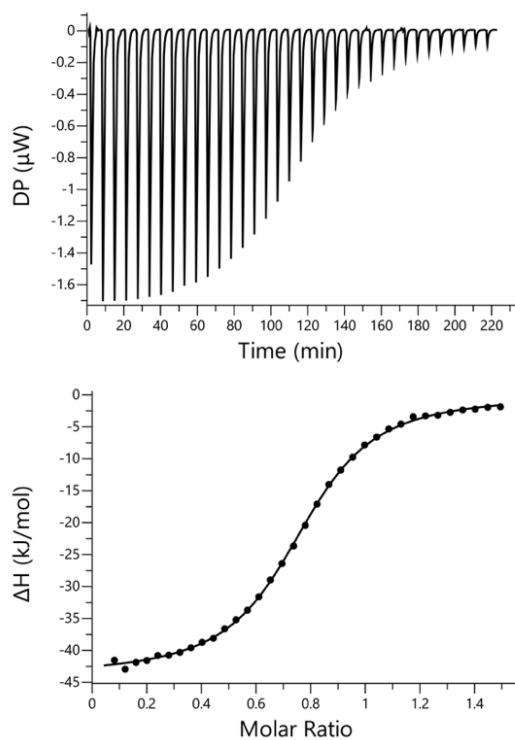


Figure S51. ITC data for titration of **14** (0.28 mM) into **3** (0.04 mM) in water at 298 K. The raw data for each injection is shown (differential power, DP), along with the least-squares-fit of the enthalpy change per mole of guest (ΔH) to a 1:1 binding isotherm.

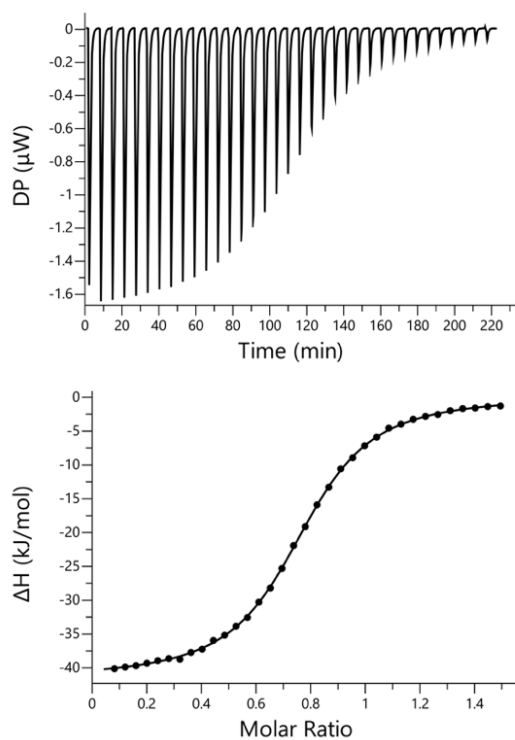


Figure S52. ITC data for titration of **15** (0.28 mM) into **3** (0.04 mM) in water at 298 K. The raw data for each injection is shown (differential power, DP), along with the least-squares-fit of the enthalpy change per mole of guest (ΔH) to a 1:1 binding isotherm.

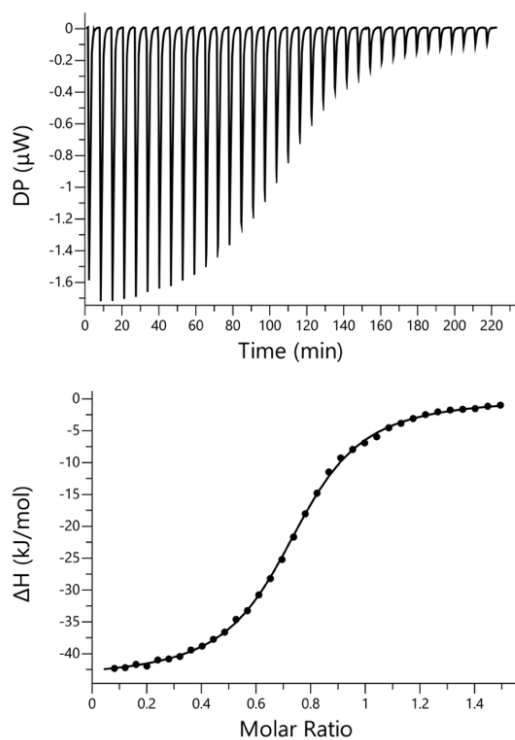


Figure S53. ITC data for titration of **16** (0.28 mM) into **3** (0.04 mM) in water at 298 K. The raw data for each injection is shown (differential power, DP), along with the least-squares-fit of the enthalpy change per mole of guest (ΔH) to a 1:1 binding isotherm.

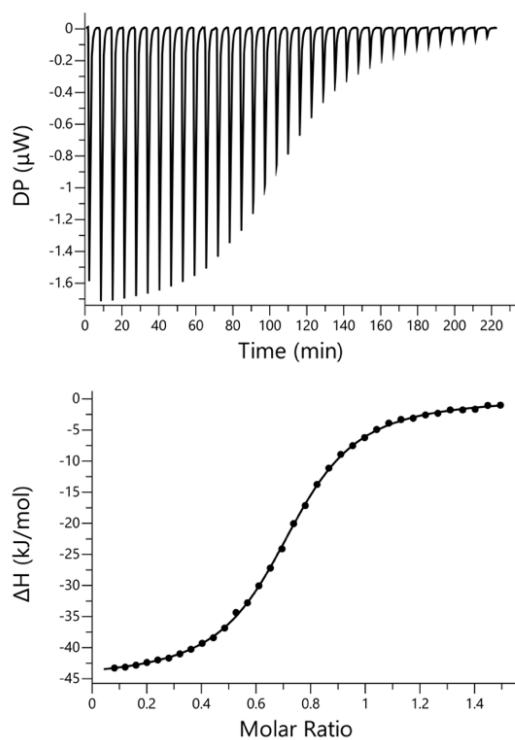


Figure S54. ITC data for titration of **17** (0.28 mM) into **3** (0.04 mM) in water at 298 K. The raw data for each injection is shown (differential power, DP), along with the least-squares-fit of the enthalpy change per mole of guest (ΔH) to a 1:1 binding isotherm.

3.3. Octachloro-super-aryl-extended calix[4]pyrrole **2**

3.3.1. Complex **C** of the DMC

The C-value for this experiment is 223, so the data could be used to determine both K and ΔH° .

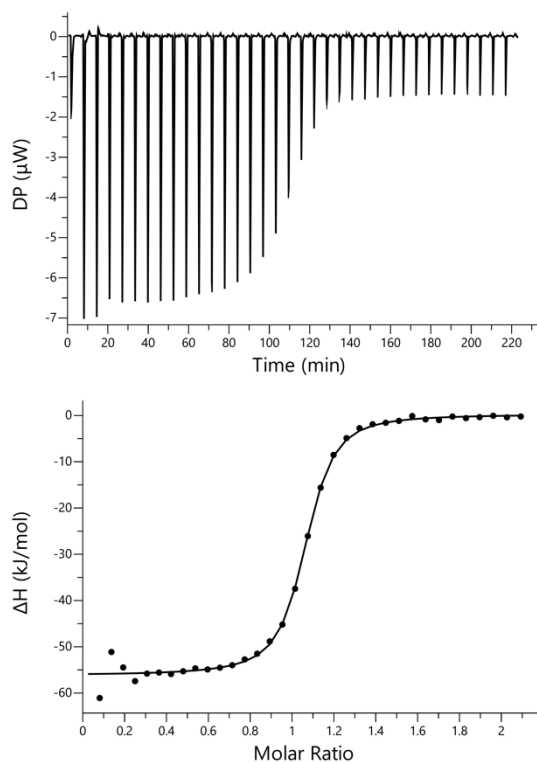


Figure S55. ITC data for titration of **PNO** (0.30 mM) into **2** (0.03 mM) in chloroform at 298 K. The raw data for each injection is shown (differential power, DP), along with the least-squares-fit of the enthalpy change per mole of guest (ΔH) to a 1:1 binding isotherm.

3.3.2. Complex A of the DMC

The C-values for these experiments are in the range $10^3 - 10^5$ so the data could only be used to determine ΔH° . The values of K were determined separately by NMR competition experiments

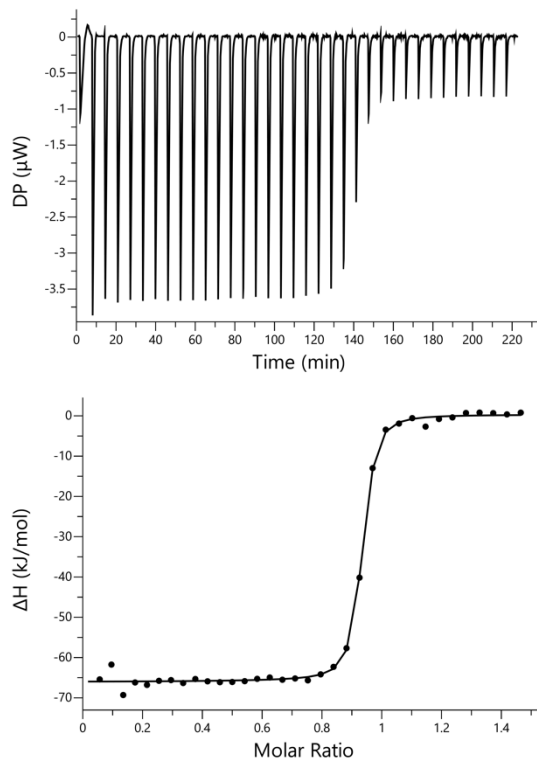


Figure S56. ITC data for titration of **5** (0.30 mM) into **2** (0.03 mM) in chloroform at 298 K. The raw data for each injection is shown (differential power, DP), along with the least-squares-fit of the enthalpy change per mole of guest (ΔH) to a 1:1 binding isotherm.

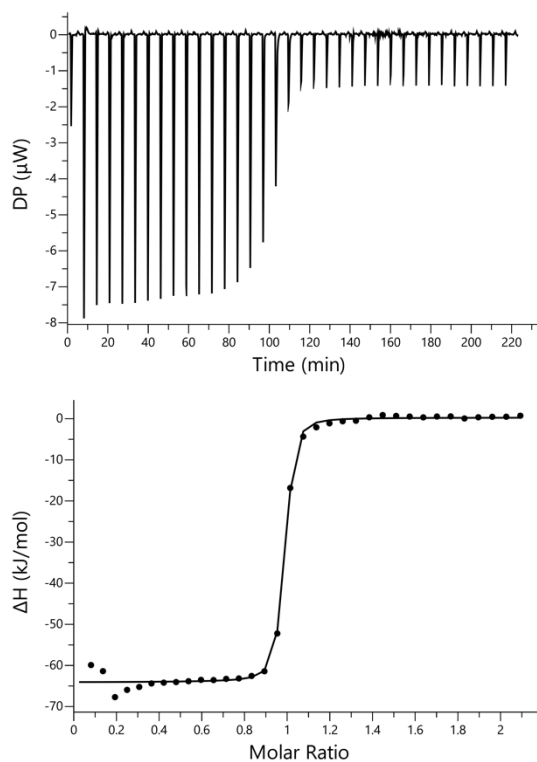


Figure S57. ITC data for titration of **6** (0.30 mM) into **2** (0.03 mM) in chloroform at 298 K. The raw data for each injection is shown (differential power, DP), along with the least-squares-fit of the enthalpy change per mole of guest (ΔH) to a 1:1 binding isotherm.

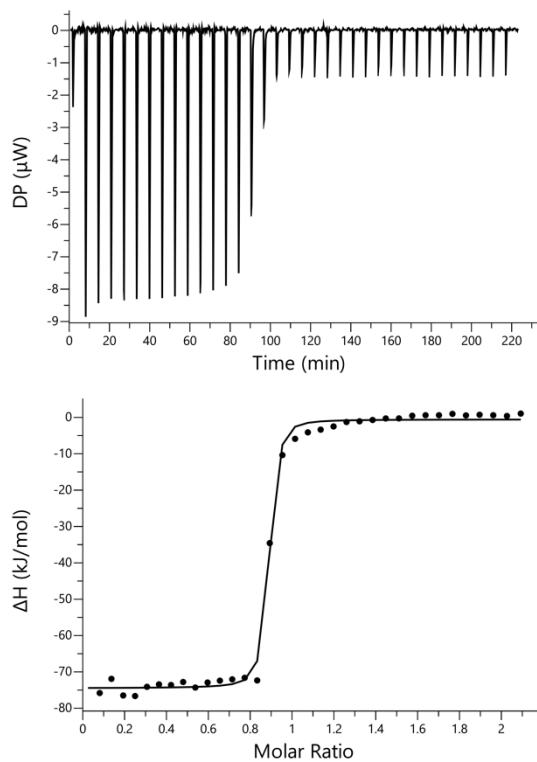


Figure S58. ITC data for titration of **7** (0.30 mM) into **2** (0.03 mM) in chloroform at 298 K. The raw data for each injection is shown (differential power, DP), along with the least-squares-fit of the enthalpy change per mole of guest (ΔH) to a 1:1 binding isotherm.

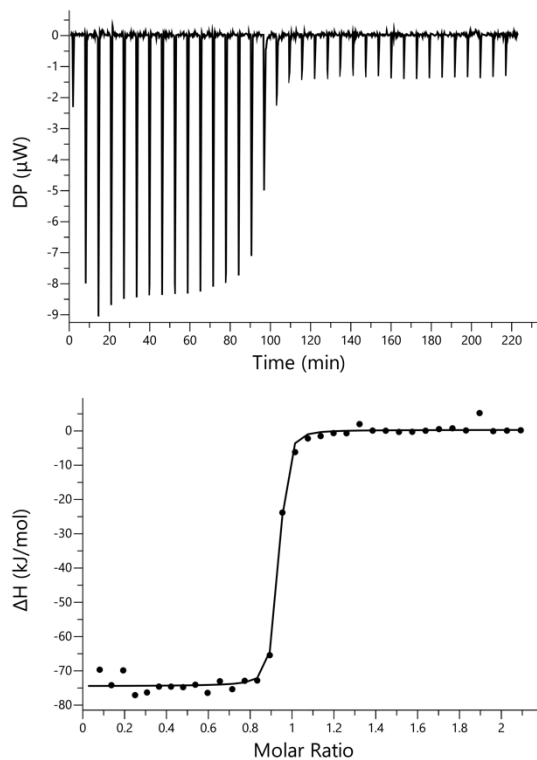


Figure S59. ITC data for titration of **8** (0.30 mM) into **2** (0.03 mM) in chloroform at 298 K. The raw data for each injection is shown (differential power, DP), along with the least-squares-fit of the enthalpy change per mole of guest (ΔH) to a 1:1 binding isotherm.

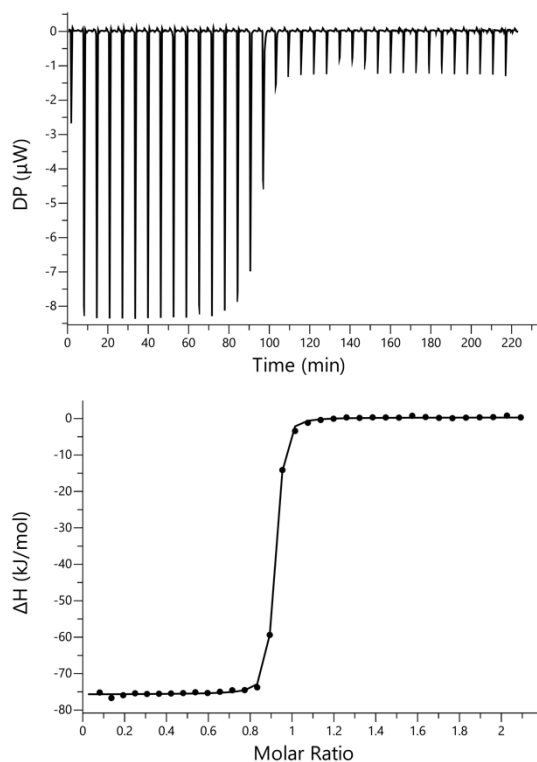


Figure S60. ITC data for titration of **9** (0.30 mM) into **2** (0.03 mM) in chloroform at 298 K. The raw data for each injection is shown (differential power, DP), along with the least-squares-fit of the enthalpy change per mole of guest (ΔH) to a 1:1 binding isotherm.

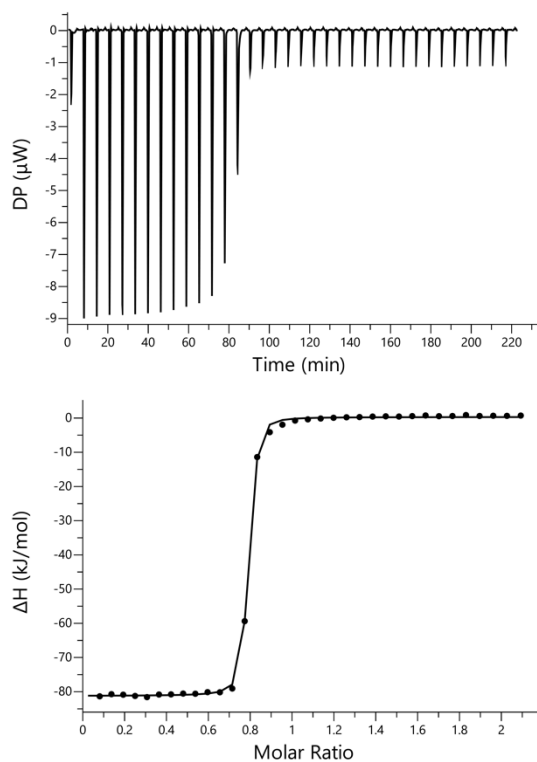


Figure S61. ITC data for titration of **10** (0.30 mM) into **2** (0.03 mM) in chloroform at 298 K. The raw data for each injection is shown (differential power, DP), along with the least-squares-fit of the enthalpy change per mole of guest (ΔH) to a 1:1 binding isotherm.

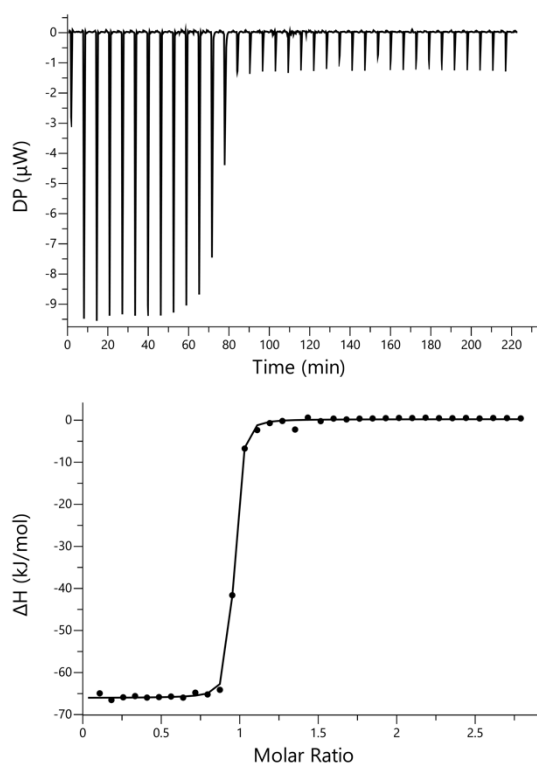


Figure S62. ITC data for titration of **11** (0.30 mM) into **2** (0.03 mM) in chloroform at 298 K. The raw data for each injection is shown (differential power, DP), along with the least-squares-fit of the enthalpy change per mole of guest (ΔH) to a 1:1 binding isotherm.

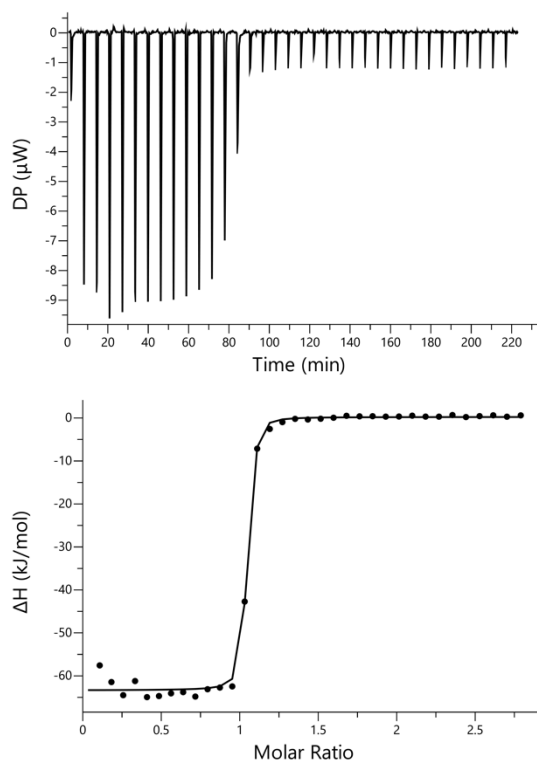


Figure S63. ITC data for titration of **12** (0.30 mM) into **2** (0.03 mM) in chloroform at 298 K. The raw data for each injection is shown (differential power, DP), along with the least-squares-fit of the enthalpy change per mole of guest (ΔH) to a 1:1 binding isotherm.

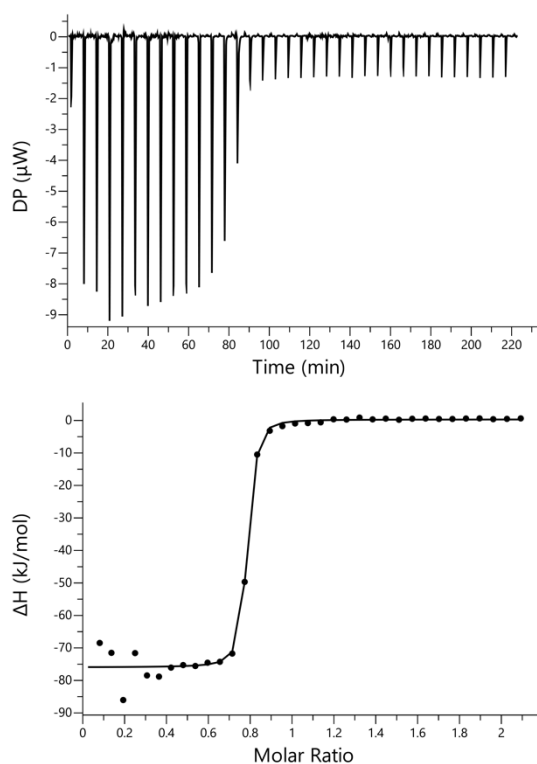


Figure S64. ITC data for titration of **13** (0.30 mM) into **2** (0.03 mM) in chloroform at 298 K. The raw data for each injection is shown (differential power, DP), along with the least-squares-fit of the enthalpy change per mole of guest (ΔH) to a 1:1 binding isotherm.

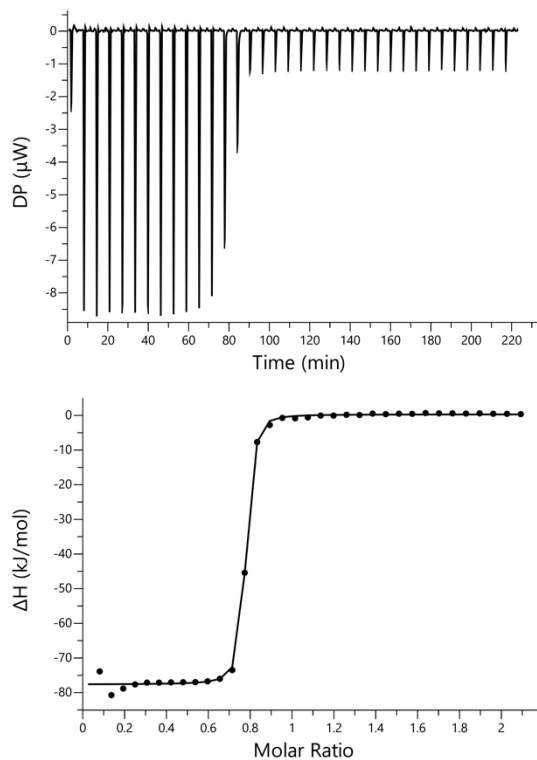


Figure S65. ITC data for titration of **14** (0.30 mM) into **2** (0.03 mM) in chloroform at 298 K. The raw data for each injection is shown (differential power, DP), along with the least-squares-fit of the enthalpy change per mole of guest (ΔH) to a 1:1 binding isotherm.

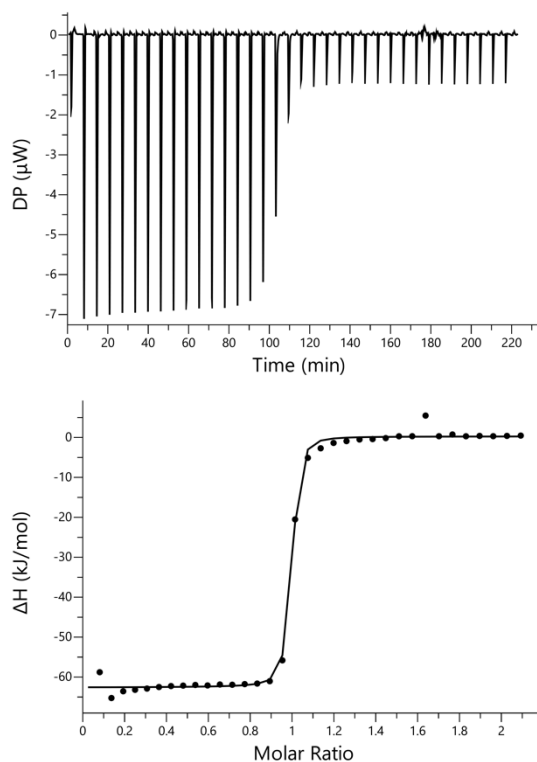


Figure S66. ITC data for titration of **15** (0.30 mM) into **2** (0.03 mM) in chloroform at 298 K. The raw data for each injection is shown (differential power, DP), along with the least-squares-fit of the enthalpy change per mole of guest (ΔH) to a 1:1 binding isotherm.

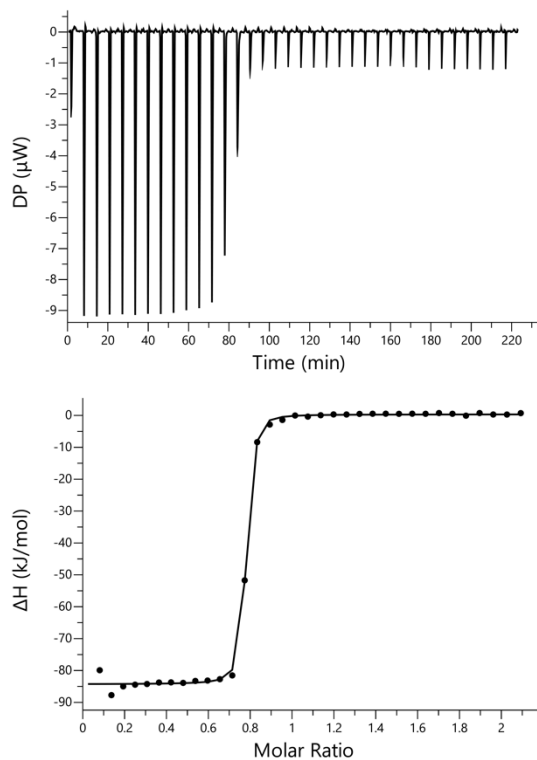


Figure S67. ITC data for titration of **16** (0.30 mM) into **2** (0.03 mM) in chloroform at 298 K. The raw data for each injection is shown (differential power, DP), along with the least-squares-fit of the enthalpy change per mole of guest (ΔH) to a 1:1 binding isotherm.

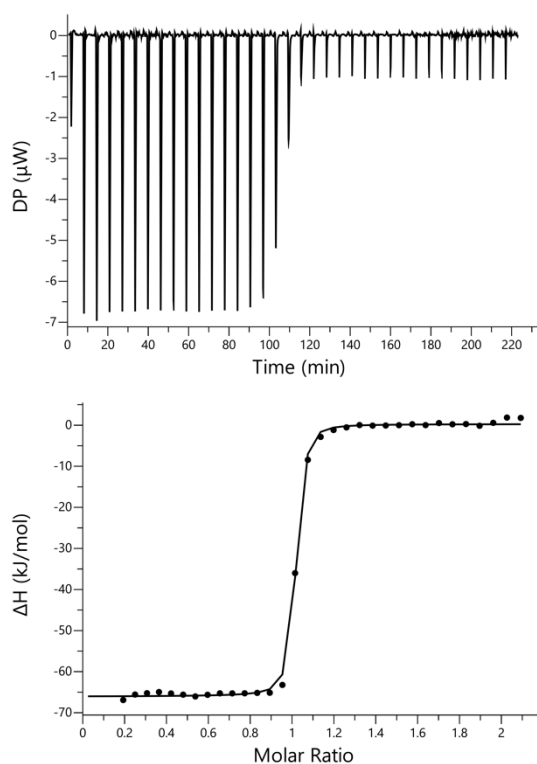


Figure S68. ITC data for titration of **17** (0.30 mM) into **2** (0.03 mM) in chloroform at 298 K. The raw data for each injection is shown (differential power, DP), along with the least-squares-fit of the enthalpy change per mole of guest (ΔH) to a 1:1 binding isotherm.

3.4. Tetrachloro-aryl-extended calix[4]pyrrole 4

3.4.1. Complex D of the DMC

The C-value for this experiment is 39, so the data could be used to determine both K and ΔH°

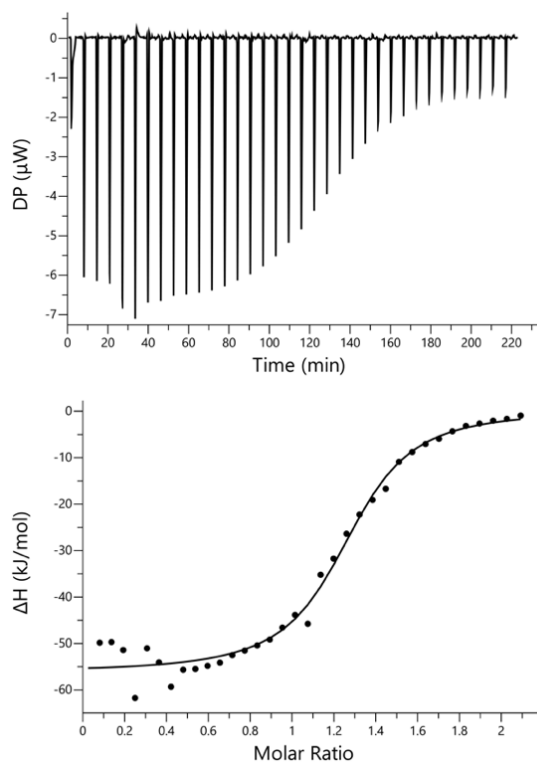


Figure S69. ITC data for titration of **PNO** (0.30 mM) into **4** (0.03 mM) in chloroform at 298 K. The raw data for each injection is shown (differential power, DP), along with the least-squares-fit of the enthalpy change per mole of guest (ΔH) to a 1:1 binding isotherm.

3.4.2. Complex B of the DMC

The C-values for these experiments are in the range 16 – 97, so the data could be used to determine both K and ΔH° .

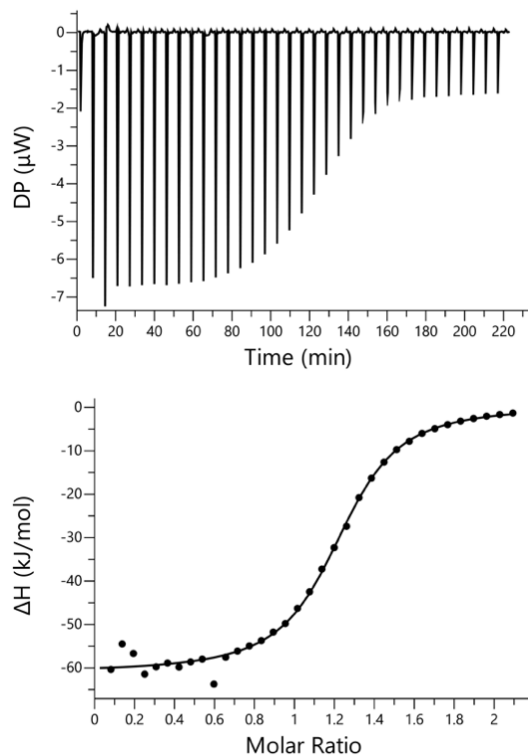


Figure S70. ITC data for titration of **5** (0.30 mM) into **4** (0.03 mM) in chloroform at 298 K. The raw data for each injection is shown (differential power, DP), along with the least-squares-fit of the enthalpy change per mole of guest (ΔH) to a 1:1 binding isotherm.

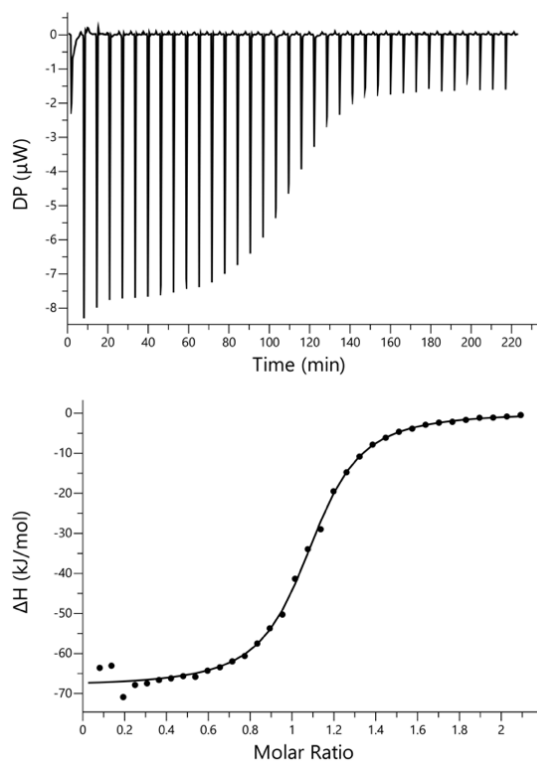


Figure S71. ITC data for titration of **6** (0.30 mM) into **4** (0.03 mM) in chloroform at 298 K. The raw data for each injection is shown (differential power, DP), along with the least-squares-fit of the enthalpy change per mole of guest (ΔH) to a 1:1 binding isotherm.

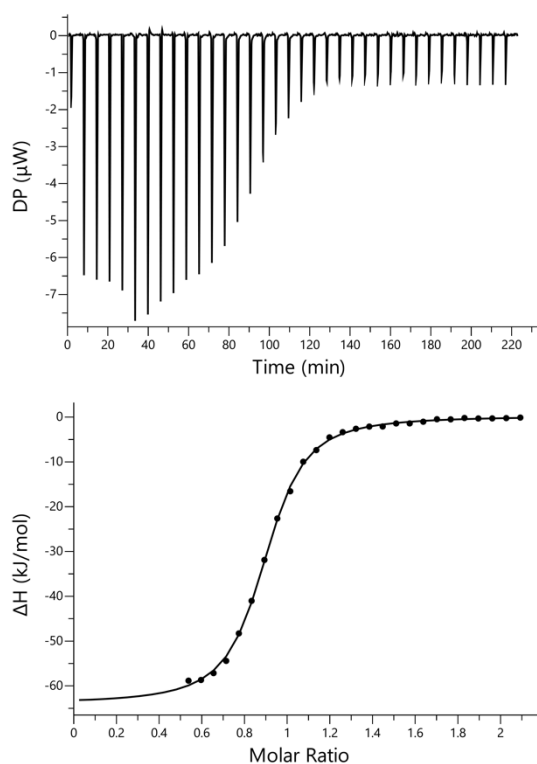


Figure S72. ITC data for titration of **7** (0.30 mM) into **4** (0.03 mM) in chloroform at 298 K. The raw data for each injection is shown (differential power, DP), along with the least-squares-fit of the enthalpy change per mole of guest (ΔH) to a 1:1 binding isotherm.

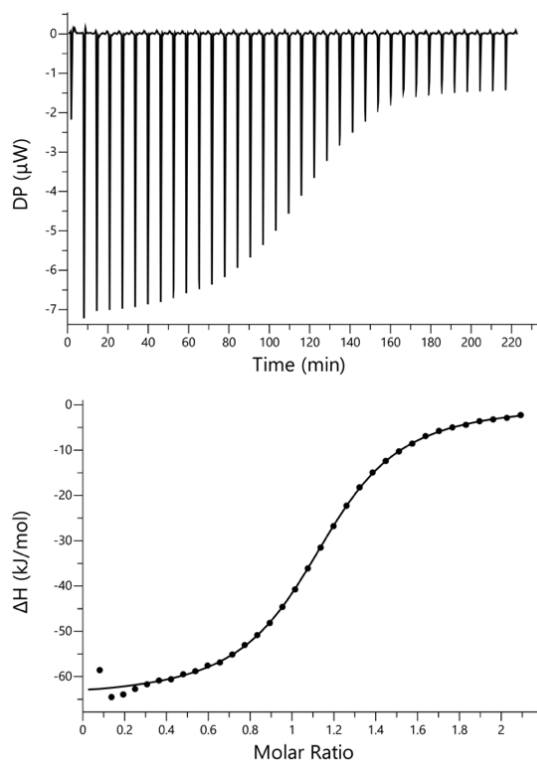


Figure S73. ITC data for titration of **8** (0.30 mM) into **4** (0.03 mM) in chloroform at 298 K. The raw data for each injection is shown (differential power, DP), along with the least-squares-fit of the enthalpy change per mole of guest (ΔH) to a 1:1 binding isotherm.

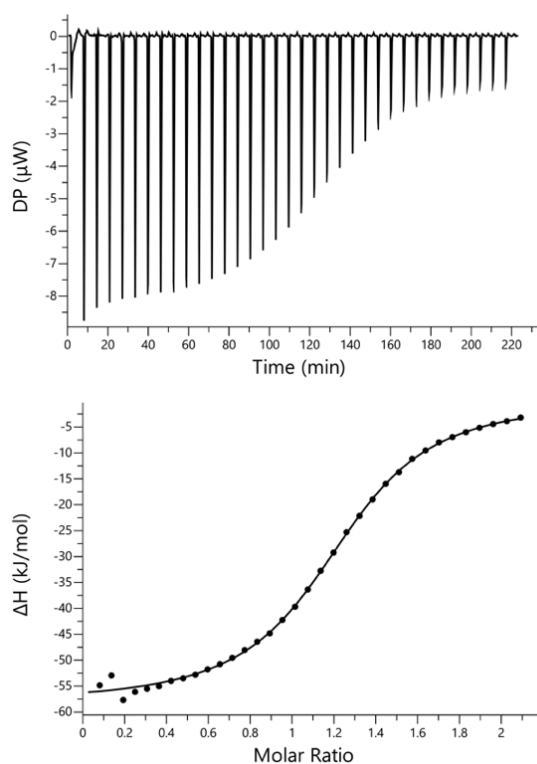


Figure S74. ITC data for titration of **9** (0.30 mM) into **4** (0.03 mM) in chloroform at 298 K. The raw data for each injection is shown (differential power, DP), along with the least-squares-fit of the enthalpy change per mole of guest (ΔH) to a 1:1 binding isotherm.

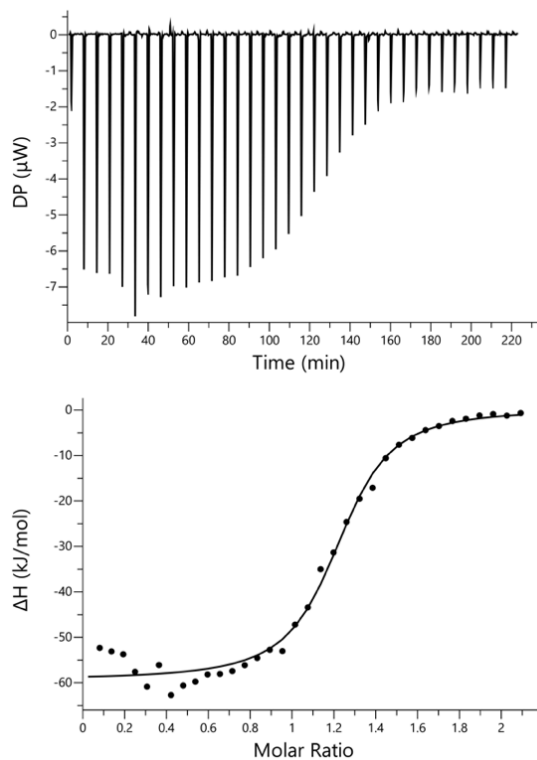


Figure S75. ITC data for titration of **10** (0.30 mM) into **4** (0.03 mM) in chloroform at 298 K. The raw data for each injection is shown (differential power, DP), along with the least-squares-fit of the enthalpy change per mole of guest (ΔH) to a 1:1 binding isotherm.

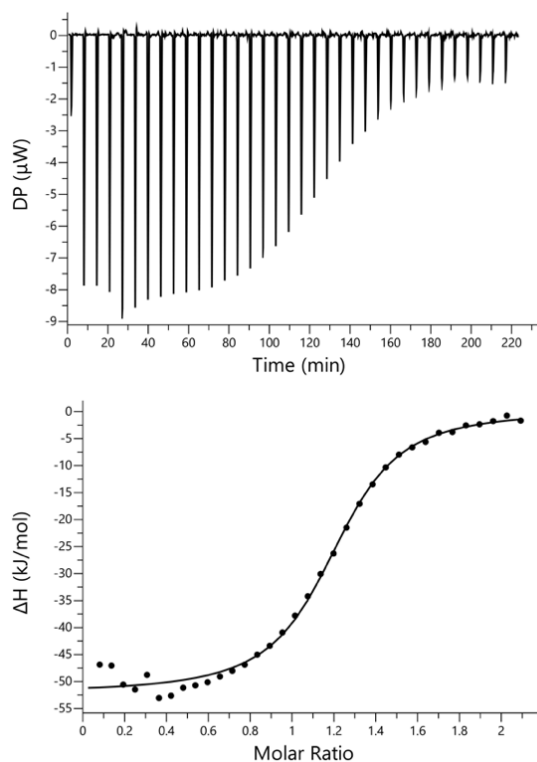


Figure S76. ITC data for titration of **11** (0.30 mM) into **4** (0.03 mM) in chloroform at 298 K. The raw data for each injection is shown (differential power, DP), along with the least-squares-fit of the enthalpy change per mole of guest (ΔH) to a 1:1 binding isotherm.

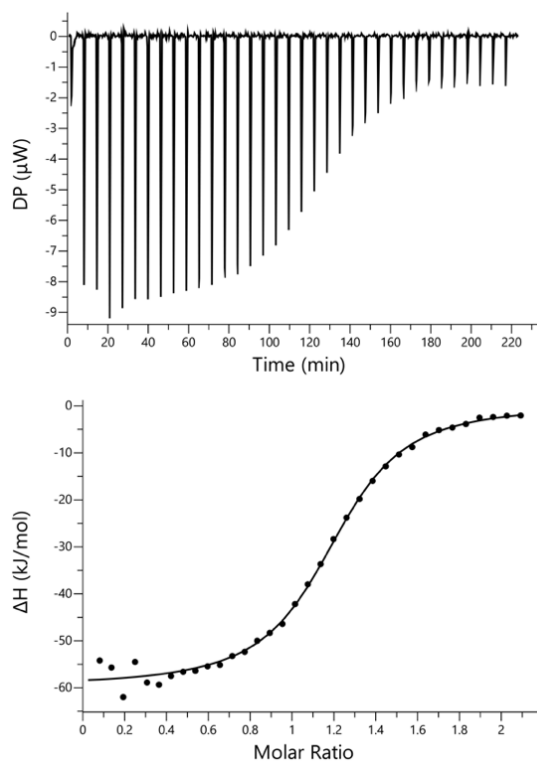


Figure S77. ITC data for titration of **12** (0.30 mM) into **4** (0.03 mM) in chloroform at 298 K. The raw data for each injection is shown (differential power, DP), along with the least-squares-fit of the enthalpy change per mole of guest (ΔH) to a 1:1 binding isotherm.

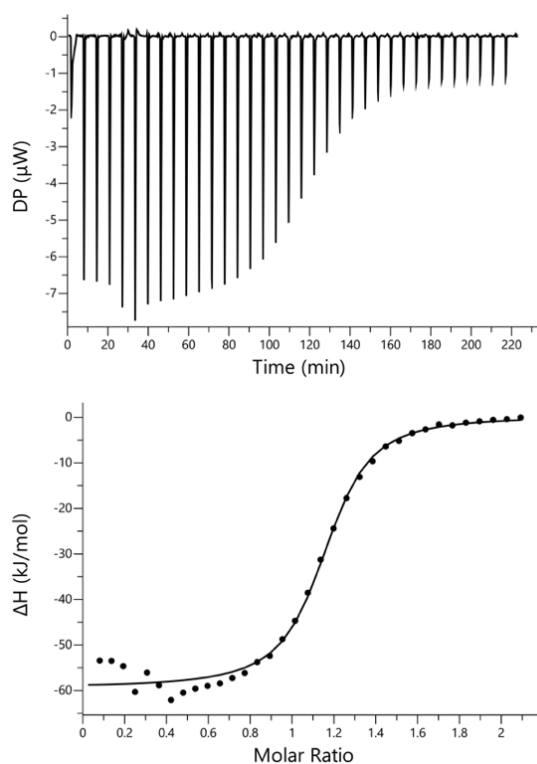


Figure S78. ITC data for titration of **13** (0.30 mM) into **4** (0.03 mM) in chloroform at 298 K. The raw data for each injection is shown (differential power, DP), along with the least-squares-fit of the enthalpy change per mole of guest (ΔH) to a 1:1 binding isotherm.

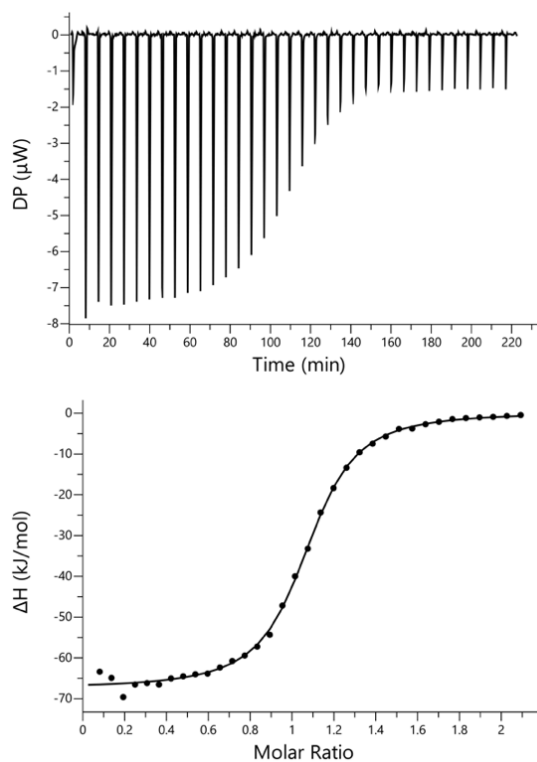


Figure S79. ITC data for titration of **14** (0.30 mM) into **4** (0.03 mM) in chloroform at 298 K. The raw data for each injection is shown (differential power, DP), along with the least-squares-fit of the enthalpy change per mole of guest (ΔH) to a 1:1 binding isotherm.

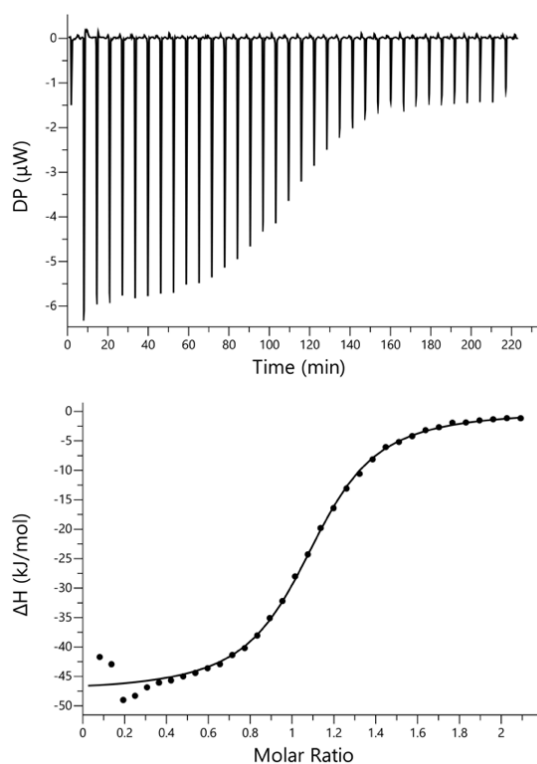


Figure S80. ITC data for titration of **15** (0.30 mM) into **4** (0.03 mM) in chloroform at 298 K. The raw data for each injection is shown (differential power, DP), along with the least-squares-fit of the enthalpy change per mole of guest (ΔH) to a 1:1 binding isotherm.

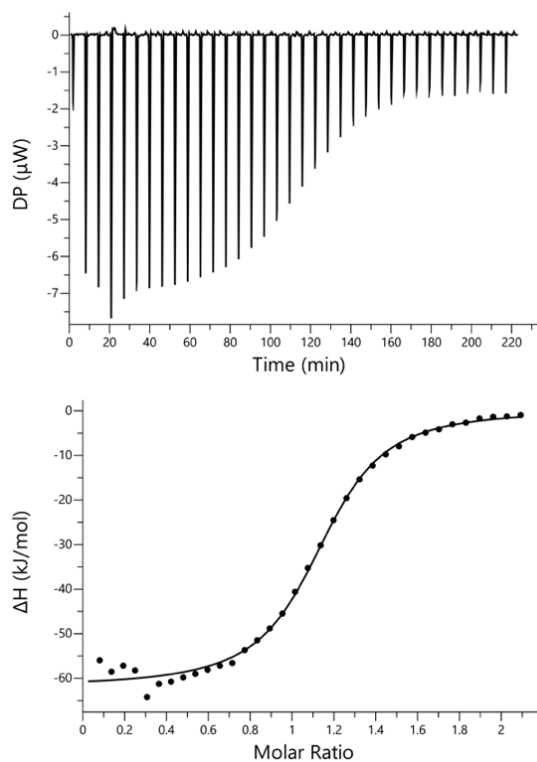


Figure S81. ITC data for titration of **16** (0.30 mM) into **4** (0.03 mM) in chloroform at 298 K. The raw data for each injection is shown (differential power, DP), along with the least-squares-fit of the enthalpy change per mole of guest (ΔH) to a 1:1 binding isotherm.

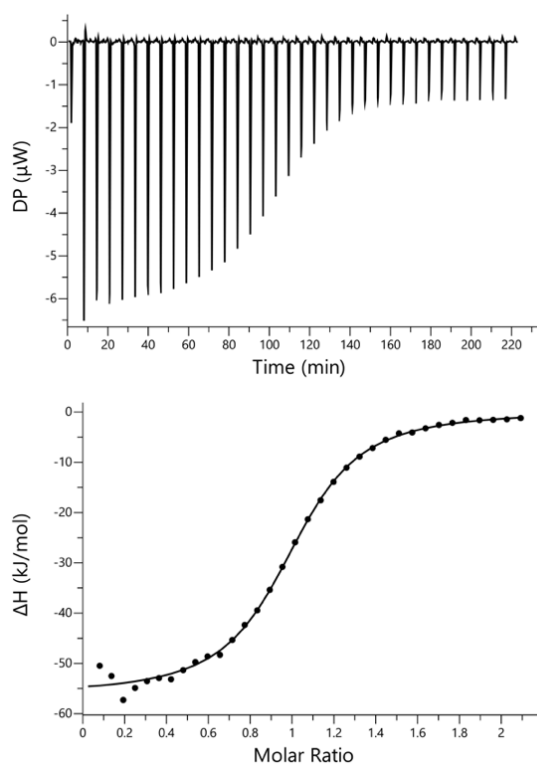


Figure S82. ITC data for titration of **17** (0.30 mM) into **4** (0.03 mM) in chloroform at 298 K. The raw data for each injection is shown (differential power, DP), along with the least-squares-fit of the enthalpy change per mole of guest (ΔH) to a 1:1 binding isotherm.

4. Pairwise ^1H NMR competitive titrations

Competitive titration experiments were performed using calix[4]pyrroles **1** and **2**, and pyridine *N*-oxides **5-17** and **PNO** in non-buffered deuterium oxide and deuteriochloroform solutions. The association constant ratios between two competing complexes were determined by integrating selected proton signals in the acquired ^1H NMR spectra.

4.1. Octapyridinium-super-aryl-extended calix[4]pyrrole **1**

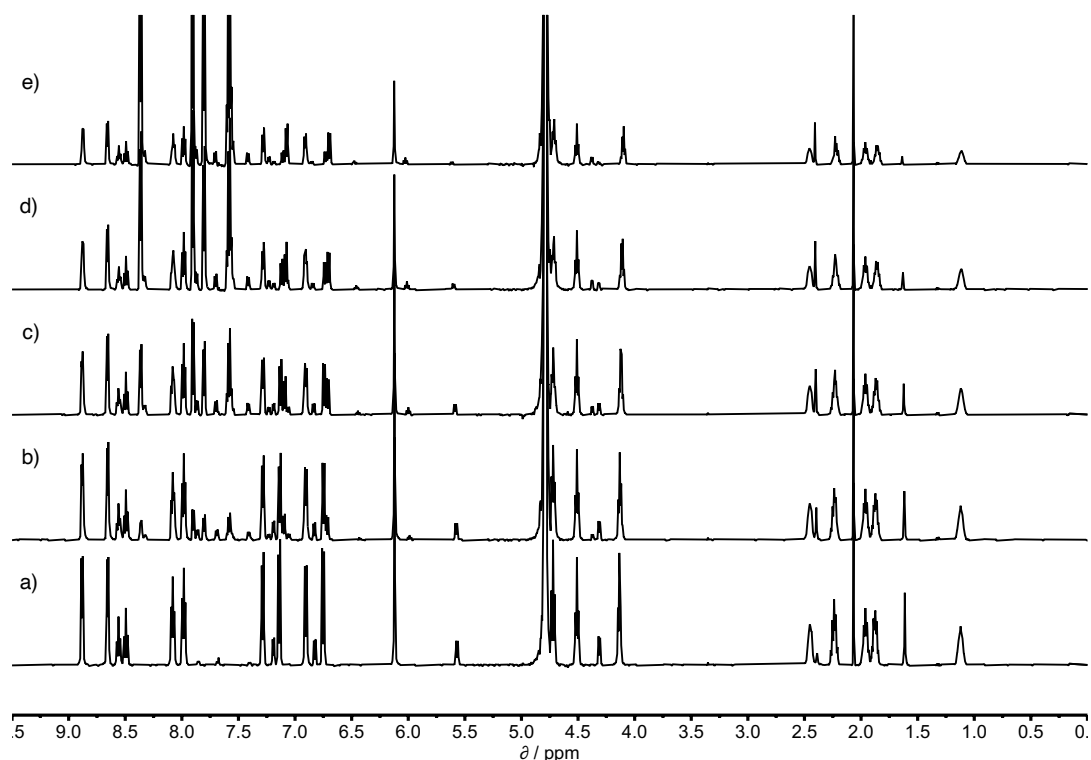


Figure S83. 500MHz ^1H NMR for titration of **5** into a mixture of **1** and **6** in D_2O at 298K. Concentrations are: a) **1**: 0.21 mM; **6**: 0.25 mM; **5**: 0 mM; b) **1**: 0.20 mM; **6**: 0.23 mM; **5**: 0.22 mM; c) **1**: 0.17 mM; **6**: 0.20 mM; **5**: 0.57 mM; d) **1**: 0.13 mM; **6**: 0.16 mM; **5**: 1.05 mM; e) **1**: 0.09 mM; **6**: 0.11 mM; **5**: 1.59 mM. Integration of selected proton signals indicated that $K(\mathbf{1}\cdot\mathbf{6}) = 7.9 \pm 0.6 \times K(\mathbf{1}\cdot\mathbf{5})$.

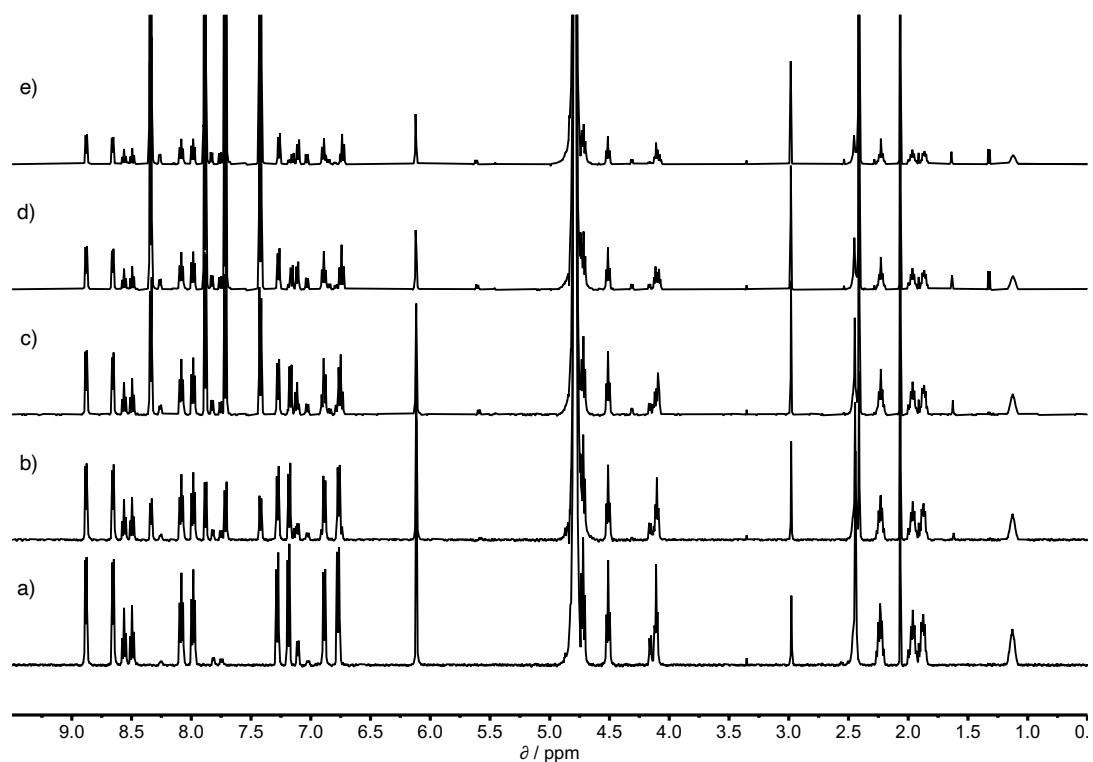


Figure S84. 500MHz ^1H NMR for titration of **6** into a mixture of **1** and **7** in D_2O at 298K. Concentrations are: a) **1**: 0.14 mM; **7**: 0.17 mM; **6**: 0 mM; b) **1**: 0.12 mM; **7**: 0.15 mM; **6**: 0.21 mM; c) **1**: 0.09mM; **7**: 0.11 mM; **6**: 0.49 mM; d) **1**: 0.07 mM; **7**: 0.08 mM; **6**: 0.79 mM; e) **1**: 0.05 mM; **7**: 0.05 mM; **6**: 1.00 mM. Integration of selected proton signals indicated that $K(\mathbf{1}\cdot\mathbf{7}) = 18.6 \pm 2.1 \times K(\mathbf{1}\cdot\mathbf{6})$.

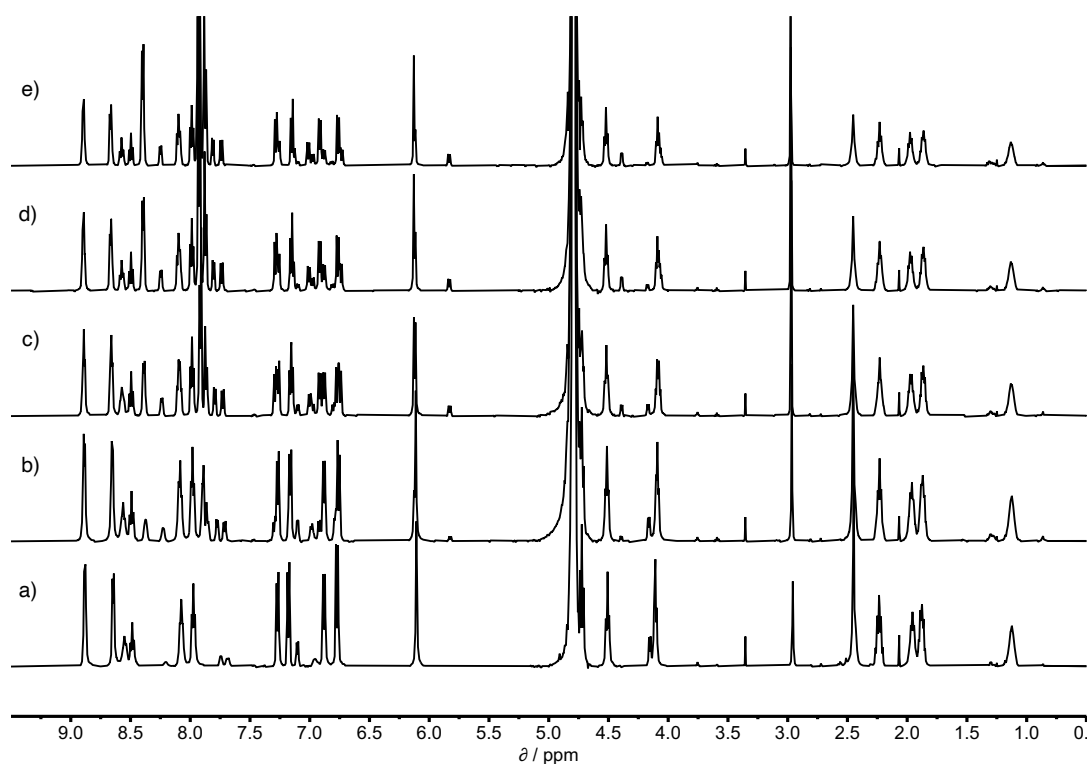


Figure S85. 500MHz ^1H NMR for titration of **8** into a mixture of **1** and **7** in D_2O at 298K. Concentrations are: a) **1**: 0.49 mM; **7**: 0.64 mM; **8**: 0 mM; b) **1**: 0.37 mM; **7**: 0.49 mM; **8**: 0.52 mM; c) **1**: 0.26 mM; **7**: 0.35 mM; **8**: 1.02 mM; d) **1**: 0.17 mM; **7**: 0.23 mM; **8**: 1.42 mM; e) **1**: 0.13 mM; **7**: 0.15 mM; **8**: 1.70 mM. Integration of selected proton signals indicated that $K(\mathbf{1}\cdot\mathbf{7}) = 2.0 \pm 0.1 \times K(\mathbf{1}\cdot\mathbf{8})$.

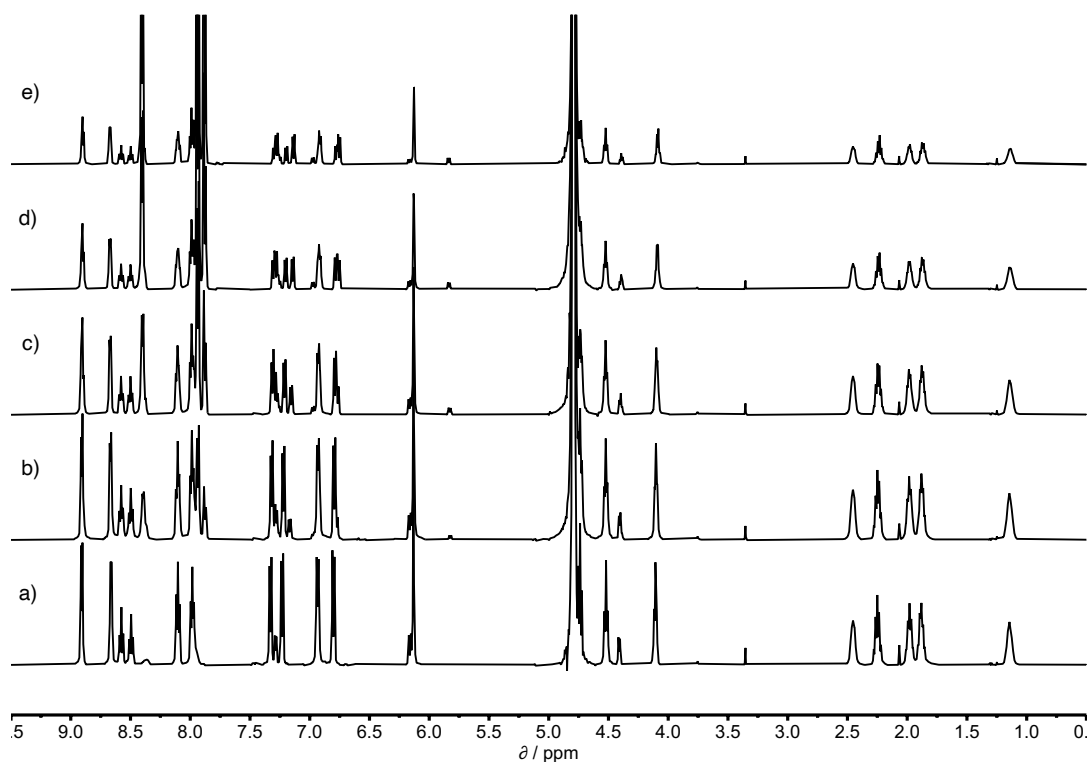


Figure S86. 500MHz ^1H NMR for titration of **8** into a mixture of **1** and **9** in D_2O at 298K. Concentrations are: a) **1**: 0.49 mM; **9**: 0.64 mM; **8**: 0 mM; b) **1**: 0.37 mM; **9**: 0.49 mM; **8**: 0.44 mM; c) **1**: 0.28 mM; **9**: 0.36 mM; **8**: 0.82 mM; d) **1**: 0.22 mM; **9**: 0.29 mM; **8**: 1.04 mM; e) **1**: 0.18 mM; **9**: 0.24 mM; **8**: 1.18 mM. Integration of selected proton signals indicated that $K(\mathbf{1}\cdot\mathbf{9}) = 14.6 \pm 0.5 \times K(\mathbf{1}\cdot\mathbf{8})$.

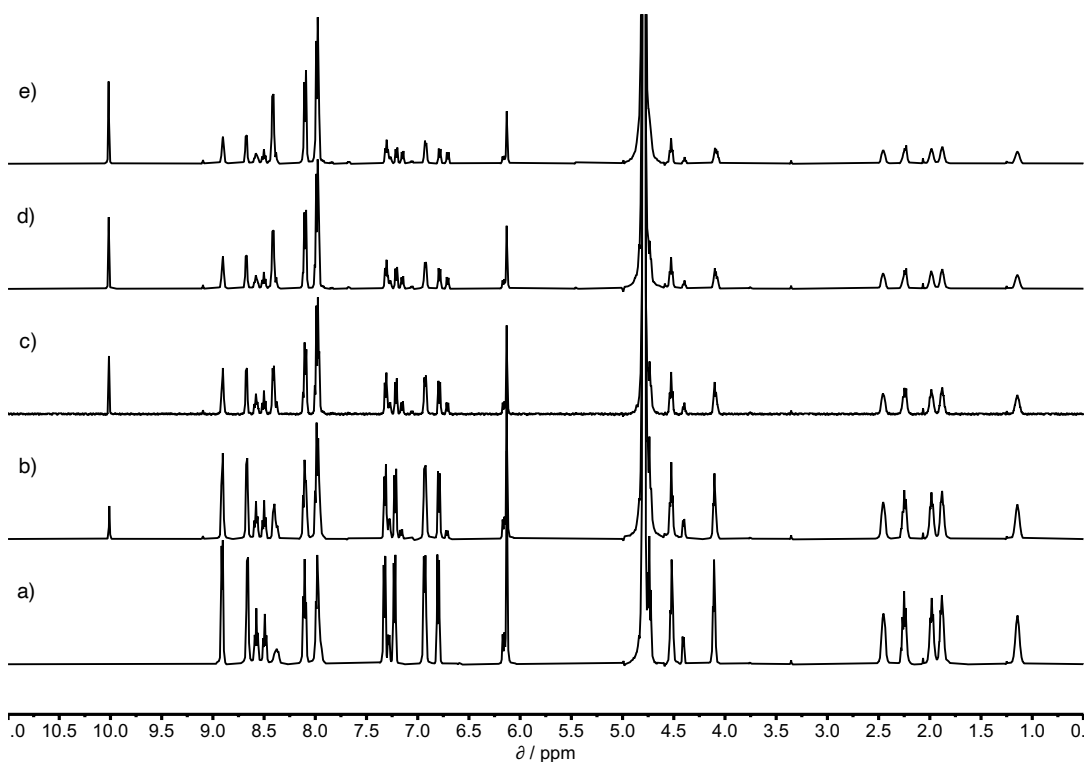


Figure S87. 500MHz ^1H NMR for titration of **11** into a mixture of **1** and **9** in D_2O at 298K. Concentrations are: a) **1**: 0.53 mM; **9**: 0.73 mM; **11**: 0 mM; b) **1**: 0.37 mM; **9**: 0.50 mM; **11**: 0.47 mM; c) **1**: 0.24 mM; **9**: 0.33 mM; **11**: 0.81 mM; d) **1**: 0.18 mM; **9**: 0.24 mM; **11**: 0.98 mM; e) **1**: 0.14 mM; **9**: 0.19 mM; **11**: 1.08 mM. Integration of selected proton signals indicated that $K(\mathbf{1}\cdot\mathbf{9}) = 12.3 \pm 1.9 \times K(\mathbf{1}\cdot\mathbf{11})$.

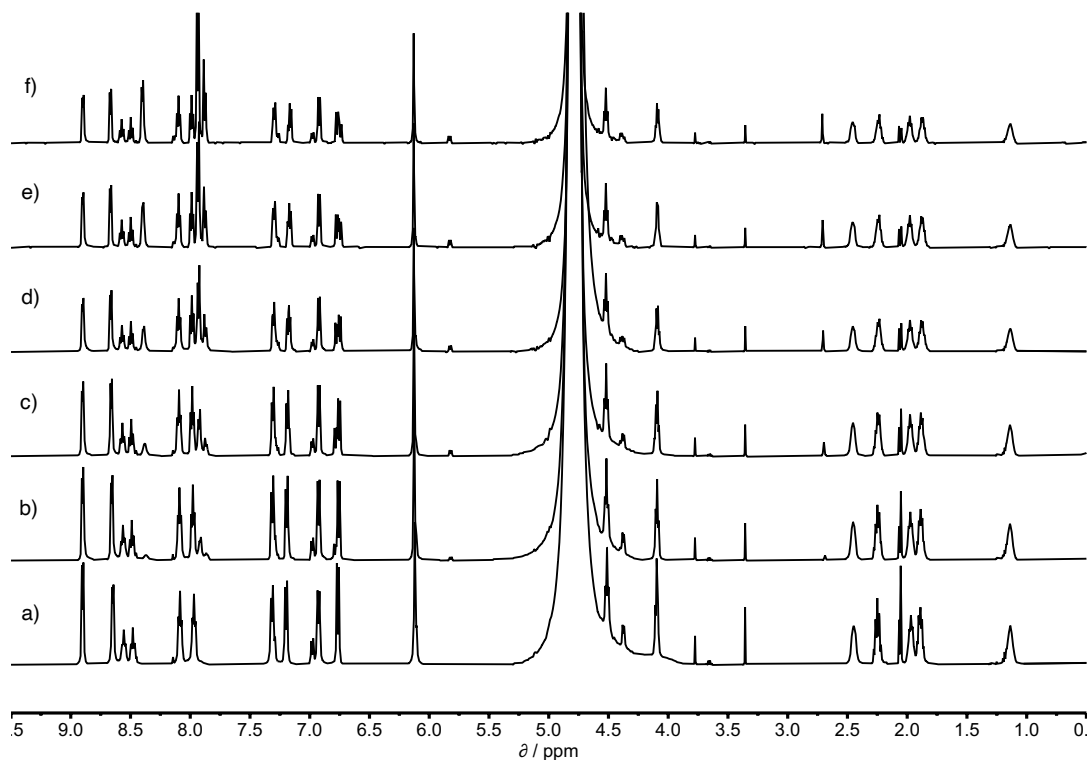


Figure S88. 500MHz ^1H NMR for titration of **8** into a mixture of **1** and **12** in D_2O at 298K. Concentrations are: a) **1**: 0.58 mM; **12**: 0.79 mM; **8**: 0 mM; b) **1**: 0.41 mM; **12**: 0.56 mM; **8**: 0.36 mM; c) **1**: 0.32 mM; **12**: 0.42 mM; **8**: 0.56 mM; d) **1**: 0.22 mM; **12**: 0.30 mM; **8**: 0.76 mM; e) **1**: 0.17 mM; **12**: 0.23 mM; **8**: 0.87 mM; f) **1**: 0.11 mM; **12**: 0.15 mM; **8**: 0.98 mM. Integration of selected proton signals indicated that $K(\mathbf{1}\cdot\mathbf{12}) = 6.3 \pm 1.8 \times K(\mathbf{1}\cdot\mathbf{8})$.

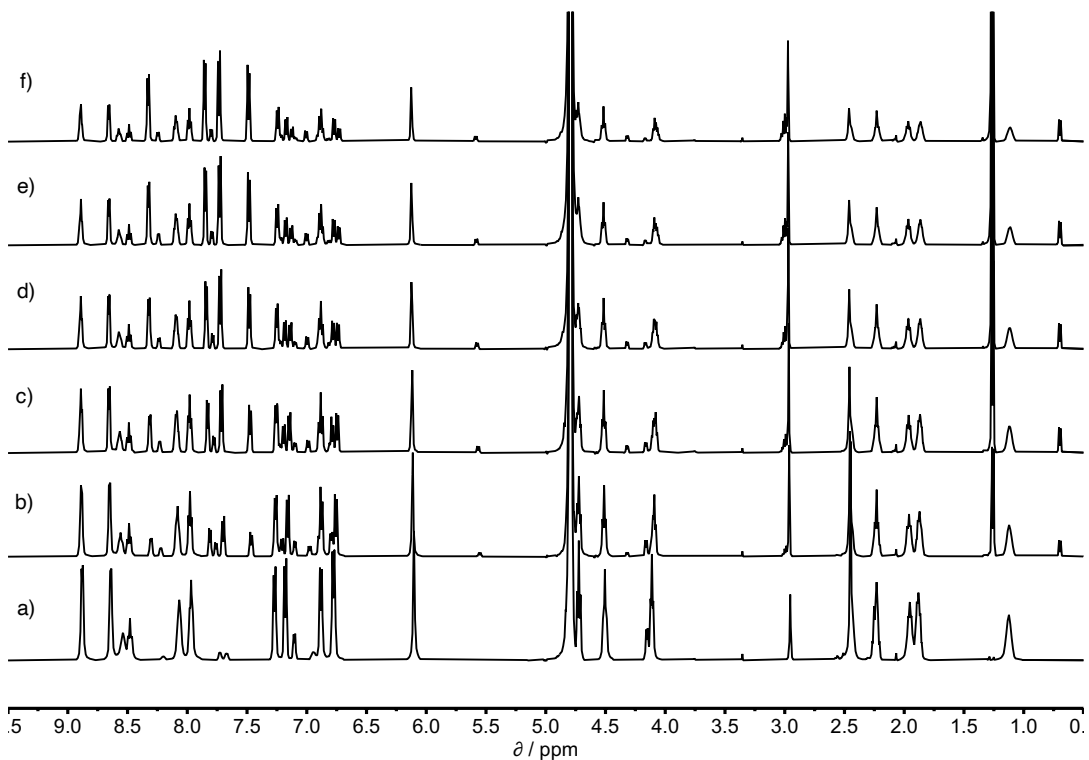


Figure S89. 500MHz ^1H NMR for titration of **13** into a mixture of **1** and **7** in D_2O at 298K. Concentrations are: a) **1**: 0.58 mM; **7**: 0.71 mM; **13**: 0 mM; b) **1**: 0.41 mM; **7**: 0.50 mM; **13**: 0.51 mM; c) **1**: 0.32 mM; **7**: 0.39 mM; **13**: 0.79 mM; d) **1**: 0.26 mM; **7**: 0.32 mM; **13**: 0.97 mM; e) **1**: 0.22 mM; **7**: 0.27 mM; **13**: 1.09 mM; f) **1**: 0.19 mM; **7**: 0.23 mM; **13**: 1.18 mM. Integration of selected proton signals indicated that $K(\mathbf{1}\cdot\mathbf{7}) = 4.2 \pm 1.0 \times K(\mathbf{1}\cdot\mathbf{13})$.

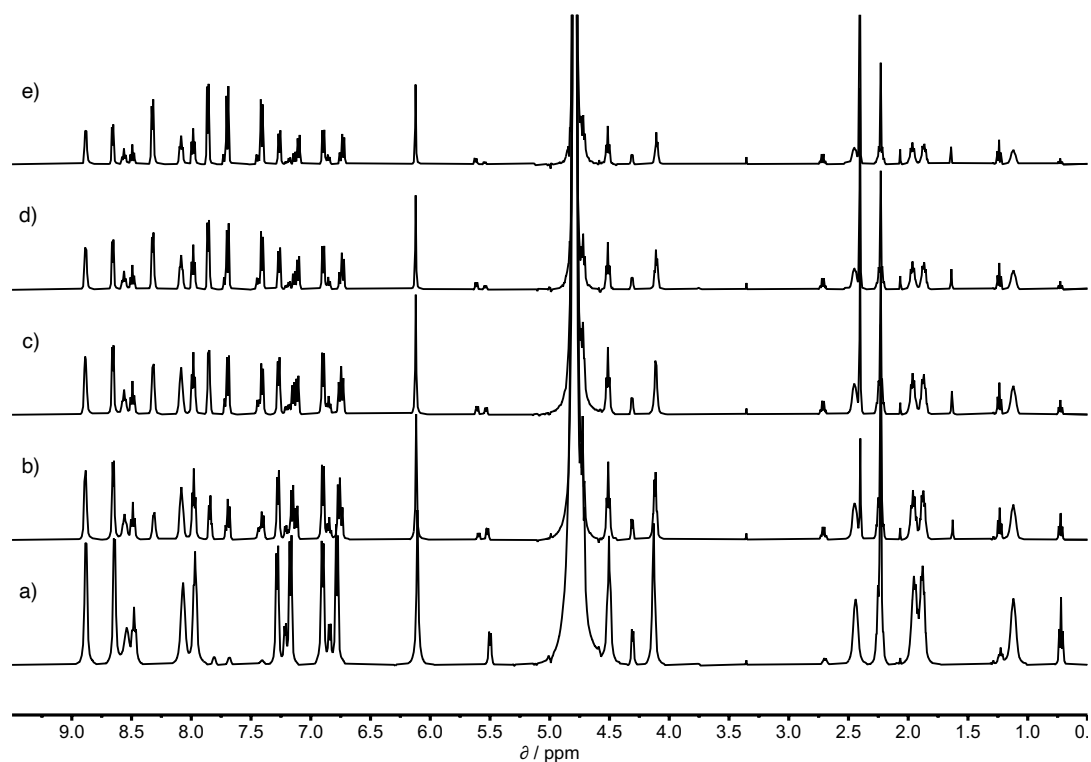


Figure S90. 500MHz ^1H NMR for titration of **6** into a mixture of **1** and **14** in D_2O at 298K. Concentrations are: a) **1**: 0.58 mM; **14**: 0.67 mM; **6**: 0 mM; b) **1**: 0.41 mM; **14**: 0.47 mM; **6**: 0.55 mM; c) **1**: 0.32 mM; **14**: 0.37 mM; **6**: 0.85 mM; d) **1**: 0.26 mM; **14**: 0.30 mM; **6**: 1.04 mM; e) **1**: 0.22 mM; **14**: 0.25 mM; **6**: 1.04 mM. Integration of selected proton signals indicated that $K(\mathbf{1}\cdot\mathbf{14}) = 2.3 \pm 0.3 \times K(\mathbf{1}\cdot\mathbf{6})$.

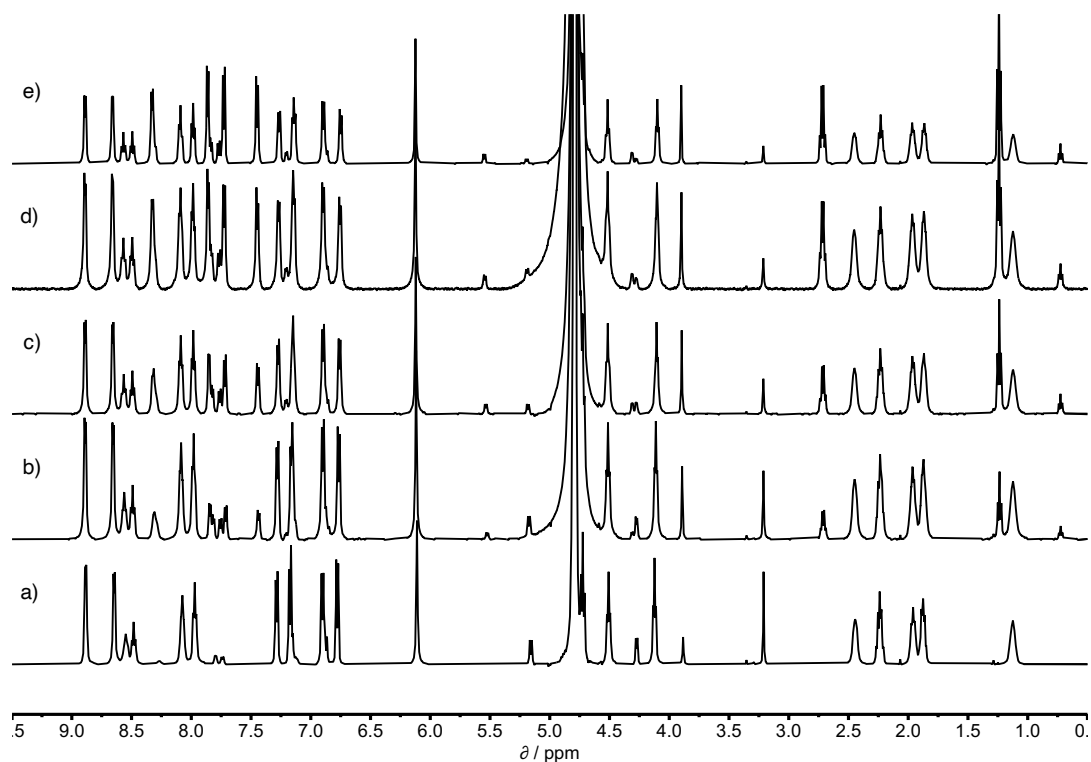


Figure S91. 500MHz ^1H NMR for titration of **14** into a mixture of **1** and **10** in D_2O at 298K. Concentrations are: a) **1**: 0.58 mM; **14**: 0 mM; **10**: 0.68 mM; b) **1**: 0.41 mM; **14**: 0.47 mM; **10**: 0.48 mM; c) **1**: 0.32 mM; **14**: 0.73 mM; **10**: 0.37 mM; d) **1**: 0.26 mM; **14**: 0.89 mM; **10**: 0.30 mM; e) **1**: 0.22 mM; **14**: 1.00 mM; **10**: 0.26 mM. Integration of selected proton signals indicated that $K(\mathbf{1}\cdot\mathbf{10}) = 2.4 \pm 0.4 \times K(\mathbf{1}\cdot\mathbf{14})$.

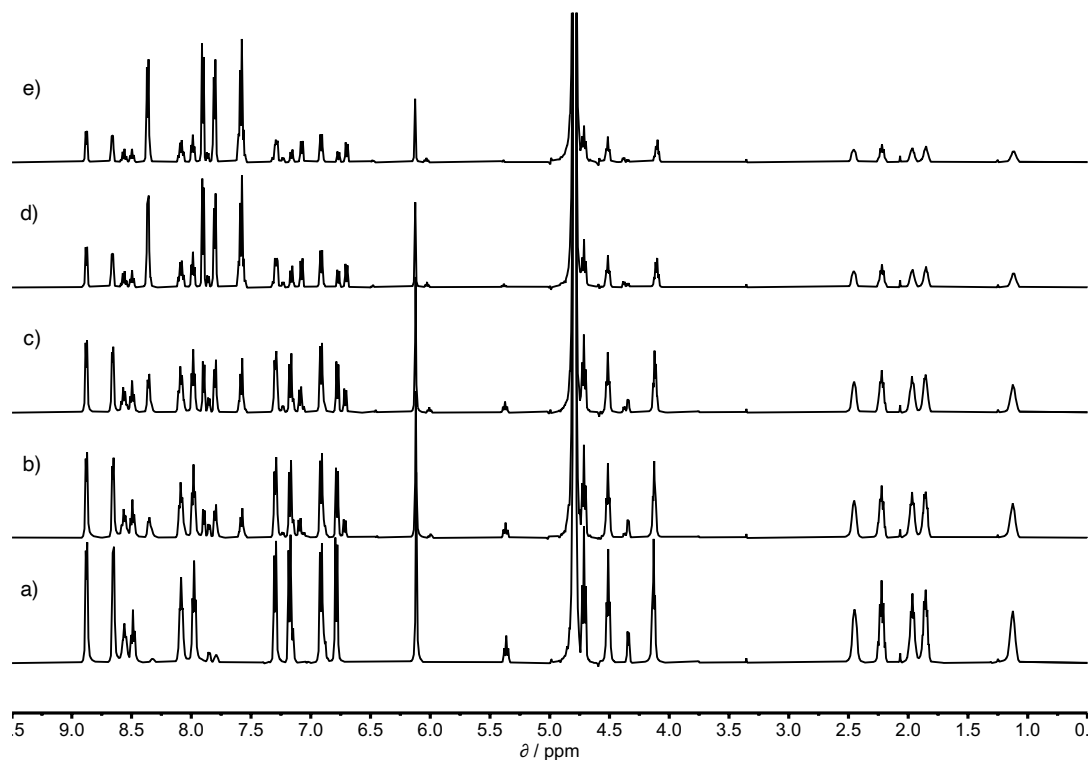


Figure S92. 500MHz ^1H NMR for titration of **5** into a mixture of **1** and **15** in D_2O at 298K. Concentrations are: a) **1**: 0.56 mM; **5**: 0 mM; **15**: 0.63 mM; b) **1**: 0.45 mM; **5**: 0.51 mM; **15**: 0.50 mM; c) **1**: 0.38 mM; **5**: 0.85 mM; **15**: 0.42 mM; d) **1**: 0.21 mM; **5**: 1.62 mM; **15**: 0.23 mM; e) **1**: 0.16 mM; **5**: 1.82 mM; **15**: 0.18 mM. Integration of selected proton signals indicated that $K(\mathbf{1}\cdot\mathbf{15}) = 8.4 \pm 1.5 \times K(\mathbf{1}\cdot\mathbf{5})$.

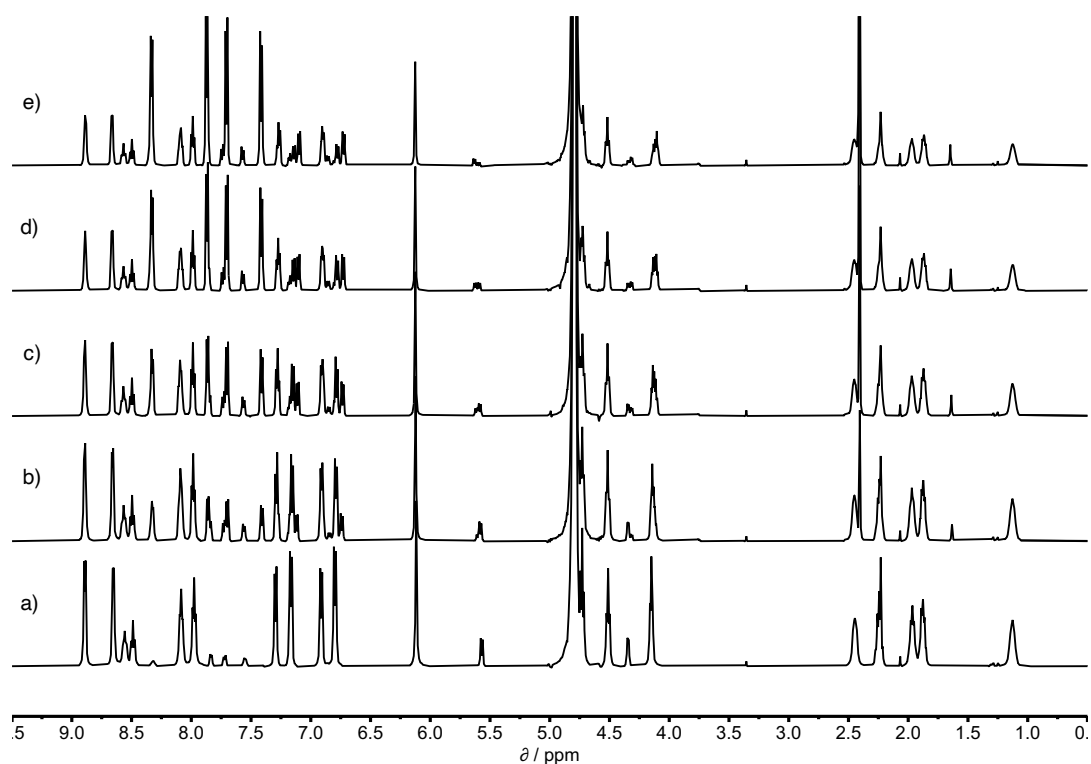


Figure S93. 500MHz ^1H NMR for titration of **6** into a mixture of **1** and **16** in D_2O at 298K. Concentrations are: a) **1**: 0.56 mM; **6**: 0 mM; **16**: 0.69 mM; b) **1**: 0.40 mM; **6**: 0.55 mM; **16**: 0.49 mM; c) **1**: 0.31 mM; **6**: 0.85 mM; **16**: 0.38 mM; d) **1**: 0.23 mM; **6**: 1.13 mM; **16**: 0.28 mM; e) **1**: 0.17 mM; **6**: 1.32 mM; **16**: 0.21 mM. Integration of selected proton signals indicated that $K(\mathbf{1}\cdot\mathbf{16}) = 5.1 \pm 1.4 \times K(\mathbf{1}\cdot\mathbf{6})$.

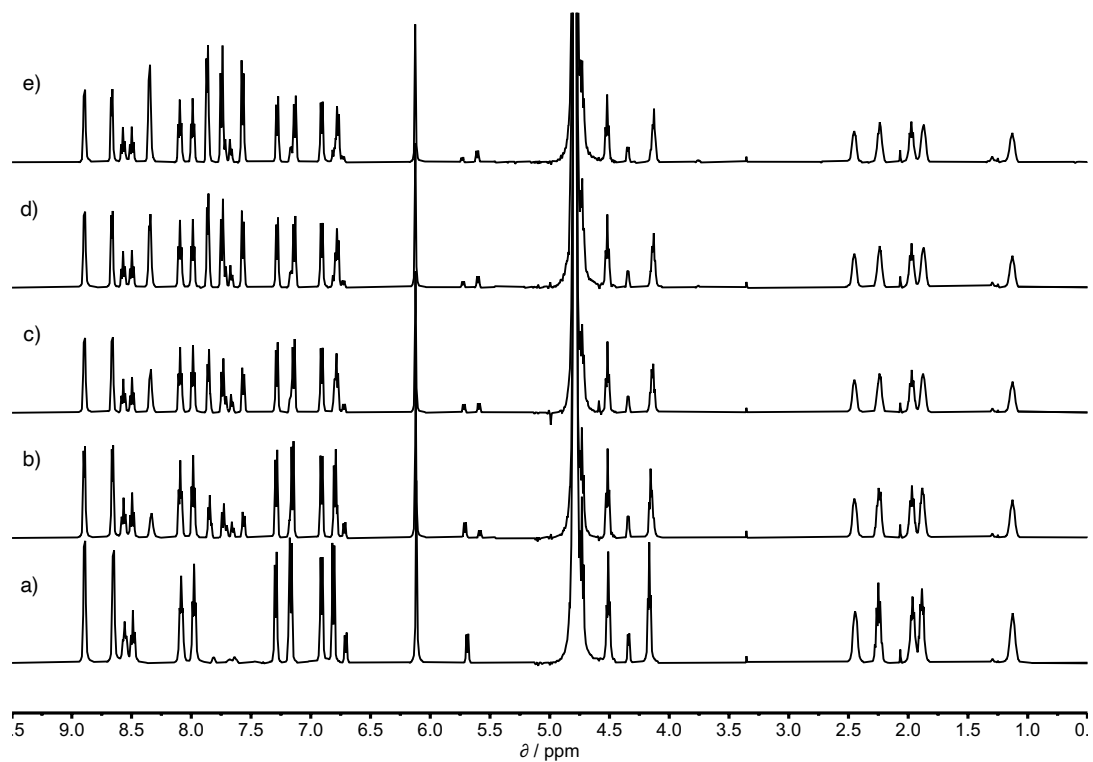


Figure S94. 500MHz ¹H NMR for titration of **16** into a mixture of **1** and **17** in D₂O at 298K. Concentrations are: a) **1**: 0.50 mM; **16**: 0 mM; **17**: 0.59 mM; b) **1**: 0.37 mM; **16**: 0.44 mM; **17**: 0.43 mM; c) **1**: 0.29 mM; **16**: 0.69 mM; **17**: 0.34 mM; d) **1**: 0.24 mM; **16**: 0.86 mM; **17**: 0.28 mM; e) **1**: 0.20 mM; **16**: 0.98 mM; **17**: 0.24 mM. Integration of selected proton signals indicated that $K(1\cdot17) = 1.8 \pm 0.1 \times K(1\cdot16)$.

4.2. Octachloro-super-aryl-extended calix[4]pyrrole **2**

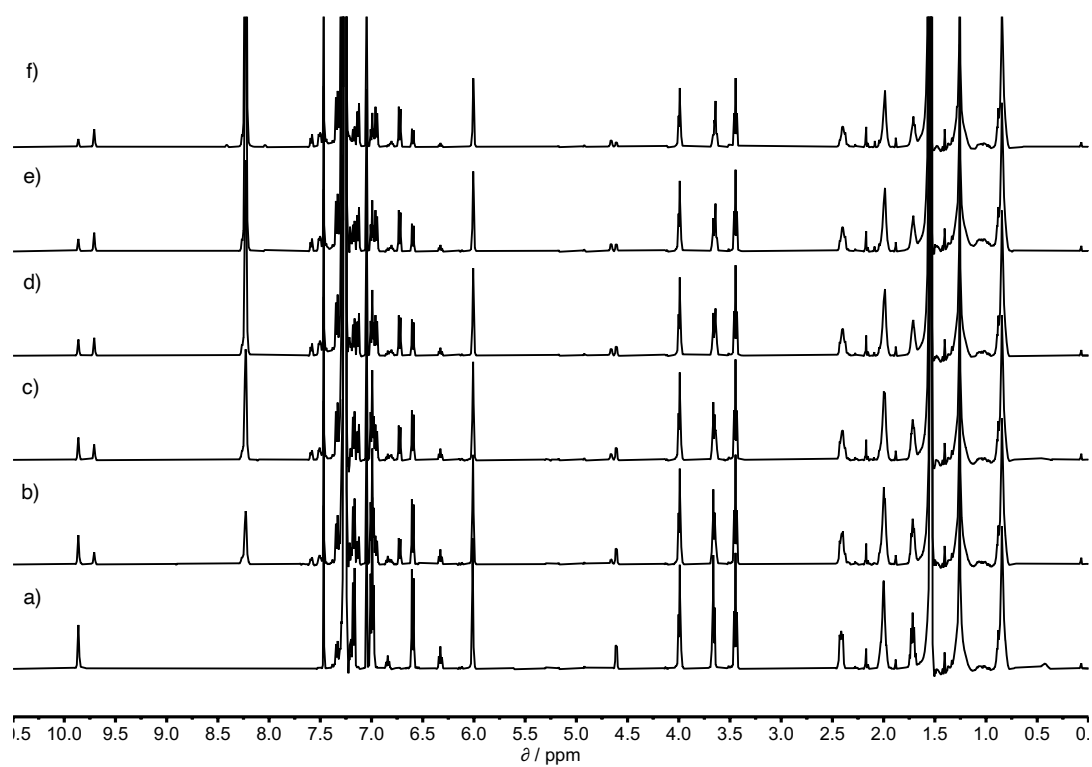


Figure S95. 500MHz ^1H NMR for titration of **PNO** into a mixture of **2** and **5** in CDCl_3 at 298K. Concentrations are: a) **2**: 0.13 mM; **PNO**: 0 mM; **5**: 0.18 mM; b) **2**: 0.12 mM; **PNO**: 0.53 mM; **5**: 0.16 mM; c) **2**: 0.11 mM; **PNO**: 0.99 mM; **5**: 0.15 mM; d) **2**: 0.10 mM; **PNO**: 1.62 mM; **5**: 0.14 mM; e) **2**: 0.09 mM; **PNO**: 2.13 mM; **5**: 0.12 mM; f) **2**: 0.08 mM; **PNO**: 2.90 mM; **5**: 0.10 mM. Integration of selected proton signals indicated that $K(\mathbf{2}\cdot\mathbf{5}) = 17.4 \pm 2.3 \times K(\mathbf{2}\cdot\mathbf{PNO})$.

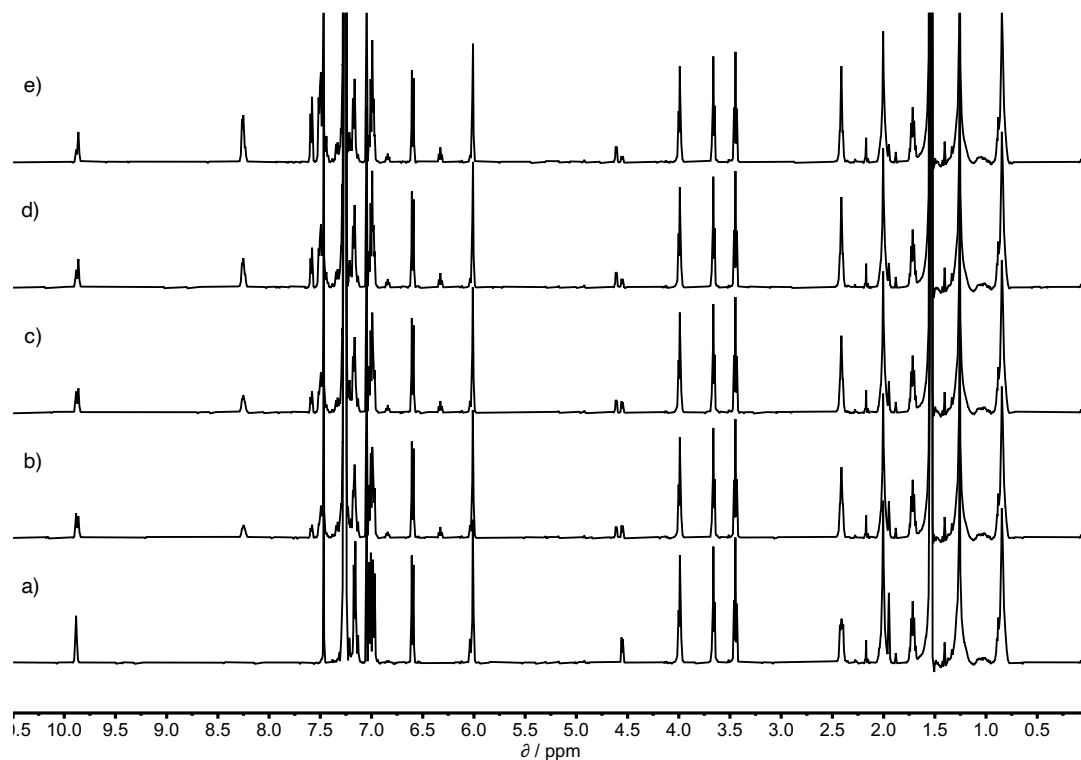


Figure S96. 500MHz ^1H NMR for titration of **5** into a mixture of **2** and **6** in CDCl_3 at 298K. Concentrations are: a) **2**: 0.13 mM; **5**: 0 mM; **6**: 0.16 mM; b) **2**: 0.12 mM; **5**: 0.17 mM; **6**: 0.16 mM; c) **2**: 0.12 mM; **5**: 0.22 mM; **6**: 0.16 mM; d) **2**: 0.12 mM; **5**: 0.32 mM; **6**: 0.15 mM; e) **2**: 0.12 mM; **5**: 0.47 mM; **6**: 0.15 mM. Integration of selected proton signals indicated that $K(\mathbf{2}\cdot\mathbf{6}) = 1.4 \pm 0.1 \times K(\mathbf{2}\cdot\mathbf{5})$.

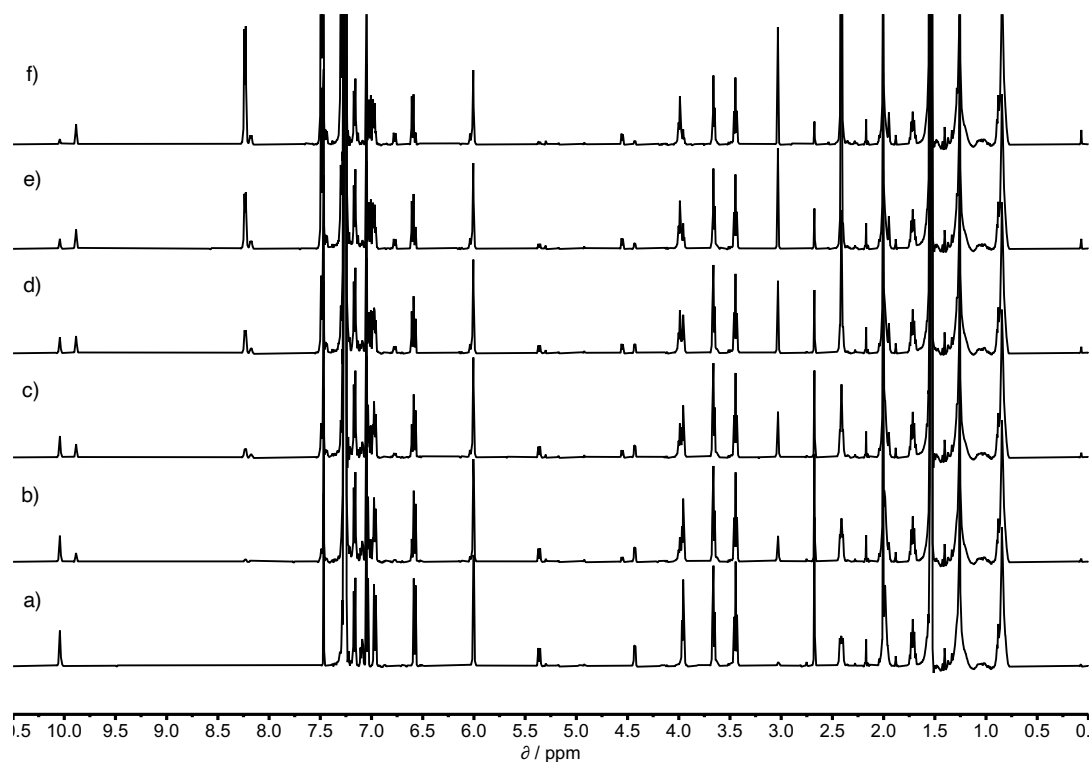


Figure S97. 500MHz ^1H NMR for titration of **6** into a mixture of **2** and **7** in CDCl_3 at 298K. Concentrations are: a) **2**: 0.13 mM; **6**: 0 mM; **7**: 0.15 mM; b) **2**: 0.12 mM; **6**: 0.08 mM; **7**: 0.15 mM; c) **2**: 0.12 mM; **6**: 0.25 mM; **7**: 0.15 mM; d) **2**: 0.12 mM; **6**: 0.29 mM; **7**: 0.14 mM; e) **2**: 0.11 mM; **6**: 0.53 mM; **7**: 0.13 mM; f) **2**: 0.09 mM; **6**: 0.88 mM; **7**: 0.11 mM. Integration of selected proton signals indicated that $K(\mathbf{2}\cdot\mathbf{7}) = 2.5 \pm 0.1 \times K(\mathbf{2}\cdot\mathbf{6})$.

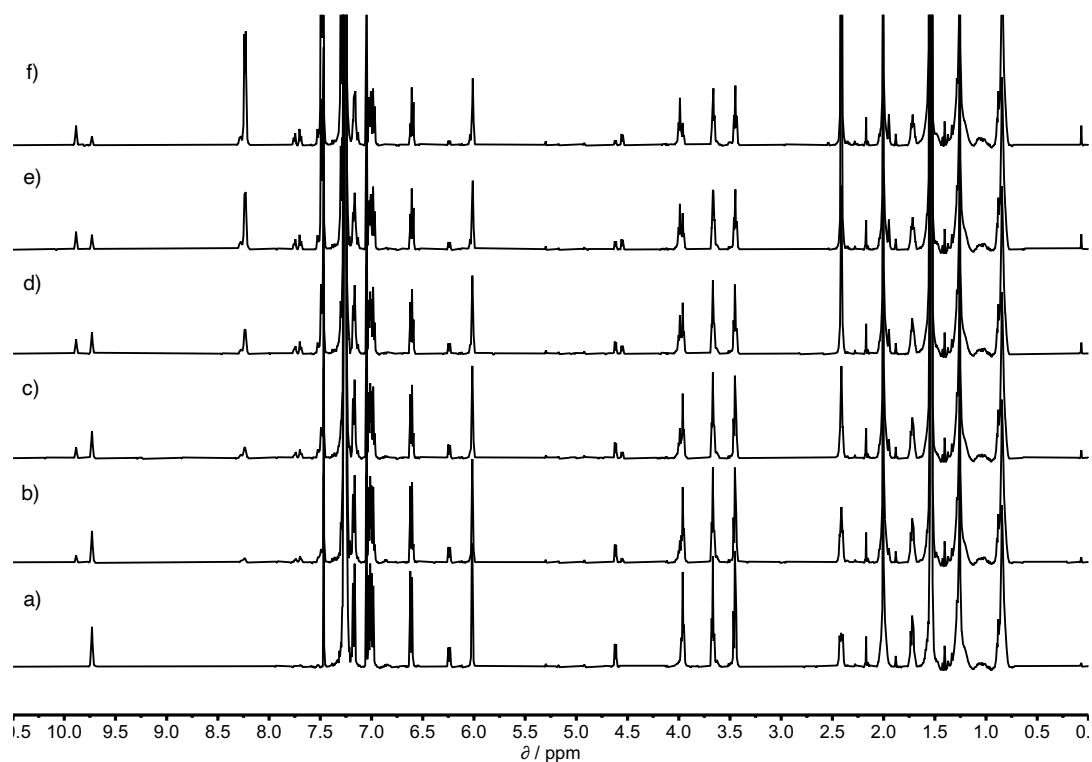


Figure S98. 500MHz ^1H NMR for titration of **6** into a mixture of **2** and **8** in CDCl_3 at 298K. Concentrations are: a) **2**: 0.13 mM; **6**: 0 mM; **8**: 0.15 mM; b) **2**: 0.12 mM; **6**: 0.08 mM; **8**: 0.15 mM; c) **2**: 0.12 mM; **6**: 0.25 mM; **8**: 0.15 mM; d) **2**: 0.11 mM; **6**: 0.29 mM; **8**: 0.14 mM; e) **2**: 0.10 mM; **6**: 0.52 mM; **8**: 0.13 mM; f) **2**: 0.09 mM; **6**: 0.87 mM; **8**: 0.11 mM. Integration of selected proton signals indicated that $K(\mathbf{2}\cdot\mathbf{8}) = 4.6 \pm 0.0 \times K(\mathbf{2}\cdot\mathbf{6})$.

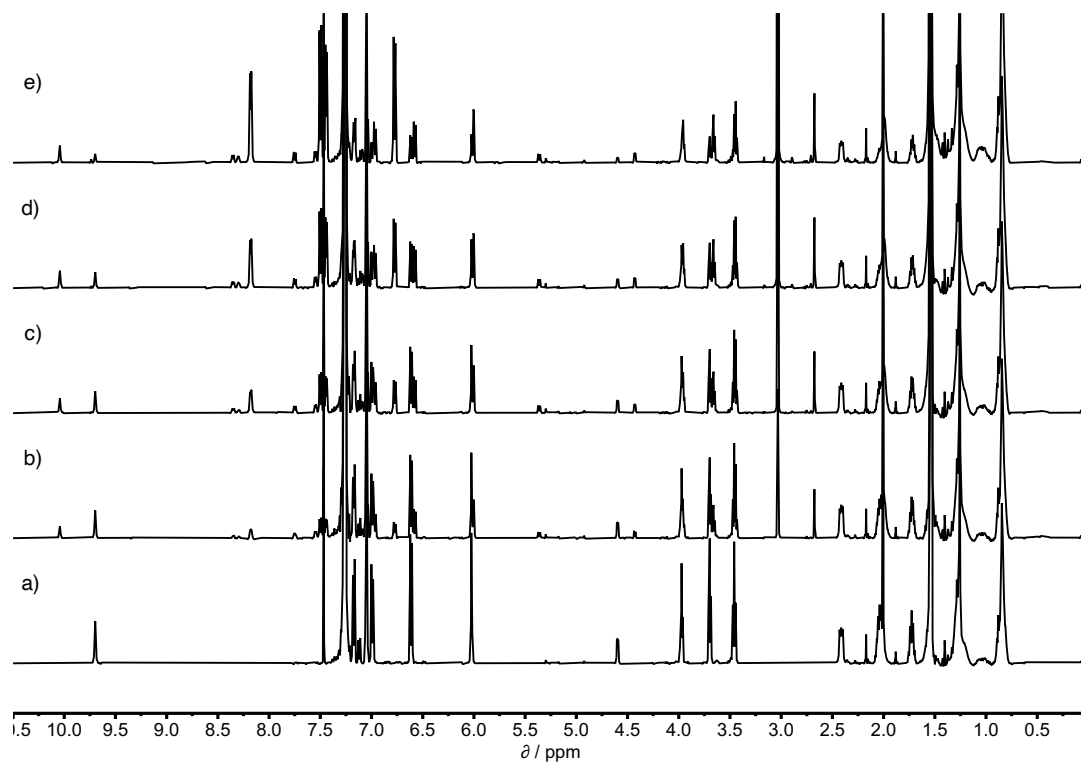


Figure S99. 500MHz ^1H NMR for titration of **7** into a mixture of **2** and **9** in CDCl_3 at 298K. Concentrations are: a) **2**: 0.13 mM; **7**: 0 mM; **9**: 0.15 mM; b) **2**: 0.12 mM; **7**: 0.16 mM; **9**: 0.14 mM; c) **2**: 0.11 mM; **7**: 0.28 mM; **9**: 0.13 mM; d) **2**: 0.10 mM; **7**: 0.47 mM; **9**: 0.11 mM; e) **2**: 0.08 mM; **7**: 0.75 mM; **9**: 0.09 mM. Integration of selected proton signals indicated that $K(\mathbf{2}\cdot\mathbf{9}) = 5.2 \pm 0.1 \times K(\mathbf{2}\cdot\mathbf{7})$.

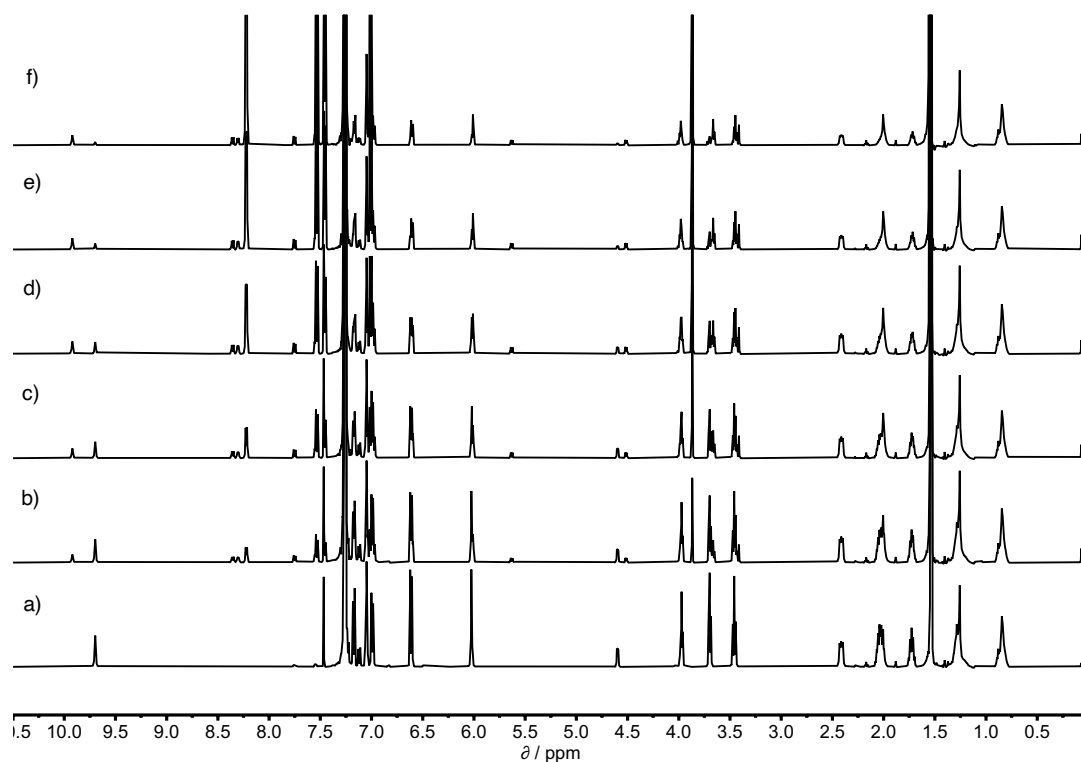


Figure S100. 500MHz ^1H NMR for titration of **10** into a mixture of **2** and **9** in CDCl_3 at 298K. Concentrations are: a) **2**: 0.20 mM; **10**: 0 mM; **9**: 0.26 mM; b) **2**: 0.18 mM; **10**: 0.23 mM; **9**: 0.23 mM; c) **2**: 0.17 mM; **10**: 0.42 mM; **9**: 0.21 mM; d) **2**: 0.14 mM; **10**: 0.73 mM; **9**: 0.18 mM; e) **2**: 0.11 mM; **10**: 1.14 mM; **9**: 0.14 mM; f) **2**: 0.08 mM; **10**: 1.51 mM; **9**: 0.10 mM. Integration of selected proton signals indicated that $K(\mathbf{2}\cdot\mathbf{9}) = 5.3 \pm 0.1 \times K(\mathbf{2}\cdot\mathbf{10})$.

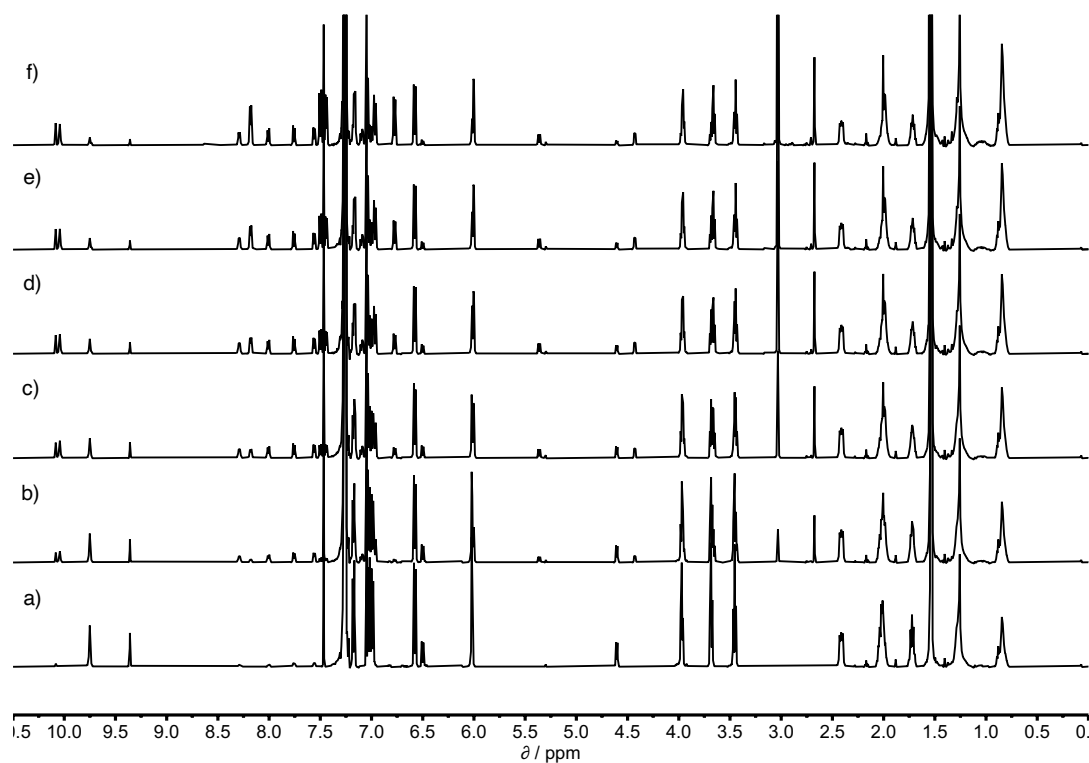


Figure S101. 500MHz ^1H NMR for titration of **7** into a mixture of **2** and **11** in CDCl_3 at 298K. Concentrations are: a) **2**: 0.20 mM; **7**: 0 mM; **11**: 0.26 mM; b) **2**: 0.19 mM; **7**: 0.11 mM; **11**: 0.25 mM; c) **2**: 0.18 mM; **7**: 0.23 mM; **11**: 0.23 mM; d) **2**: 0.17 mM; **7**: 0.33 mM; **11**: 0.22 mM; e) **2**: 0.16 mM; **7**: 0.42 mM; **11**: 0.21 mM; f) **2**: 0.14 mM; **7**: 0.59 mM; **11**: 0.19 mM. Integration of selected proton signals indicated that $K(\mathbf{2}\cdot\mathbf{11}) = 1.2 \pm 0.1 \times K(\mathbf{2}\cdot\mathbf{7})$.

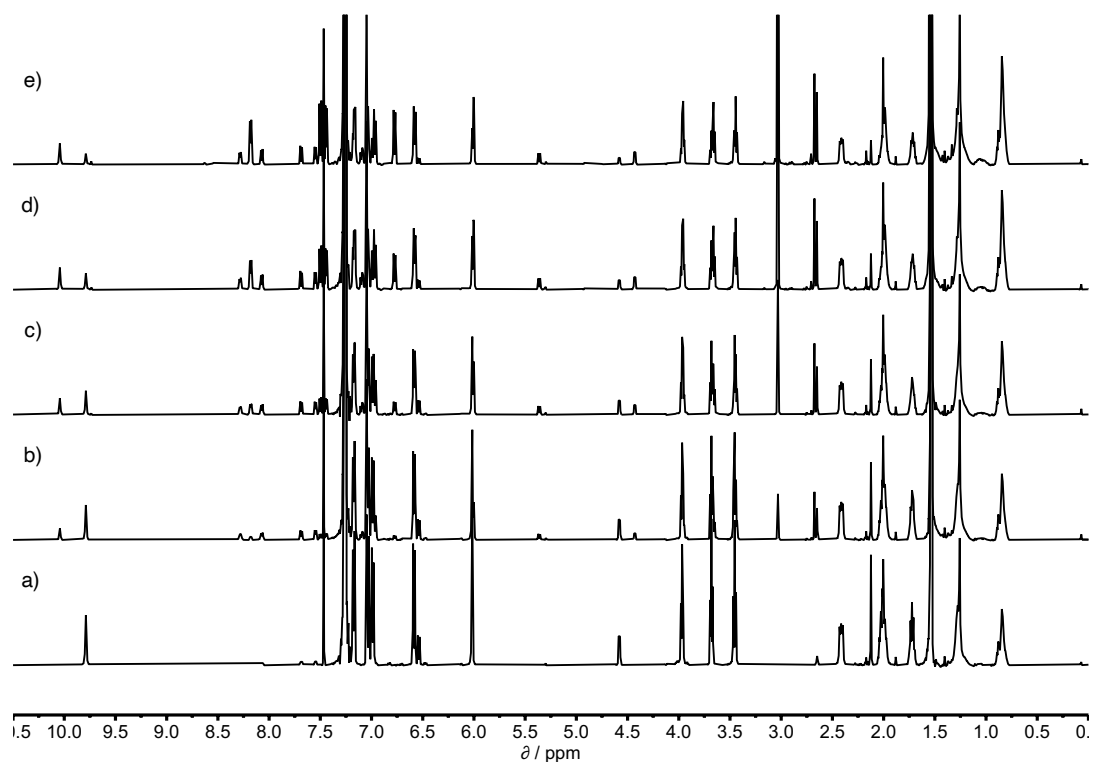


Figure S102. 500MHz ^1H NMR for titration of **7** into a mixture of **2** and **12** in CDCl_3 at 298K. Concentrations are: a) **2**: 0.21 mM; **7**: 0 mM; **12**: 0.27 mM; b) **2**: 0.20 mM; **7**: 0.11 mM; **12**: 0.25 mM; c) **2**: 0.18 mM; **7**: 0.23 mM; **12**: 0.23 mM; d) **2**: 0.16 mM; **7**: 0.43 mM; **12**: 0.21 mM; e) **2**: 0.14 mM; **7**: 0.59 mM; **12**: 0.19 mM. Integration of selected proton signals indicated that $K(\mathbf{2}\cdot\mathbf{12}) = 1.8\pm 0.1 \times K(\mathbf{2}\cdot\mathbf{7})$.

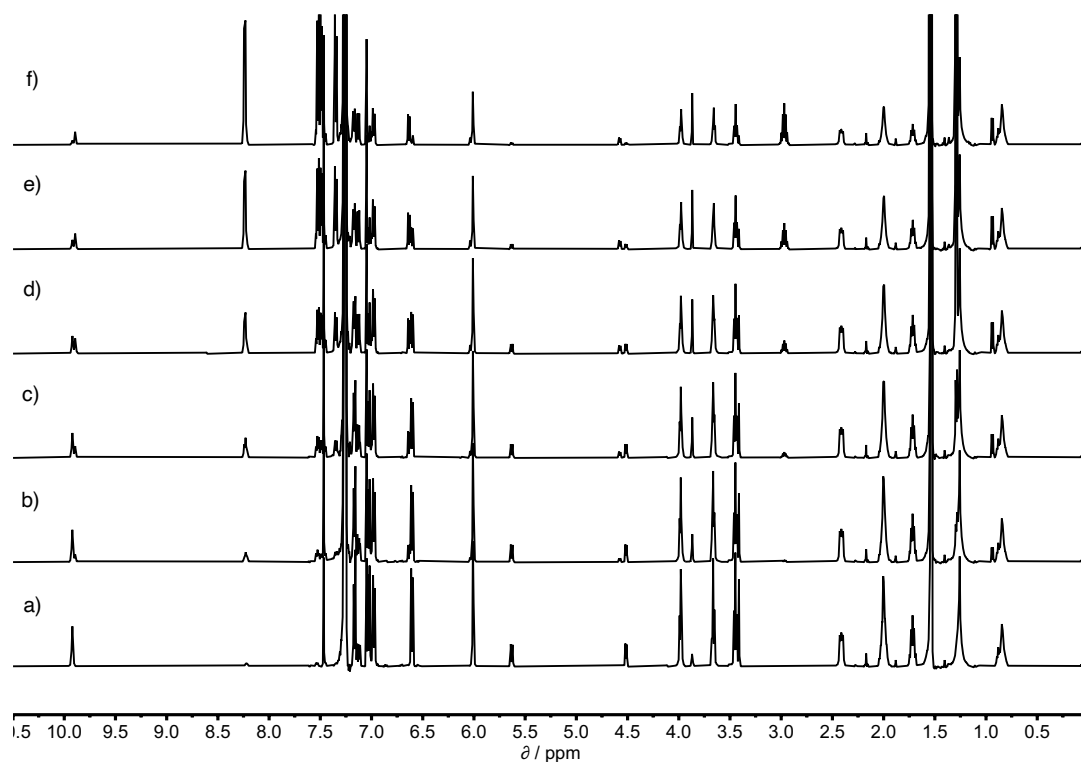


Figure S103. 500MHz ^1H NMR for titration of **13** into a mixture of **2** and **10** in CDCl_3 at 298K. Concentrations are: a) **2**: 0.20 mM; **13**: 0 mM; **10**: 0.26 mM; b) **2**: 0.19 mM; **13**: 0.10 mM; **10**: 0.24 mM; c) **2**: 0.18 mM; **13**: 0.22 mM; **10**: 0.23 mM; d) **2**: 0.16 mM; **13**: 0.41 mM; **10**: 0.20 mM; e) **2**: 0.13 mM; **13**: 0.68 mM; **10**: 0.16 mM; f) **2**: 0.09 mM; **13**: 1.00 mM; **10**: 0.12 mM. Integration of selected proton signals indicated that $K(\mathbf{2}\cdot\mathbf{10}) = 3.3\pm 0.6 \times K(\mathbf{2}\cdot\mathbf{13})$.

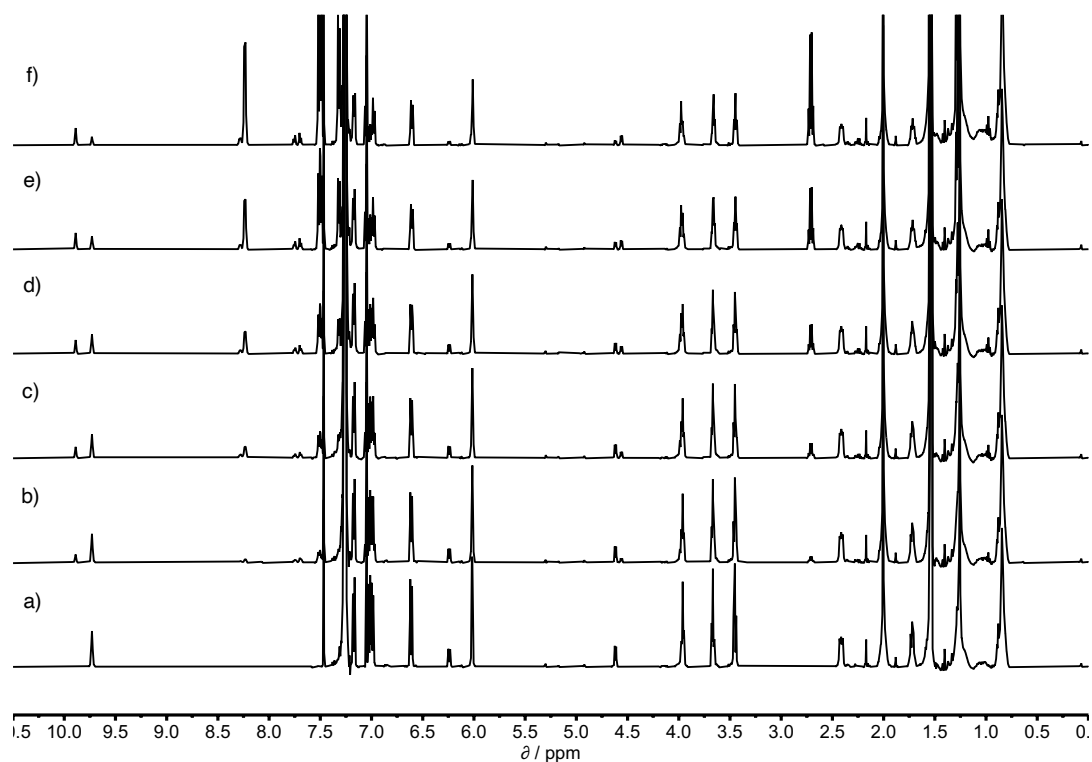


Figure S104. 500MHz ^1H NMR for titration of **14** into a mixture of **2** and **8** in CDCl_3 at 298K. Concentrations are: a) **2**: 0.13 mM; **14**: 0 mM; **8**: 0.15 mM; b) **2**: 0.12 mM; **14**: 0.09 mM; **8**: 0.15 mM; c) **2**: 0.12 mM; **14**: 0.17 mM; **8**: 0.14 mM; d) **2**: 0.11 mM; **14**: 0.28 mM; **8**: 0.14 mM; e) **2**: 0.10 mM; **14**: 0.50 mM; **8**: 0.12 mM; f) **2**: 0.08 mM; **14**: 0.81 mM; **8**: 0.08 mM. Integration of selected proton signals indicated that $K(\mathbf{2}\cdot\mathbf{8}) = 4.6 \pm 0.7 \times K(\mathbf{2}\cdot\mathbf{14})$.

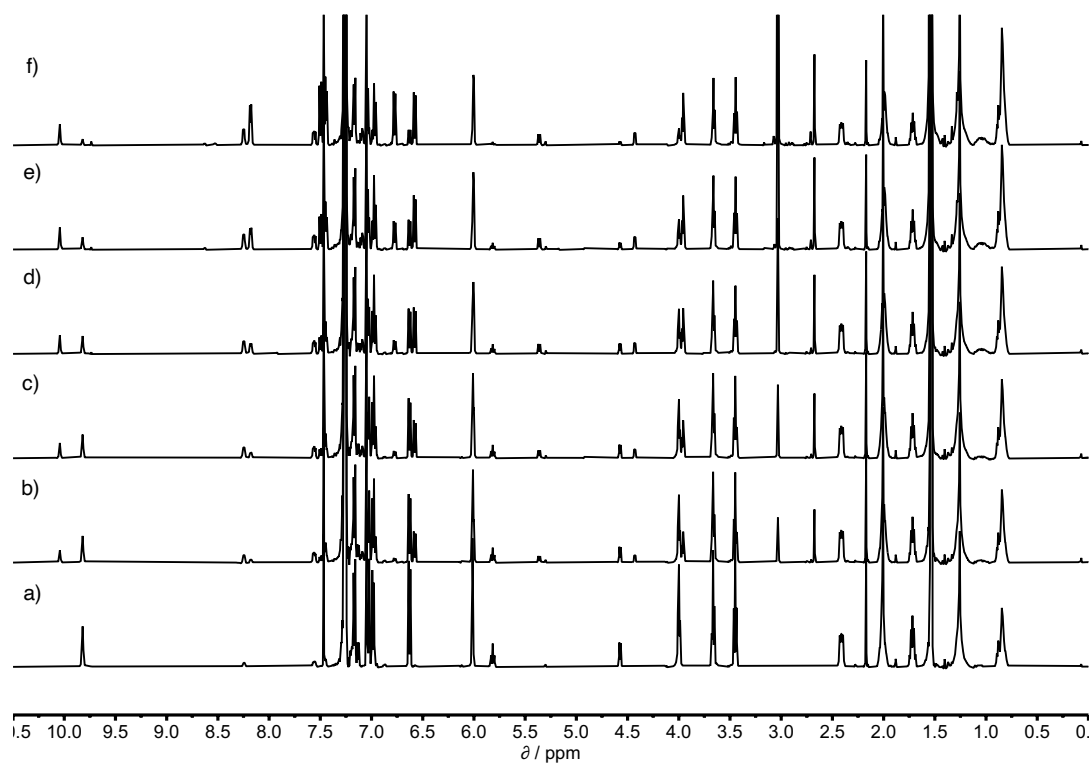


Figure S105. 500MHz ^1H NMR for titration of **7** into a mixture of **2** and **15** in CDCl_3 at 298K. Concentrations are: a) **2**: 0.19 mM; **7**: 0 mM; **15**: 0.25 mM; b) **2**: 0.18 mM; **7**: 0.13 mM; **15**: 0.23 mM; c) **2**: 0.18 mM; **7**: 0.17 mM; **15**: 0.22 mM; d) **2**: 0.17 mM; **7**: 0.26 mM; **15**: 0.21 mM; e) **2**: 0.15 mM; **7**: 0.41 mM; **15**: 0.19 mM; f) **2**: 0.13 mM; **7**: 0.63 mM; **15**: 0.17 mM. Integration of selected proton signals indicated that $K(\mathbf{2}\cdot\mathbf{15}) = 1.3 \pm 0.3 \times K(\mathbf{2}\cdot\mathbf{7})$.

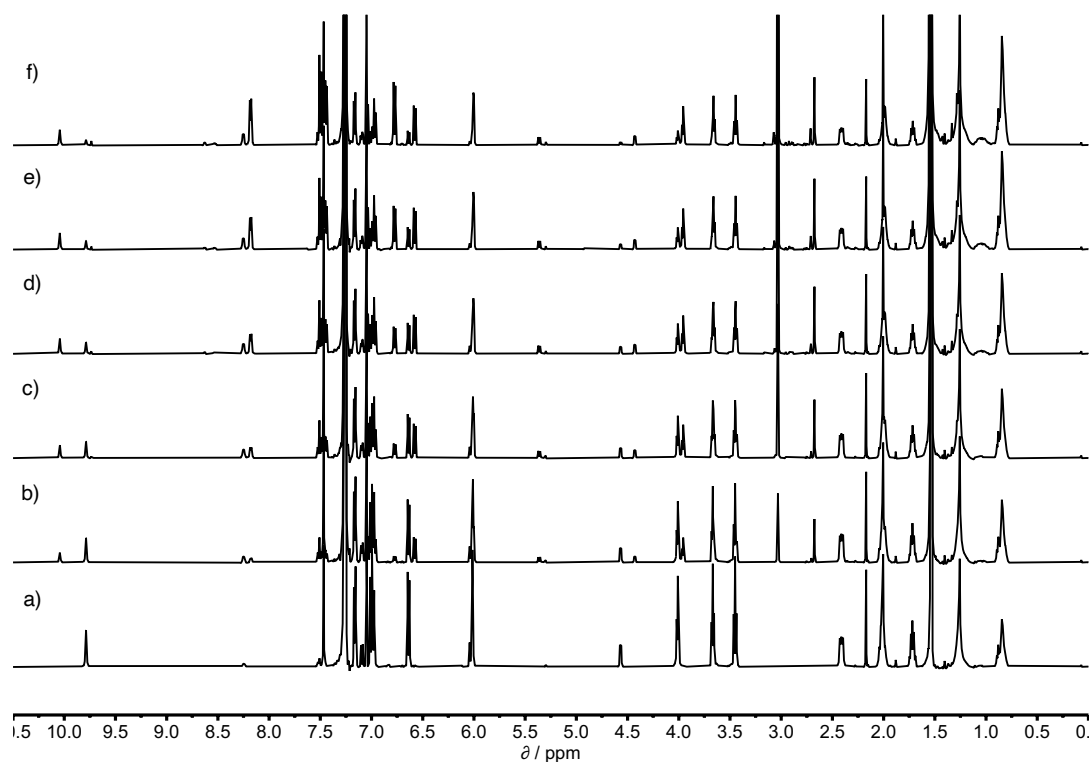


Figure S106. 500MHz ^1H NMR for titration of **7** into a mixture of **2** and **16** in CDCl_3 at 298K. Concentrations are: a) **2**: 0.20 mM; **7**: 0 mM; **16**: 0.26 mM; b) **2**: 0.18 mM; **7**: 0.16 mM; **16**: 0.24 mM; c) **2**: 0.17 mM; **7**: 0.29 mM; **16**: 0.22 mM; d) **2**: 0.16 mM; **7**: 0.44 mM; **16**: 0.20 mM; e) **2**: 0.14 mM; **7**: 0.60 mM; **16**: 0.18 mM; f) **2**: 0.12 mM; **7**: 0.78 mM; **16**: 0.16 mM. Integration of selected proton signals indicated that $K(\mathbf{2}\cdot\mathbf{16}) = 2.3 \pm 0.5 \times K(\mathbf{2}\cdot\mathbf{7})$.

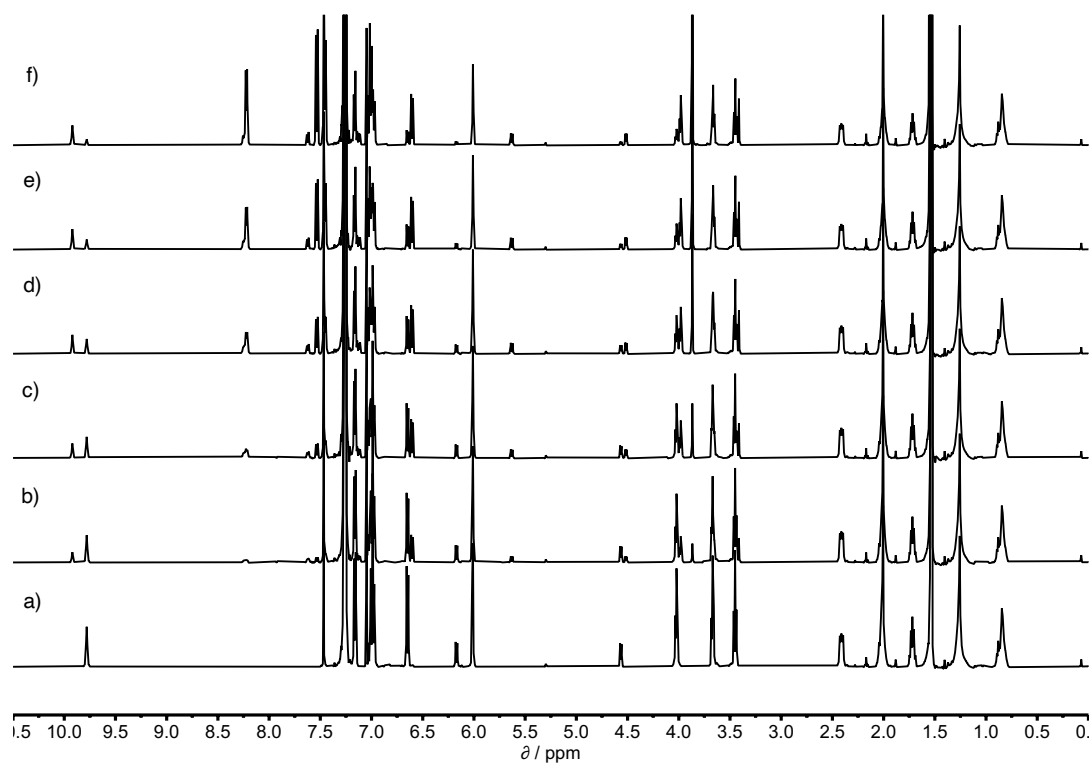


Figure S107. 500MHz ^1H NMR for titration of **10** into a mixture of **2** and **17** in CDCl_3 at 298K. Concentrations are: a) **2**: 0.20 mM; **10**: 0 mM; **17**: 0.25 mM; b) **2**: 0.19 mM; **10**: 0.10 mM; **17**: 0.24 mM; c) **2**: 0.18 mM; **10**: 0.20 mM; **17**: 0.23 mM; d) **2**: 0.17 mM; **10**: 0.36 mM; **17**: 0.22 mM; e) **2**: 0.15 mM; **10**: 0.57 mM; **17**: 0.20 mM; f) **2**: 0.13 mM; **10**: 0.84 mM; **17**: 0.17 mM. Integration of selected proton signals indicated that $K(\mathbf{2}\cdot\mathbf{17}) = 1.5 \pm 0.2 \times K(\mathbf{2}\cdot\mathbf{10})$.

4.3. Tetrachloro-aryl-extended calix[4]pyrrole 4

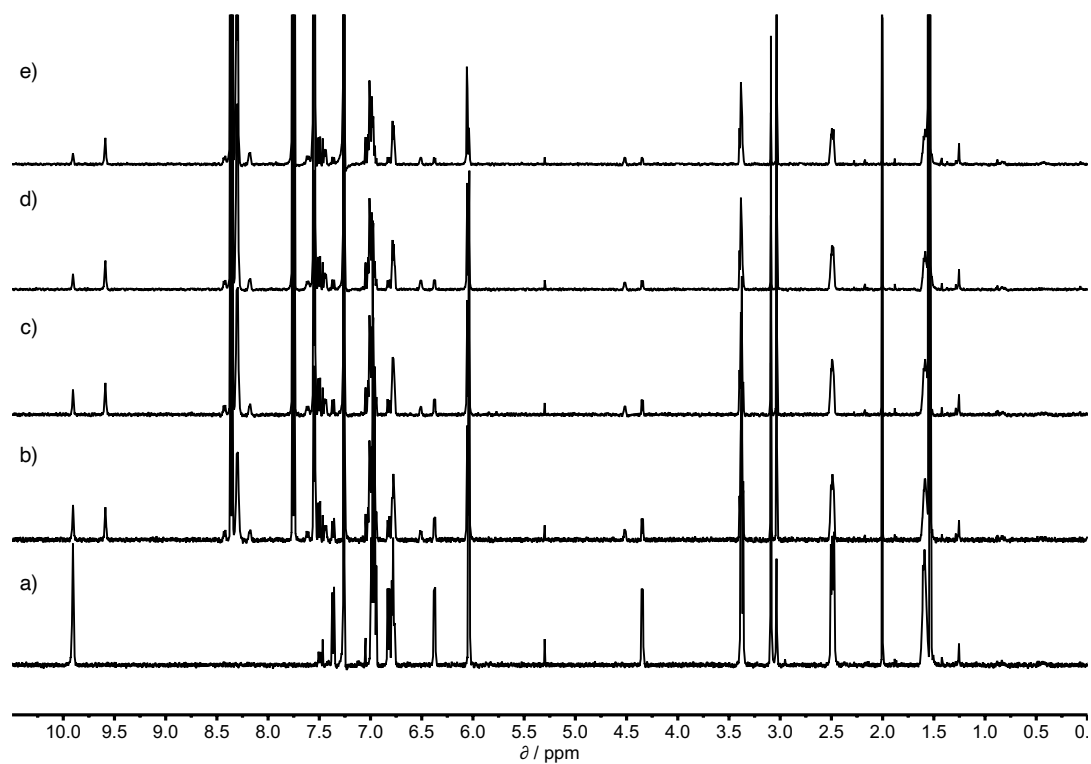


Figure S108. 500MHz ^1H NMR for titration of **9** into a mixture of **4** and **7** in CDCl_3 at 298K. Concentrations are: a) **4**: 0.79 mM; **7**: 0.93 mM; **9**: 0 mM; b) **4**: 0.45 mM; **7**: 0.53 mM; **9**: 2.12mM; c) **4**: 0.37 mM; **7**: 0.44 mM; **9**: 2.62mM; d) **4**: 0.29 mM; **7**: 0.34 mM; **9**: 3.15mM; e) **4**: 0.23 mM; **7**: 0.28 mM; **9**: 3.48 mM. Integration of selected proton signals indicated that $K(\mathbf{4}\cdot\mathbf{7}) = 6.3 \pm 0.7 \times K(\mathbf{4}\cdot\mathbf{9})$

5. Results of titration experiments

Table S1. Thermodynamic parameters for formation of 1:1 complexes in water at 298 K.^a

Guest	X	Host							
		1				3			
		K / M^{-1b}	$\Delta G^\circ / \text{kJ mol}^{-1b}$	$\Delta H^\circ / \text{kJ mol}^{-1b}$	$-T\Delta S^\circ / \text{kJ mol}^{-1b}$	K / M^{-1c}	$\Delta G^\circ / \text{kJ mol}^{-1c}$	$\Delta H^\circ / \text{kJ mol}^{-1c}$	$-T\Delta S^\circ / \text{kJ mol}^{-1c}$
PNO	-	$3.5 \pm 0.1 \times 10^6$	-37.4 ± 0.0	-43.8 ± 0.1	6.4 ± 0.2	$3.3 \pm 0.6 \times 10^5$	-31.5 ± 0.4	-34.3 ± 0.3	2.8 ± 0.6
5	H	$2.6 \pm 0.6 \times 10^9$	-53.7 ± 0.6	-56.8 ± 0.6	3.0 ± 0.7	$1.2 \pm 0.1 \times 10^6$	-34.7 ± 0.4	-41.9 ± 1.4	7.1 ± 1.3
6	Me	$2.3 \pm 0.9 \times 10^{10}$	-59.1 ± 1.0	-62.8 ± 0.3	3.7 ± 1.0	$1.4 \pm 0.1 \times 10^6$	-35.0 ± 0.2	-43.6 ± 2.2	8.6 ± 2.3
7	NMe ₂	$4.1 \pm 1.3 \times 10^{11}$	-66.2 ± 0.8	-72.7 ± 1.7	6.5 ± 1.9	$1.2 \pm 0.0 \times 10^6$	-34.7 ± 0.1	-41.7 ± 3.1	7.0 ± 3.1
8	CF ₃	$1.9 \pm 0.7 \times 10^{11}$	-64.4 ± 1.0	-67.4 ± 0.8	3.0 ± 1.3	$1.1 \pm 0.1 \times 10^6$	-34.4 ± 0.2	-45.3 ± 2.1	10.9 ± 1.9
9	NO ₂	$4.1 \pm 1.9 \times 10^{12}$	-72.0 ± 1.2	-89.8 ± 1.4	17.9 ± 1.8	$9.3 \pm 1.0 \times 10^5$	-34.1 ± 0.3	-46.9 ± 1.7	12.7 ± 1.4
10	OMe	$1.4 \pm 0.7 \times 10^{11}$	-63.6 ± 1.2	-75.4 ± 0.4	11.8 ± 1.2	$1.2 \pm 0.2 \times 10^6$	-34.8 ± 0.5	-43.5 ± 0.7	8.7 ± 1.1
11	CHO	$3.6 \pm 1.6 \times 10^{11}$	-65.9 ± 1.1	-79.2 ± 0.8	13.3 ± 1.4	$1.1 \pm 0.1 \times 10^6$	-34.4 ± 0.1	-46.5 ± 2.7	12.0 ± 2.7
12	COMe	$1.2 \pm 0.5 \times 10^{12}$	-68.9 ± 1.0	-84.8 ± 1.1	15.3 ± 1.5	$9.2 \pm 1.6 \times 10^5$	-34.0 ± 0.4	-45.3 ± 0.6	11.3 ± 0.8
13	iPr	$9.8 \pm 4.0 \times 10^{10}$	-62.7 ± 1.0	-61.3 ± 0.7	-1.4 ± 1.2	$1.3 \pm 0.0 \times 10^6$	-35.0 ± 0.1	-50.8 ± 0.4	15.8 ± 0.5
14	Et	$5.9 \pm 2.8 \times 10^{10}$	-61.4 ± 1.2	-58.4 ± 2.3	-3.0 ± 2.6	$1.1 \pm 0.2 \times 10^6$	-34.4 ± 0.4	-43.1 ± 1.0	8.5 ± 1.3
15	F	$2.2 \pm 0.6 \times 10^{10}$	-59.0 ± 0.7	-61.6 ± 0.6	2.6 ± 0.9	$1.1 \pm 0.1 \times 10^6$	-34.4 ± 0.3	-42.2 ± 0.9	7.7 ± 1.0
16	Cl	$1.1 \pm 0.4 \times 10^{11}$	-62.9 ± 0.9	-65.8 ± 2.3	2.9 ± 2.4	$1.1 \pm 0.1 \times 10^6$	-34.4 ± 0.2	-43.6 ± 1.7	9.1 ± 1.8
17	Br	$1.9 \pm 0.7 \times 10^{11}$	-64.3 ± 0.9	-60.1 ± 1.6	-4.3 ± 1.8	$1.1 \pm 0.1 \times 10^6$	-34.5 ± 0.1	-42.4 ± 0.6	7.9 ± 0.7

^a Every measurement was repeated at least twice, and errors are quoted as twice the standard deviation. ^b Determined by pair-wise ¹H NMR competitive experiments. ^c Determined by ITC experiments

Table S2. Thermodynamic parameters for formation of 1:1 complexes in chloroform at 298 K.^a

Guest	X	Host							
		2				4			
		K / M^{-1b}	$\Delta G^\circ / \text{kJ mol}^{-1b}$	$\Delta H^\circ / \text{kJ mol}^{-1b}$	$-T\Delta S^\circ / \text{kJ mol}^{-1b}$	K / M^{-1c}	$\Delta G^\circ / \text{kJ mol}^{-1c}$	$\Delta H^\circ / \text{kJ mol}^{-1c}$	$-T\Delta S^\circ / \text{kJ mol}^{-1c}$
PNO	-	$7.5 \pm 0.7 \times 10^6$	-39.2 ± 0.2	-58.1 ± 3.7	18.8 ± 3.7	$1.3 \pm 0.0 \times 10^6$	-34.9 ± 0.1	-61.0 ± 2.7	26.0 ± 2.5
5	H	$1.4 \pm 0.3 \times 10^8$	-46.3 ± 0.4	-69.8 ± 6.2	22.6 ± 6.2	$1.8 \pm 0.4 \times 10^6$	-35.6 ± 0.6	-63.6 ± 4.5	28.0 ± 3.8
6	Me	$2.0 \pm 0.4 \times 10^8$	-47.1 ± 0.4	-64.3 ± 0.1	17.2 ± 0.4	$2.2 \pm 0.1 \times 10^6$	-36.1 ± 0.1	-70.3 ± 4.3	34.1 ± 4.5
7	NMe ₂	$5.0 \pm 1.0 \times 10^8$	-49.4 ± 0.4	-74.9 ± 1.4	25.5 ± 1.5	$3.2 \pm 0.0 \times 10^6$	-37.1 ± 0.0	-65.6 ± 4.1	28.4 ± 4.1
8	CF ₃	$9.1 \pm 1.8 \times 10^8$	-50.9 ± 0.4	-76.2 ± 1.4	25.3 ± 1.5	$9.9 \pm 1.5 \times 10^5$	-34.2 ± 0.3	-64.2 ± 3.1	30.0 ± 3.3
9	NO ₂	$2.6 \pm 0.5 \times 10^9$	-53.5 ± 0.4	-74.7 ± 3.4	21.2 ± 3.4	$5.4 \pm 0.2 \times 10^5$	-32.7 ± 0.1	-58.2 ± 2.5	35.5 ± 2.4
10	OMe	$4.9 \pm 1.0 \times 10^8$	-53.5 ± 0.4	-82.3 ± 2.3	28.8 ± 2.3	$2.0 \pm 0.9 \times 10^6$	-35.9 ± 1.1	-65.0 ± 2.1	29.0 ± 3.3
11	CHO	$6.1 \pm 1.3 \times 10^8$	-49.9 ± 0.5	-65.6 ± 1.7	15.7 ± 1.8	$8.7 \pm 1.3 \times 10^5$	-33.9 ± 0.4	-57.5 ± 3.1	23.4 ± 2.8
12	COMe	$9.0 \pm 1.9 \times 10^8$	-50.8 ± 0.5	-86.4 ± 2.8	35.6 ± 2.9	$9.4 \pm 1.5 \times 10^5$	-34.1 ± 0.4	-61.4 ± 3.7	27.3 ± 3.3
13	iPr	$1.5 \pm 0.4 \times 10^8$	-49.3 ± 0.4	-76.3 ± 4.0	27.0 ± 4.0	$2.5 \pm 0.5 \times 10^6$	-36.5 ± 0.5	-63.3 ± 0.1	26.7 ± 0.3
14	Et	$2.0 \pm 1.8 \times 10^8$	-50.9 ± 0.4	-77.6 ± 0.6	26.7 ± 0.7	$2.7 \pm 0.7 \times 10^6$	-36.7 ± 0.6	-67.5 ± 1.3	30.8 ± 2.0
15	F	$6.5 \pm 1.0 \times 10^8$	-50.0 ± 0.7	-61.5 ± 4.0	11.5 ± 4.0	$1.2 \pm 0.1 \times 10^6$	-34.7 ± 0.3	-51.4 ± 3.8	16.5 ± 3.8
16	Cl	$1.1 \pm 0.3 \times 10^9$	-51.4 ± 0.7	-82.2 ± 4.0	30.8 ± 4.0	$1.4 \pm 0.1 \times 10^6$	-35.0 ± 0.1	-62.7 ± 0.0	27.6 ± 0.0
17	Br	$7.4 \pm 1.7 \times 10^8$	-50.3 ± 0.5	-64.5 ± 4.8	14.2 ± 4.8	$1.2 \pm 0.1 \times 10^6$	-34.6 ± 0.2	-56.1 ± 0.1	21.5 ± 0.4

^a Every measurement was repeated at least twice, and errors are quoted as twice the standard deviation. ^b Determined by pair-wise ¹H NMR competition experiments. ^c Determined by ITC experiments.

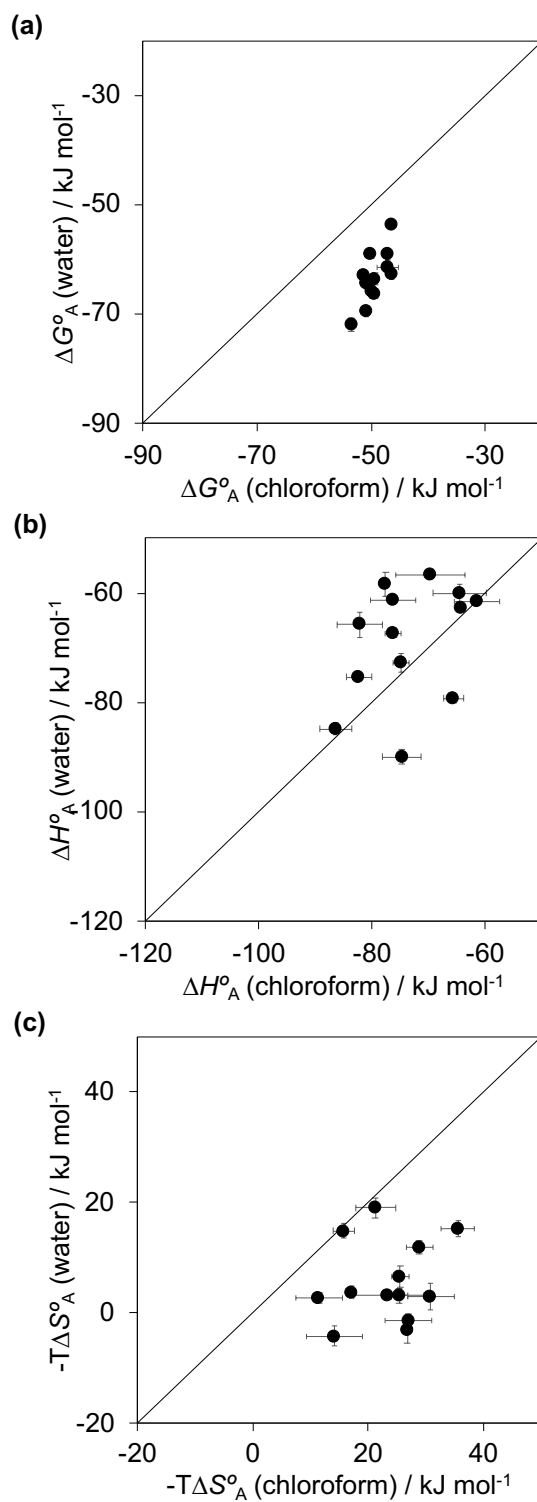


Figure S109. Thermodynamic parameters measured for formation of complex A of the DMC in water compared with the corresponding values measured in chloroform at 298 K. (a) ΔG° , (b) ΔH° and (c) ΔS° . The line corresponds to $y = x$ in each case.

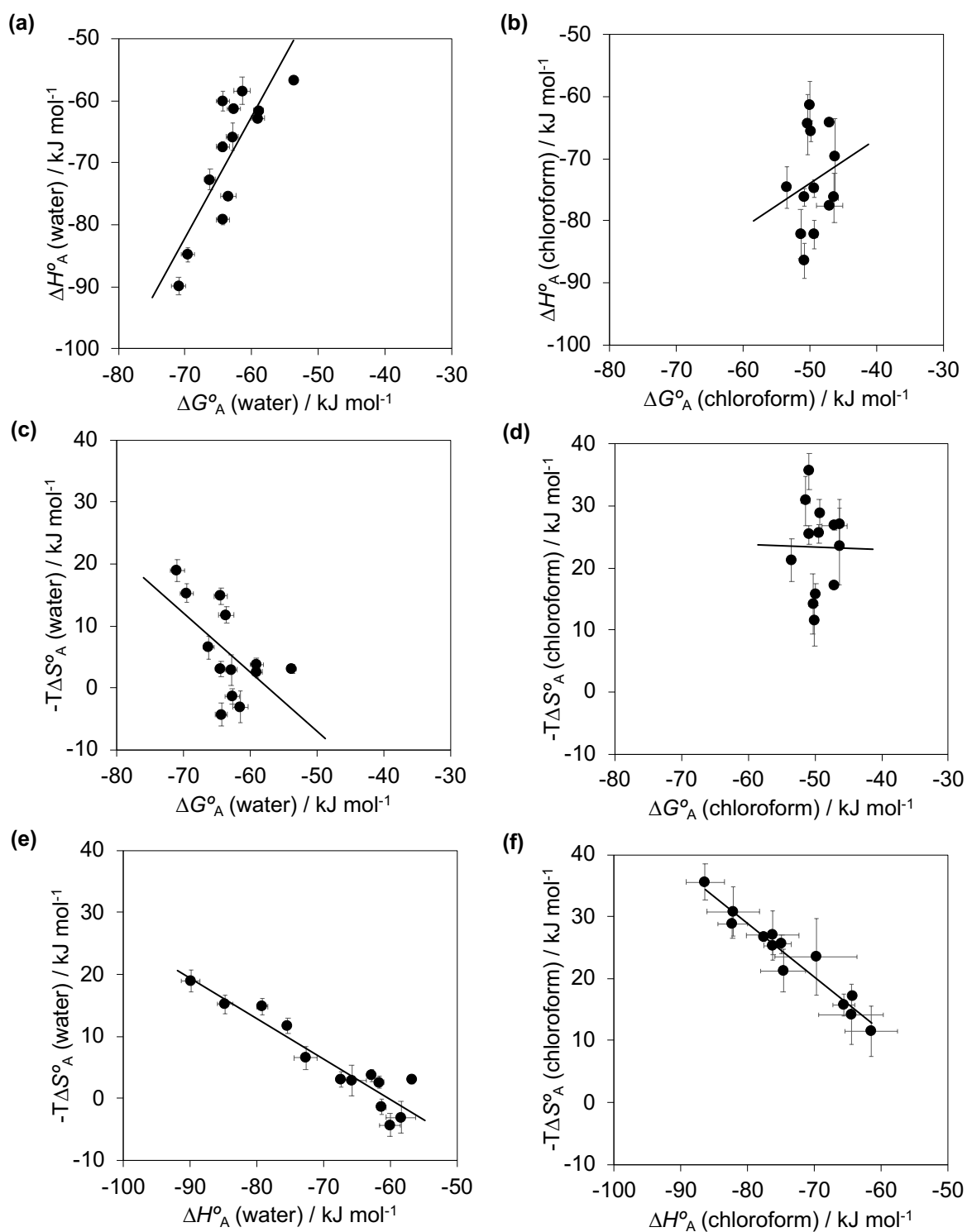


Figure S110. Comparison of ΔG° , ΔH° and ΔS° measured for formation of complex A of the DMC in water (a, c, e) and chloroform (b, d, f). The line of best fit is a) $y = 2.0x + 45.5$ ($R^2 = 0.68$); b) $y = 0.7x - 38.2$ ($R^2 = 0.04$); c) $y = -1.0x - 54.6$ ($R^2 = 0.34$); d) $y = -0.1x + 21.4$ ($R^2 = 0.00$); e) $y = -0.7x - 39.2$ ($R^2 = 0.88$); f) $y = -0.9x - 40.4$ ($R^2 = 0.94$).

6. ¹H NMR analysis of the structures of complex A of the DMC

Table S3. Limiting complexation-induced changes in ¹H NMR chemical shift ($\Delta\delta$ in ppm) for the guest signals in complex A of the DMC.^a

	Solvent	Water		Chloroform	
	Host	1		2	
Guest	X	H ₁	H ₄	H ₁	H ₄
5	H	-4.0	-1.6	-3.7	-1.1
6	Me	-4.0	-1.9	-3.7	-1.3
7	NMe ₂	-4.1	n.d.	-3.8	-1.4
8	CF ₃	-4.0	-2.1	-3.7	-1.3
9	NO ₂	-4.0	-2.3	-3.8	-1.7
10	OMe	-4.1	-2.0	-3.7	-1.4
11	CHO	-4.1	-1.9	-3.7	-1.5
12	COMe	-4.0	-2.0	-3.7	-1.6
13	iPr	-4.0	-2.0	-3.7	-1.3
14	Et	-4.0	-2.0	-3.7	-1.3
15	F	-4.0	-2.0	-3.7	-1.4
16	Cl	-4.0	-2.0	-3.7	-1.5
17	Br	-4.0	-2.0	-3.7	-1.5

^a Values for H₂ and H₃ could not be determined due to signal overlap.

Table S4. Differences between the ^1H chemical shift of the host signal in host-guest complexes compared with the chemical shift in the corresponding host-5 complex ($\Delta\delta$ in ppm) at 298 K.

Guest	X	Solvent													
		D ₂ O							CDCl ₃						
		H _a	H _b	H _c	H _d	H _e	H _f	H _g	H _a	H _b	H _c	H _d	H _e	H _f	H _g
6	Me	n.d. ^a	0.0	0.0	0.0	0.0	0.0	0.0	0.0	0.0	0.0	0.0	0.0	0.0	0.0
7	NMe ₂	n.d.	0.0	0.0	0.0	0.0	0.0	0.0	0.0	+0.2	0.0	0.0	0.0	0.0	0.0
8	CF ₃	n.d.	0.0	0.0	0.0	+0.1	+0.1	0.0	-0.1	0.0	0.0	0.0	0.0	0.0	0.0
9	NO ₂	n.d.	0.0	0.0	0.0	+0.1	+0.1	0.0	-0.2	0.0	0.0	+0.1	0.0	0.0	0.0
10	OMe	n.d.	0.0	0.0	0.0	+0.1	+0.1	0.0	+0.1	0.0	0.0	0.0	0.0	0.0	0.0
11	CHO	n.d.	0.0	0.0	0.0	0.0	0.0	0.0	-0.1	0.0	0.0	0.0	0.0	0.0	0.0
12	COMe	n.d.	0.0	0.0	0.0	+0.1	0.0	0.0	-0.1	0.0	0.0	0.0	0.0	0.0	0.0
13	iPr	n.d.	0.0	0.0	0.0	+0.1	+0.1	0.0	0.0	0.0	0.0	0.0	0.0	0.0	0.0
14	Et	n.d.	0.0	0.0	0.0	+0.1	+0.1	0.0	0.0	0.0	0.0	+0.1	0.0	0.0	0.0
15	F	n.d.	0.0	0.0	0.0	+0.1	+0.1	0.0	0.0	0.0	0.0	0.0	0.0	0.0	0.0
16	Cl	n.d.	0.0	0.0	0.0	+0.1	+0.1	0.0	-0.1	0.0	0.0	0.0	0.0	0.0	0.0
17	Br	n.d.	0.0	0.0	0.0	+0.1	+0.1	0.0	-0.1	0.0	0.0	0.0	0.0	+0.1	0.0

^a n.d. values could not be determined.

7. Analysis of the DMC results

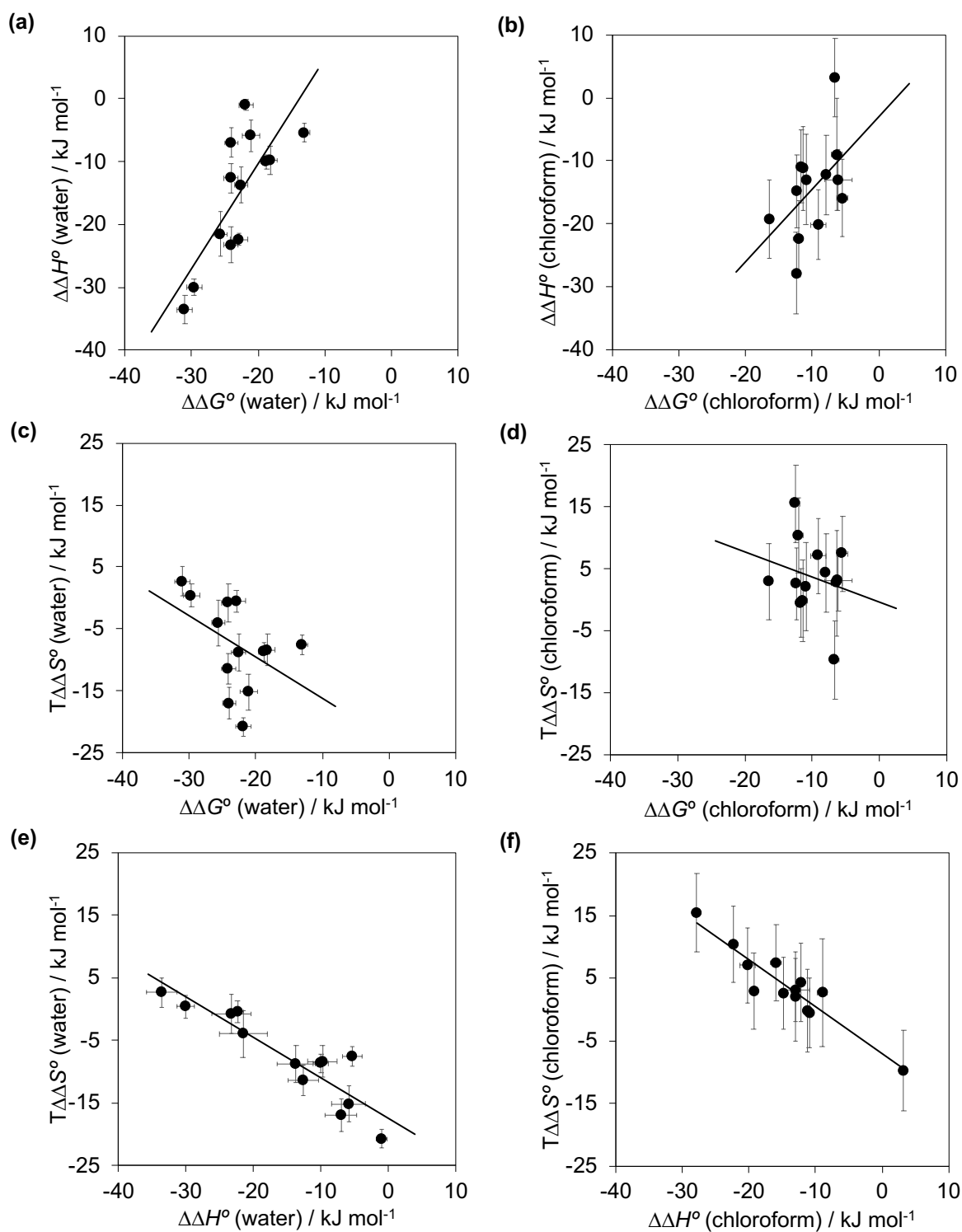


Figure S111. Comparison of $\Delta\Delta G^\circ$, $\Delta\Delta H^\circ$ and $\Delta\Delta S^\circ$ contributions measured with the DMC in water (a, c, e) and chloroform (b, d, f). The line of best fit is a) $y = 1.7x + 23.0$ ($R^2 = 0.60$); b) $y = 1.2x - 2.9$ ($R^2 = 0.25$); c) $y = -0.7x - 22.9$ ($R^2 = 0.19$); d) $y = -0.4x - 0.3$ ($R^2 = 0.05$); e) $y = -0.6x - 17.4$ ($R^2 = 0.83$); f) $y = -0.7x - 7.0$ ($R^2 = 0.88$).

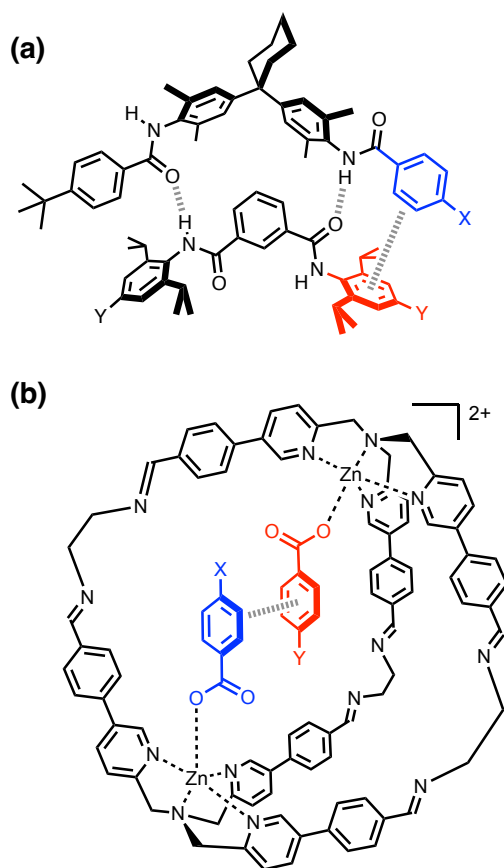


Figure S112. Aromatic interactions between the blue and red rings were measured as a function of substituents *X* and *Y* using DMCs. (a) An edge-to-face interaction in a H-bonded complex in chloroform. (b) A stacking interaction inside a self-assembled coordination cage in acetonitrile.

DMCs have been used previously to measure substituent effects on the free energy contributions of individual aromatic interactions to the stabilities of quite different supramolecular complexes (Figure 1).^{4,5} Figure S112a shows a H-bonded complex that was used to investigate substituent effects on edge-to-face aromatic interactions in chloroform. Figure S112b shows a coordination cage complex that was used to measure substituent effects on aromatic stacking interactions relative to solvation by alkyl groups. In both cases, substituents *X* and *Y* on the two interacting rings were varied, and good correlations were found with the Hammett substituent constants. Eq. 1 describes the edge-to-face interaction illustrated in Figure S112a, and Eq. 2 describes the stacking interaction illustrated in Figure S112b.

$$\Delta\Delta G^\circ(\text{edge-to-face}) / \text{kJ mol}^{-1} = 5.2 \sigma_x \sigma_Y - 1.9 \sigma_x + 1.4 \sigma_Y - 1.5 \quad \text{Eq. (1)}$$

$$\Delta\Delta G^\circ(\text{stacking}) / \text{kJ mol}^{-1} = 0.7 \sigma_x \sigma_Y - 1.5 \sigma_x - 1.5 \sigma_Y - 0.4 \quad \text{Eq. (2)}$$

Although there are differences in solvent and in the orientation of the substituents compared with the calix[4]pyrrole complexes, and Equations 1 and 2 were determined using *para* Hammett parameters, the results are in good agreement with the total aromatic interaction energy measured by the DMC in

Figure 2. Substituent effects on edge-to-face and stacking interactions with the π -face of an alkoxy substituted aromatic ring can be estimated by setting $\sigma_V = -0.27$ in Equations 1 and 2. The edge-to-face interaction is proportional to $3.3\sigma_X$, and the stacking interaction, which is less sensitive to the X substituent, is proportional to $1.7\sigma_X$. Summing over the four interactions in the calix[4]pyrrole complex predicts that $\Delta\Delta G^\circ$ should be proportional to $10\sigma_X$, which is similar to the equation of the line of best fit in Figure 10 (Eq. 3). We conclude that the magnitudes of the substituent effects on the aromatic interactions measured in the calix[4]pyrrole complexes in chloroform are in quantitative agreement with the literature and are dominated by electrostatic effects. Equations 1 and 2 suggest that the magnitude of the substituent effect on the edge-to-face interactions in the calix[4]pyrrole complexes is roughly double the effect on the stacking interactions.

$$\Delta\Delta G^\circ(\text{chloroform}) / \text{kJ mol}^{-1} = -7.4 - 11.7 \sigma_X \quad \text{Eq. (3)}$$

where σ_X is the Hammett constant for substituent X on the pyridine *N*-oxide guest.

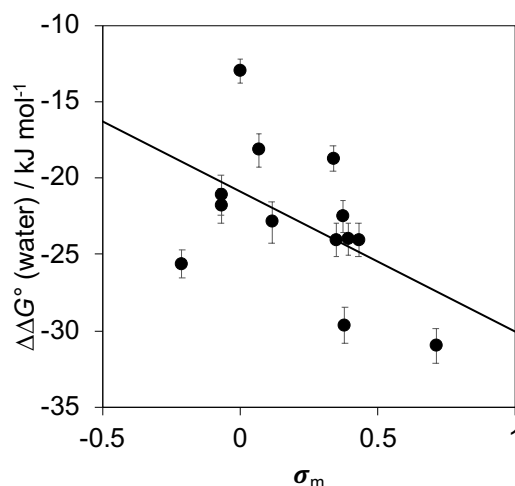


Figure S113. The free energy contributions due to aromatic interactions in complex A of the DMC ($\Delta\Delta G^\circ$) plotted as a function of the Hammett constant for substituent X (σ_m) for DMCs carried out in water. The line of best fit is $y = -9.2x - 20.9$ ($R^2 = 0.27$).

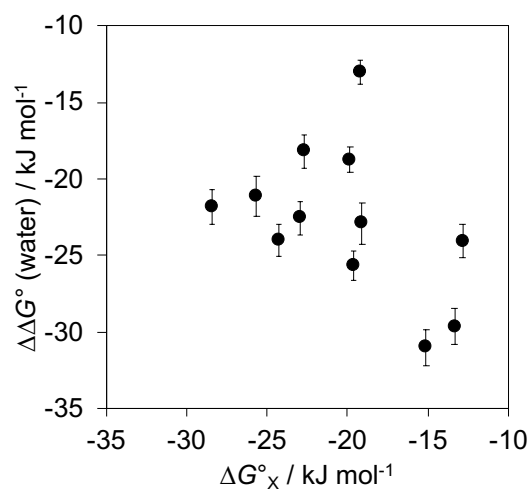


Figure S114. The free energy contributions due to aromatic interactions in complex A of the DMC ($\Delta\Delta G^\circ$) measured using DMCs in water compared with the corresponding values for the free energy of transfer of PhX from water into n-hexadecane (ΔG°_X).

8. References

- 1 L. Escobar and P. Ballester, *Org. Chem. Front.*, 2019, **6**, 1738–1748.
- 2 A. Díaz-Moscoso, D. Hernández-Alonso, L. Escobar, F. A. Arroyave and P. Ballester, *Org. Lett.*, 2017, **19**, 226–229.
- 3 L. Escobar, A. Díaz-Moscoso and P. Ballester, *Chem. Sci.*, 2018, **9**, 7186–7192.
- 4 F. J. Carver, C. A. Hunter, D. J. Livingstone, J. F. McCabe and E. M. Seward, *Chem. - A Eur. J.*, 2002, **8**, 2847.
- 5 C. Bravin, J. A. Piękoś, G. Licini, C. A. Hunter and C. Zonta, *Angew. Chemie - Int. Ed.*, 2021, **60**, 23871–23877.